technische universität dortmund

IMPRS FOR LIVING MATTER
International Max Planck Research School

Recursion quantification analysis reveals a cellular Morphodynamics - ERK activity recursive relationship

Dissertation

Zur Erlangung des akademischen Grades eines
Doktors der Naturwissenschaften
(Dr. rer. nat.)

bei der Fakultät Chemie und Chemische Biologie der Technischen Universität Dortmund

vorgelegt von Manuel Campos-Medina
October 2022

Deklaration

Tag der Abgabe Dissertation:
14. Oktober 2022

von Manuel Campos-Medina

Gutachter:

Prof. Dr. Philippe I.H. Bastiaens

Prof. Dr. Jan Kierfeld

The work presented in this dissertation was performed in the laboratory of Prof. Dr. Philippe I.H. Bastiaens at the Max Planck Institute of Molecular Physiology, Dortmund (Germany).

Manuel Campos-Medina was affiliated with the International Max Planck Research School in Chemical and Molecular Biology, Dortmund (Germany).

Eidesstattliche Versicherung (Affidavit)

Campos Medina, Manuel
Name, Vorname
(Surname, first name)

216146
Matrikel-Nr.
(Enrolment number)

Belehrung:

Wer vorsätzlich gegen eine die Täuschung über Prüfungsleistungen betreffende Regelung einer Hochschulprüfungsordnung verstößt, handelt ordnungswidrig. Die Ordnungswidrigkeit kann mit einer Geldbuße von bis zu 50.000,00 € geahndet werden. Zuständige Verwaltungsbehörde für die Verfolgung und Ahndung von Ordnungswidrigkeiten ist der Kanzler/die Kanzlerin der Technischen Universität Dortmund. Im Falle eines mehrfachen oder sonstigen schwerwiegenden Täuschungsversuches kann der Prüfling zudem exmatrikuliert werden, § 63 Abs. 5 Hochschulgesetz NRW.

Die Abgabe einer falschen Versicherung an Eides statt ist strafbar.

Wer vorsätzlich eine falsche Versicherung an Eides statt abgibt, kann mit einer Freiheitsstrafe bis zu drei Jahren oder mit Geldstrafe bestraft werden, § 156 StGB. Die fahrlässige Abgabe einer falschen Versicherung an Eides statt kann mit einer Freiheitsstrafe bis zu einem Jahr oder Geldstrafe bestraft werden, § 161 StGB.

Die oben stehende Belehrung habe ich zur Kenntnis genommen:

Official notification:

Any person who intentionally breaches any regulation of university examination regulations relating to deception in examination performance is acting improperly. This offence can be punished with a fine of up to EUR 50,000.00. The competent administrative authority for the pursuit and prosecution of offences of this type is the chancellor of the TU Dortmund University. In the case of multiple or other serious attempts at deception, the candidate can also be unenrolled, Section 63, paragraph 5 of the Universities Act of North Rhine-Westphalia.

The submission of a false affidavit is punishable.

Any person who intentionally submits a false affidavit can be punished with a prison sentence of up to three years or a fine, Section 156 of the Criminal Code. The negligent submission of a false affidavit can be punished with a prison sentence of up to one year or a fine, Section 161 of the Criminal Code.

I have taken note of the above official notification.

Dortmund, 14/10/22
Ort, Datum
(Place, date)

Campos Medina, Manuel
Unterschrift
(Signature)

Titel der Dissertation:
(Title of the thesis):

Recursion quantification analysis reveals a cellular Morphodynamics - ERK activity recursive relationship

Ich versichere hiermit an Eides statt, dass ich die vorliegende Dissertation mit dem Titel selbstständig und ohne unzulässige fremde Hilfe angefertigt habe. Ich habe keine anderen als die angegebenen Quellen und Hilfsmittel benutzt sowie wörtliche und sinngemäße Zitate kenntlich gemacht.
Die Arbeit hat in gegenwärtiger oder in einer anderen Fassung weder der TU Dortmund noch einer anderen Hochschule im Zusammenhang mit einer staatlichen oder akademischen Prüfung vorgelegen.

I hereby swear that I have completed the present dissertation independently and without inadmissible external support. I have not used any sources or tools other than those indicated and have identified literal and analogous quotations.

The thesis in its current version or another version has not been presented to the TU Dortmund University or another university in connection with a state or academic examination.*

*Please be aware that solely the German version of the affidavit ("Eidesstattliche Versicherung") for the PhD thesis is the official and legally binding version.

Dortmund, 14/10/22
Ort, Datum
(Place, date)

Campos Medina, Manuel
Unterschrift
(Signature)

Table of Contents

Abstract

One of the enigmas of cellular biology is the process by which eukaryotic cells, abandoning their unitary role, organize to form complex systems of organs. Despite the details of such pattern emergence process are yet to be elucidated, there is a significant degree of coordination among adjacent cells. For decades, several proteins have been monitored to track cellular communication. Although advancements have been made regarding our understanding of the internal cellular signaling network, there is no clear answer regarding how cells can communicate. One of the most studied families of proteins is the Extracellular-signal-regulated-kinases. Due to its myriad interactions and influence over most major cellular processes, it has been established as a central node in the cellular signaling network. However, the number of studies regarding its dynamic behavior is limited. Although its connection with cellular morphodynamics has also been well-documented, there is no consensus on the time scale of their relationship.

By studying ERK's dynamics upon growth factor stimulation, we found that the local cellular environment influences ERK's activation tendencies. Nonetheless, this effect is more significant at low growth factor concentrations. We employed a non-linear dynamics multidimensional analysis to explore the existence of recurring patterns within ERK dynamics and cellular morphodynamics. We focused on the high-frequency components of each of these dynamics during the basal state of cells and after either EGF or HRG stimulation. After cells were exposed to cell-fate-decision induing dosages of growth factors, our analysis showed an increase in the persistence of ERK dynamics and cellular morphodynamics recurrence patterns. Furthermore, we found that the recurrences that exist within ERK dynamics and cellular morphodynamics occur at similar time scales. Moreover, our results showed that these two dynamic processes are intrinsically related, and their relationship is not modified upon growth factor stimulation.

By extending the recurrence analysis to neighboring cells' dynamic behavior, we corroborated our findings on the influence of the local cellular environment on ERK dynamics and cellular morphodynamics. ERK dynamics in neighboring cells kept their communication pattern after EGF stimulation. However, cellular morphodynamics

between neighboring cells synchronized only after stimulation with low concentrations of EGF.

Our work sets the framework for conceiving ERK dynamics and cellular morphodynamics as inseparable processes. It also sheds light on conceptualizing cellular communication as a process that could occur via physiological concentrations of EGF among MCF-7 cells.

Zusammenfassung

Eines der Rätsel der Zellbiologie ist der Prozess, durch den sich eukaryotische Zellen unter Aufgabe ihrer einheitlichen Rolle zu komplexen Organsystemen organisieren. Obwohl die Einzelheiten eines solchen Musterbildungsprozesses noch nicht geklärt sind, gibt es ein erhebliches Maß an Koordination zwischen benachbarten Zellen. Seit Jahrzehnten werden verschiedene Proteine überwacht, um die zelluläre Kommunikation zu verfolgen. Obwohl unser Verständnis des internen zellulären Signalnetzwerks Fortschritte gemacht hat, gibt es keine klare Antwort darauf, wie Zellen kommunizieren können. Eine der am meisten untersuchten Proteinfamilien ist die der extrazellulären signalregulierten Kinasen. Aufgrund ihrer unzähligen Interaktionen und ihres Einflusses auf die meisten wichtigen zellulären Prozesse hat sie sich als zentraler Knotenpunkt im zellulären Signalnetzwerk etabliert. Die Zahl der Studien zu ihrem dynamischen Verhalten ist jedoch begrenzt. Obwohl sein Zusammenhang mit der zellulären Morphodynamik gut dokumentiert ist, gibt es keinen Konsens über die Zeitskala ihrer Beziehung.

Bei der Untersuchung der ERK-Dynamik nach Stimulation durch Wachstumsfaktoren haben wir festgestellt, dass die lokale zelluläre Umgebung die Aktivierungstendenzen von ERK beeinflusst. Dieser Effekt ist jedoch bei niedrigen Konzentrationen des Wachstumsfaktors stärker ausgeprägt. Wir setzten eine multidimensionale Analyse der nichtlinearen Dynamik ein, um die Existenz wiederkehrender Muster innerhalb der ERK-Dynamik und der zellulären Morphodynamik zu untersuchen. Wir konzentrierten uns auf die hochfrequenten Komponenten jeder dieser Dynamiken während des Grundzustands der Zellen und nach EGF- oder HRG-Stimulation. Nachdem die Zellen einer den Zellzustand beeinflussenden Dosis von Wachstumsfaktoren ausgesetzt wurden, zeigte unsere Analyse eine Zunahme der Persistenz der ERK-Dynamik und der zellulären Morphodynamik-Rezidivmuster. Darüber hinaus stellten wir fest, dass die Wiederholungen innerhalb der ERK-Dynamik und der zellulären Morphodynamik auf ähnlichen Zeitskalen auftreten. Darüber hinaus zeigten unsere Ergebnisse, dass diese beiden dynamischen Prozesse eng miteinander verbunden sind und ihre Beziehung durch die Stimulation mit Wachstumsfaktoren nicht verändert wird.

Indem wir die Rekurrenzanalyse auf das dynamische Verhalten benachbarter Zellen ausdehnten, konnten wir unsere Erkenntnisse über den Einfluss der lokalen zellulären Umgebung auf die ERK-Dynamik und die zelluläre Morphodynamik untermauern. Die ERK-Dynamik in benachbarten Zellen behielt ihr Kommunikationsmuster nach der EGF-Stimulation bei. Die zelluläre Morphodynamik zwischen benachbarten Zellen synchronisierte sich jedoch nur nach Stimulation mit niedrigen EGF-Konzentrationen.

Unsere Arbeit bildet den Rahmen, um die ERK-Dynamik und die zelluläre Morphodynamik als untrennbare Prozesse zu begreifen. Sie wirft auch ein Licht auf die Vorstellung, dass zelluläre Kommunikation ein Prozess ist, der durch physiologische EGF-Konzentrationen zwischen MCF-7-Zellen stattfinden könnte.

1 Introduction

The hallmark of eukaryotic cells can be entrusted to their ability to form arrangements with groups of their peers to develop complex structures with highly specified functions. Regardless of the size of these structures, the organization of tissues leads to the formation of organs. These organs are grouped into systems and, in turn, create an organism. This entire process solely relies on the ability of cells to interact with their environment and coordinate with the surrounding cells. The cellular environment is conformed by mechano-chemical signals that convey information to the cell. This compendium of stimulus, in turn, integrates said information and responds according to several factors that can be resumed as its current state. Consequently, the cell's morphological or chemical reciprocation contains information about the cellular signaling network and how the stimulus was processed by the cell. Although said cellular responses are fast-paced, the effects of stimulation that reaches a cell can develop into long-lasting morphological changes (Guo et al., 2020; Mayr et al., 2019; von Kriegsheim et al., 2009; Yarden and Sliwkowski, 2001; Yoon and Seger, 2006). The difficulty of predicting the outcome of a particular stimulus resides in the complexity of the signaling network within the cell. A complex system that comprises thousands of protein interactions, some of which are negligible, others transcendental. Fortunately, extensive work has been done on characterizing one family of proteins that could be considered a central node of this signaling network, "Extracellular regulated kinases" (ERK).

1.1 Extracellular regulated kinases (ERK)

The term ERK is used to refer to two protein complexes, ERK1 and ERK2. ERK interacts with diverse proteins, and thanks to decades of studies, its mechanism of action and effect on several cellular processes have been identified (Roskoski, 2012). However, the main focus of the study of ERK has been how its activity is affected by the transduction of membrane-receptor-emitted signals due to the exposure of cells to

external chemical cues such as epidermal growth factor (EGF), Hereguling (HRG), and fibroblast growth factor (FGF) (Lavoie et al., 2020).

ERK proteins are members of the family of kinases called "Mitogen-activated protein kinases" (MAPKs). MAPKs covey signals emitted by receptors located at the cellular membrane and transmit them to downstream effectors through phosphorylation (Cargnello and Roux, 2011). ERK is mainly involved in the transduction of growth factor-triggered reactions and mitogen-induced signals affecting the RAS GTPases' family. First, GTP-loaded RAS activates the kinase RAF, which then phosphorylates the kinase MEK, which activates ERK by direct phosphorylation (Cargnello and Roux, 2011; Lavoie and Therrien, 2015). Once phosphorylated, ERK keeps on the conveys the signal initiated by RAS via phosphorylation of a myriad of substrates in different cellular regions. Among the primary substrates of ERK are the protein complexes RSK and MSK. However, ERK's extensive collection of direct phosphorylation sites comprises a much broader range of compounds(Ünal et al., 2017).

1.2 ERK spatial localization

Although the details of ERK spatiotemporal activation remain to be clarified, its relationship has been established with RAS-GTPases. RAS-GTPases locations and their connection with ERK initiating reactions bring as a consequence the localization of ERK activation mainly to the plasma membrane, and in a lesser role, to the endoplasmatic reticulum, endosomes, and other endomembrane-rich cellular structures (Good et al., 2009; Tsukada et al., 2008). Once activated, ERK species can be identified on the cytoplasm or can translocate to the nucleus. ERK cytoplasmic activity and its eventual nuclear translocation have been used to characterize several cellular processes, and despite the inability to achieve ERK translocation has been described as a sign of quiescence, the specific role of each type of ERK is yet to be fully understood(Harding et al., 2005; Raina et al., 2022; Stanoev et al., 2018). However, it has been suggested that dimerized ERK is mainly found in the cytoplasm, whereas nuclear ERK proteins are primarily monomers. Interestingly, dimerized ERK has been reported to possess autophosphorylating properties. The ability of

cytoplasmic ERK to self-activation suggests that this species is more dynamic than its nuclear counterpart (Herrero et al., 2015; Lai and Pelech, 2016; Lorenz et al., 2009).

1.3 ERK as a central node of the cellular signaling network

Despite ERK proteins are mainly identified with the MAPK cellular signaling network, they have been found to have de involved in cellular processes such as migration, proliferation, survival, growth, metabolism, and differentiation (Lavoie et al., 2020).

1.3.1 Cell migration and motility

ERK signaling is responsible for cellular morphodynamics by its effect on downstream proteins that regulate membrane retraction and protrusion and are capable of inducing cell-matrix adhesion (Tanimura and Takeda, 2017). Thus, ERK monitoring yields information about cell motility and migration. Our previous research showed that ERK phosphorylation and the subsequent KSR activation are characteristics of growth factor-induced cell migration. This ERK phosphorylation is characterized by being localized at the plasma membrane (Brüggemann et al., 2021). Simultaneously, It has been reported that when there is an overexpression or a gain-of-function mutation in one of the proteins upstream of ERK, it is responsible for epithelial to mesenchymal transition. Polarized epithelial cells can transform into mesenchymal cells, which are associated with invasive metastatic tumors (Yang and Weinberg, 2008) .

In addition, ERK phosphorylation and post-activation interactions are associated with cellular membrane protrusions via filopodia and lamellipodia. ERK interacts with a protein called WAVE, which enhances actin polymerization, which indicates modification of the cytoskeleton and, thus, morphodynamic activity. Furthermore, it has been reported that the ERK-mediated WAVE activity may induce sustained cell motility and migration (Mendoza et al., 2011; Miki et al., 1999).

Regarding cell spreading regulation, ERK is also related to the protein Vinexin, which decreases cell motility via surface adhesion (Parsons et al., 2010). ERK-phosphorylated Vinein has been localized to the leading edge of migrating cells colocalized with active ERK. Intriguingly ERK forms a complex with a protein complex called FAK. The ERK-FAK complex serves as a scaffold protein for MEK, an upstream phosphorylator of ERK, which activates a complex called calpain. Calpain, specifically calpain 2, cleaves proteins that fixate the cytoskeleton to focal adhesion complexes. Thus, diminishing cell-to-surface adhesion and enhancing cellular motility(Case and Waterman, 2015; Eblen et al., 2004; Parsons et al., 2010; Slack-Davis et al., 2003). In addition, ERK phosphorylates a protein complex called FAK, and a protein complex called paxillin disturbs the association ratio between them. This interaction ultimately leads to the dissociation of FAK from the FAK-paxillin complex, which releases cell adhesion sites (Nayal et al., 2006; Sundberg-Smith et al., 2005). The release of these sites enhances cell spreading. In addition, it enables the formation of protrusions in the form of lamellipodia and filopodia. Naturally, the release of the cells from adhesion sites enables the extension of the cellular membrane, which is necessary for cellular motility.

Though the details of the mechanism involved in cellular motion have not been clarified, a continuous balance between cellular adhesion, and cellular spreading, combined with protrusions of the cellular membrane, appears to revolt around ERK activity and to be a constant in moving cells. Despite the details remain unclear as to how ERK phosphorylates Myosionn light chain kinase (MLCK), once it activates it, they are colocalized on the leading edge of migrating cells. MLCK phosphorylates the Myosin II light chain, which regulates Myosin II (Brahmbhatt and Klemke, 2003; Klemke et al., 1997; Webb et al., 2004). The latter interacts with actin and generates the contractile force that drives the cellular motion and is associated with the extension of the cellular membrane.

Cell movement appears to be a consequence of attachment on the leading edge. At the same time, force is generated by the myosin II complex and detachment of the following end of the cells. Once the following recoiling end of the cell approaches the leading edge, the latter detaches. The cellular membrane extends while the

following edge of the cell is attached until the myosin II generates enough force to reset the process. Cellular retraction is mainly linked to Rho GTPases which stabilize actin and enhance cellular retraction via myosin. This process is negatively regulated by Rho phosphorylation (Brahmbhatt and Klemke, 2003). Once phosphorylated, Rho is marked for its ubiquitin-proteasome-dependent degradation . Despite the fact that the mechanism has not been clarified, it is known that ERK phosphorylates, whether directly or indirectly, Rho (Vicente-Manzanares et al., 2009; Webb et al., 2004). Thus, further linking ERK to the retraction process involved in cellular motility.

1.3.2 Proliferation

The transition between cell cycle phases G1 and S depends on ERK activation via RAS. Namely, the activation of ERK through RAS induces the transition from G1 to the S phase of the cell cycle (Drosten et al., 2010; Stacey and Kung, 1984). Thus perennial activation of RAS or gain of function mutation that leads to trigger-friendly phosphorylation of RAS and subsequent phosphorylation of ERK is associated with uncontrollably dividing cells, such as many types of cancer cells (Deschênes-Simard et al., 2014; Koseska and Bastiaens, 2017).

Interestingly, Up-regulated ERK is likely to be responsible for cellular senesce induction cell cycle exit. Additionally to the RAS-related effect on the cell cycle, ERK's substrate RSK, once phosphorylated, increases the binding of serum response factors (SRF) to DNA (Fowler et al., 2011; Lavoie and Therrien, 2015). SRF forms tetramer with three ternary complex factors (TCF), later phosphorylated by ERK. Once phosphorylated, TCF induces chromatin modifications that lead to methylation, acetylation, and transcription initiation (Hollenberg and Gregory, 1980; Rivera et al., 1993). The location of these modifications upregulates cell proliferation and is linked to some types of cancer.

In addition, ERK directly phosphorylates proteins that belong to the FOS and JUN family complexes. This phosphorylation blocks their proteasomal degradation and increases their DNA binding activity, enhancing their transactivation. FOS and JUN family complexes are strongly related to cell proliferation induction (Lopez-Bergami et al., 2010; Murphy et al., 2002). ERK signaling has been found to be

necessary for the transcription of G1-specific cyclin and late G1-specific cyclin that induces feedforward loops that lead to the irreversibility of S phase induction (Albanese et al., 1995).

1.3.3 Cell survival

Cell population and genetic stability are maintained by the induction of programmed cell death or apoptosis. This process maintains tissue stability and prevents cells with significant DNA damage from pass-down mutations (Matsuura et al., 2016; Mohammad et al., 2015). Conversely, inhibition of pro-apoptotic mechanisms induces abnormal growth in tissues due to excessive cell population and accumulation of mutations that could develop into malignant transformations (Bakhoum and Cantley, 2018; Lukow et al., 2021).

According to the literature, receptor tyrosine kinases (RTK) mediated ERK activation is mainly involved in inhibiting pro-apoptotic signals. RTK are protein complexes responsible of the transduction of extracellular chemical signals cytoplasm (Lemmon and Schlessinger, 2010). The evidence suggests that ERK-mediated inhibition of apoptosis is focused on stopping the permeabilization of the mitochondria despite the cell death-inducing signals (Ostrakhovitch and Cherian, 2005). It has been found that ERK inhibits a pro-apoptotic protein called BIM, responsible for oligomerizing proteins that form pores on the mitochondrial membrane. Apoptosis is blocked by blocking the release of cellular death-inducing proteins such as Cytochrome C, BAK, and BAX (Chen et al., 2005; Edlich, 2018; Kale et al., 2018). In addition, ERK phosphorylates FOXO3A, a transcription activation factor that encodes the above-mentioned BIM (Lopez et al., 2012). ERK phosphorylation of FOXO3A promotes its cellular exclusion and enhances its degradation at the proteasome (Yang et al., 2008).

In addition, ERK phosphorylation has also been positively correlated with the disruption of other pro-apoptotic complexes such as BIK and BAD. ERK induces proteasomal degradation of BIK by direct phosphorylation (Lopez et al., 2012). In the case of the BAD protein complex, ERK-activated RSK enables the translocation of BAD from the mitochondrial membrane to the cytosol, which blocks its negative control

over the anti-apoptotic factors BCL-2 and BCL-xL (Bonni et al., 1999; Shao and Aplin, 2012). ERK has also been linked to inhibiting protein complexes that are released post-mitochondrial permeabilization. For example, caspase 9, a crucial protein that, once active, marks the irreversibility of programmed cell death, Is phosphorylated and inhibited by ERK (Allan et al., 2003). Furthermore, ERK also enhances the viability of anti-apoptotic complexes. MCL1 and BIRC5, both anti-apoptotic proteins, have been found to be positively regulated by high ERK and ERK-related activity (Bonni et al., 1999; Ye et al., 2014).

1.3.4 Cell growth

Cell size and its modification in response to environmental cues dictate the triggering of cell proliferation. The size of the cells, influenced by the biomass intake from the cellular environment, has been linked to the G1/S transition in proliferating cells (Ginzberg et al., 2015). However, the G1/S transition also depends on the type and concentration of extracellular chemical cues and the nature of the cell involved in the process. Cues that induce growth in cells are conveyed to the intrinsic building machinery by specific nodes of the cell signaling network. Although cell growth is not dominated by ERK activity, it is involved in several cell volume regulatory mechanisms by the induction of ribosomal DNA transcription (Ginzberg et al., 2015). Specifically, ERK phosphorylates the transcription factor RRN3, which enhances the production of Pol I and Pol III. Consequently, this upregulates the uptake of biomass (Bywater et al., 2013; Zhao et al., 2003).

Furthermore, ERK activity has been linked to mTOR complex 1 mediated mRNA regulation. mTOR-1 significant effect on cell size has been well documented (Saxton and Sabatini, 2017). mTOR complex 1 interacts with several cellular metabolic sensors and conveys the availability of nutrients in the cellular environment to the internal signaling network. It has also been shown that ERK phosphorylation of RAPTOR leads to mTORC1 activation, which subsequently enhances protein synthesis (Carrière et al., 2008).

1.3.5 Cellular metabolism

ERK is involved in 2 different cellular metabolic processes. One of these is directly related to ATP. Releasing of energy by ATP dissociation is enhanced by active AMP-dependent kinase (AMPK) (Herzig and Shaw, 2018). This kinase is negatively regulated by the AMP: ATP ratio. ERK antagonizes AMPK and indiscriminately induces ATP production. Interestingly, AMPK opposes ERK-mediated ATP production by inhibiting BRAF, one of ERK effectors (Shen et al., 2013).

The other mechanism of energy production that involves ERK is aerobic glycolysis. Otherwise known as the Warburg effect, it is a well-known trait of rapidly dividing cells, undifferentiated cells, and cancer cells (Warbug, 1956). Although the mechanism and targets of ERK phosphorylation are yet to be clarified, ERK activity has been positively correlated with aerobic glycolysis. However, it is likely that ERK impedes anaerobic glycolysis by suppressing pyruvate dehydrogenase activity due to its direct phosphorylation of MYC and hypoxia-inducible factor 1 α (HIF1 α) (Mylonis et al., 2006; Parmenter et al., 2014; Richard et al., 1999).

Upregulated ERK has been found to promote the Warburg effect by silencing the aerobic generation of energy in the mitochondria (Herzig and Shaw, 2018). Interestingly, ERK's pharmacological inhibition turns off glycolysis-mediated ATP production and shifts energy generation to an oxidative-phosphorylation-mediated process (Haq et al., 2013). Furthermore, this change in the energy generation mechanism has been found to prevent metastasis in melanoma cells (Houles et al., 2018). In addition, ERK activity has been linked to "Dynamin-related protein 1" activation and subsequent mitochondrial morphology modification (Serasinghe et al., 2015). Consequently, with its influence over the Warburg effect, ERK activity favors anabolic reactions that involve glycolysis. These reactions include the activation of non-oxidative pentose phosphatase-mediated reactions and phosphorylation of carbamoyl phosphate synthase, which stimulates pyrimidine synthesis (Graves et al., 2000).

1.3.6 Differentiation

Cell fate and tissue fate decisions have been described as processes that strongly rely on ERK activity (Patel and Shvartsman, 2018; Saba-El-Leil et al., 2016). For example, ERK's effect on cellular development is found in stem cell self-renewal and differentiation. In addition, homeostasis in osteocytes, cardiocytes, and brain cells is dependent on balanced ERK activity (Lavoie et al., 2020).

Embryonic stem cells are maintained undifferentiated in-vitro by being cultured on media that inhibits ERK signaling. However, the mechanism by which ERK-driven differentiation occurs remains a topic of discussion (Burdon et al., 1999). Recent evidence suggests that by silencing ERK's effector MEK, partial inhibition of ERK induces continuous switching between partial ERK-signalling and negligible ERK activity (Ying et al., 2008). It has been described that Fibroblast growth factor exposure induces ERK that results in the damping of the pluripotency transcription factors NANOG, KLF4, and KLF2 (Dhaliwal et al., 2018; Spelat et al., 2012). In addition, by direct phosphorylation, ERK inhibits these three transcription factors and OCT4, another key pluripotency transcription factor (Brumbaugh et al., 2014). Furthermore, ERK directly phosphorylates other transcription factors associated with BMP signaling, mainly STAT3. This inhibition suppresses STAT3 DNA binding and consequently nullifies the ability of the transcription factor to maintain cells in naive pluripotency (Huang et al., 2014). SMAD transcription factors, another set of complexes linked to BMP signaling, are phosphorylated by ERK and subsequently driven towards degradation (Fuentealba et al., 2007).

Additionally, ERK activity limits stem-cell self-renewal by damping BMP signaling and inducing cell differentiation. As negative feedback, BMP4 reduces ERK signaling and supports pluripotency as well as self-renewal of embryonic stem cells (Huang et al., 2014). Although differentiation-associated pathologies are usually found on cells with abnormally high ERK activity, decreased ERK activity has also been linked to developmental diseases. These medical conditions are characterized by symptoms that often include facial dysmorphism, cardiac malformations, cutaneous and musculoskeletal anomalies, cognitive impairment, and increased cancer susceptibility (Dinsmore and Soriano, 2018; Nakamura et al., 2009; Newbern et al.,

2008). During embryonic development, a group of cells that arise from the ectoderm germ layer called the neural crest is particularly susceptible to ERK imbalances.

These neural crest cells are crucial for skeletal development, specifically cranial development. In these cells, it has been found that ERK phosphorylates and activates transcription factors that are suspected of inducing abnormal osteogenesis. Thus, upregulated ERK induces malformations in the cranial region (Rauen, 2013; Twigg et al., 2013). Similarly, neural crest cells are responsible for supporting the formation of aortic walls, valves, and the intraventricular septum (Nakamura et al., 2009). ERK imbalance affects the development of these structures by perturbing the normal functioning of the cell signaling network in neural crest cells. Interestingly, neighboring cell communication has been found to be partially responsible for propagating abnormal cell differentiation in cardiomyocytes during embryonic development (Yin et al., 2017). However, ERK-related interactions in developmental cardiopathies are yet to be fully described.

Normal ERK signaling is crucial for proper brain development. Abnormally high ERK activity has been linked to several levels of cognitive disabilities, autism spectrum disorder, attention deficit hyperactivity disorder, and memory impairment (Atkins et al., 1998; Lu et al., 2017). Furthermore, the ERK-induced activity of complexes MNK1 and MNK2 are associated with the control translation factors involved in neuronal plasticity (Ueda Takeshi et al., 2004). Furthermore, it has been reported that these MNK complexes phosphorylate the protein eIF4R in hippocampal neurons, which could be related to cognitive impairment traits similar to the fragile X syndrome (Napoli et al., 2008).

1.4 Erk phosphorylation by either EGF or HRG simulation

How it was mentioned in the previous section, ERK has a pivotal role in a myriad of cellular processes. Such a significant impact on cellular behavior requires an equally important precise output of responses. ERK dynamics robustness has been its broad range of interactions, especially the complex reversible reactions (Obatake et al., 2019; Ünal et al., 2017). In addition, the competition between ERK substrates and

ERK phosphatases affects the ERK dynamics, which also contributes to the stability of the network (Legewie et al., 2007; Liu et al., 2011). ERKs robustness It has also been linked to the co-existence of several feedback loops with two different periodicities, one with a periodicity between 15 and 30 mins and another slower-occurring feedback with a periodicity between 1 to 2 hours (Blüthgen and Herzel, 2003; Brandman et al., 2005; Dessauges et al., 2022; Fritsche-Guenther et al., 2011; Kochańczyk et al., 2017; Shankaran and Wiley, 2010). Considering the presence of different time scales embedded in the signaling network implies that the duration of ERK's activity internal cycles can convey important information about its signaling network.

Regarding ERK activity duration, RTK of ERK can range between a few minutes up to several hours. The duration of RTK-mediated ERK activity depends on the ligand concentration and the type of activated receptor (Bergeron et al., 2016). The dynamics of ERK are also highly dependent, as it has been corroborated by previous work of this lab, on the internalization and further degradation mechanism of the ligand-activated receptor, which is also ligand concentration dependent (Stanoev et al., 2018). This project focused on studying ERK's dynamics after EGF or HRG stimulation.

1.4.1 ERK activation by EGF

The epidermal growth factor (EGF) is a protein with an estimated molecular weight of 6-kDa that was discovered in1980s (Hollenberg and Gregory, 1980). Even though this protein has been majorly associated with cell anti-apoptotic and proliferation, there is emerging evidence that depending on its concentration, stimulation with EGF develops into a broader range of ERK-mediated cellular behaviors. EGF-induced cellular proliferation and survival have been reported at concentrations higher than 100 ng/mL (Lee et al., 2009; Li et al., 2019; Maachi et al., 2020; Siromolot et al., 2020); its other effects have been found at lower concentrations. Concentrations of 50 ng/mL of EGF have been found to increase biomass intake, which is a sign of cellular volumetric growth (Deshpande et al., 1996; Phuc and Taniguchi, 2017; Wang et al., 2018; Zhao et al., 2003). Similarly, stimulations with concentrations up to 40ng/mL of EGF have been found to facilitate cellular

differentiation (Li et al., 2019; Smitz et al., 1998). At concentrations ranging between 10ng/mL and 25 ng/mL, EGF-stimulation inhibited aerobic-glycolysis and enhanced L-lactate production, as mentioned in the previous section, is what is described as the Warburg effect, a characteristic switch found in cancer cells (Lee et al., 2015; Xu et al., 2017). As reported in our previous results, EGF-stimulation at concentrations as low as 1ng/mL leads to the activation of the KSR-ERK complex, eventually resulting in cell migration (Brüggemann et al., 2021). Such EGF-concentration-dependent distinct behaviors corroborate independent research that states the effect of EGF concentration is a smooth curve regarding ERK phosphorylation and its subsequent effect on cell-fate decisions (Birtwistle et al., 2007; Masunaga et al., 2017).

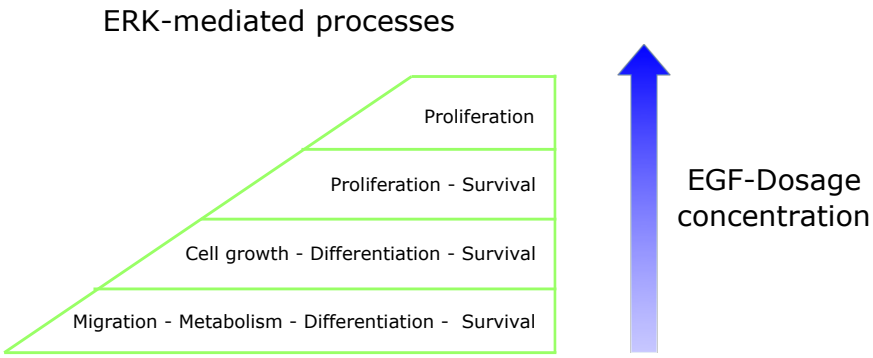

Figure 1. ERK-mediated process diversity dependency with EGF concentration

EGF directly stimulates the Epidermal growth factor receptor (EGFR), a well-characterized member of the ErbB family. This family of receptors is composed of 4 members EGFR (ErbB1), ErbB2,3, and 4. Its downstream signaling network is intrinsically linked to cell-fate decisions and the consequent tissue organization processes (Parker et al., 2020; Yarden and Sliwkowski, 2001). Active ErbB receptors undergo allosteric reactions that can result in the formation of homo- or heterodimers (Zhang et al., 2006). Interestingly, depending on the aggregation state of these receptors, their internalization and further degradation are different (Grecco et al., 2011; Moran et al., 1990; Stallaert et al., 2018; Stanoev et al., 2018). In our previous study, we found that EGF binding to EGFR at concentrations of 1ng/mL induces the heterodimerization between EGFR and ErbB2 or ErbB3. In contrast, a concentration of 100ng/mL led to the formation of EGFR homodimers (Baumdick et al., 2018, 2015;

Brüggemann et al., 2021). Interestingly, EGFR-homodimers are rapidly internalized by endosomes and degraded at the lysosomes (Sigismund et al., 2008). As a mechanism to ensure the robustness of the signaling response, the endosomal system down-regulates the receptor activation rate by breaking the chain of transmission between ligands, receptors, and the other components of the signaling network. Despite the fact that active EGFRs can maintain their signaling activity from endosomes, their access to the downstream signaling relievers is constrained (Villaseñor et al., 2016). The internalization of EGFR-homodimers results in transient ERK activity. In contrast, EGFR-heterodimers are internalized by the action of a protein called Clathrin. The protein complex Clathrin forms a polyhedral lattice around the EGFR-heterodimer, internalizes it, and recycles it back to the cell surface (Liu et al., 2020; Sigismund et al., 2008). This recycling re-sensitizes the membrane to further growth factor stimulation or autocatalytic phosphorylation by active EGFR monomers (Baumdick et al., 2015; Sanderson et al., 2006; Stanoev et al., 2018). The Clathrin-dependent internalization of EGFR results in sustained EGF-mediated ERK activity.

1.4.2 ERK activation by HRG

Heregullin (HRG) is a protein with a predicted molecular weight of 66.8 kDa, which contains EGF-like domains (Shamir and Buonanno, 2010). This protein acts as a ligand of the ErbB2, ErbB3, and ErbB4 members of the ErbB transmembrane receptor family. HRG-stimulation leads to the formation of ErbB2/ErbB3 dimers (Balañá et al., 1999; Bourguignon et al., 2007; Kawamoto et al., 2015; Keely and Barrett, 1999, p. 2; Negro et al., 2004). Despite its inability to autophosphorylate, even low HRG concentrations (1 ng/mL) are sufficient for ErbB3 activation; this leads to downstream-proteins phosphorylation through heterodimerization with ErbB2 (Steinkamp et al., 2014). This characteristic of ErbB3 has been attributed to the higher motility of its inactive form. Once activated, ErbB3 receptors' motility significantly decreases (Váradi et al., 2019); the complexes become collision targets for the mobile inactive ErbB2 complexes, which leads to the formation of ErbB2/ErbB3 dimers (Bertelsen and Stang, 2014; Ghosh et al., 2013, p. 3; Steinkamp et al., 2014). HRG-stimulation of ERK is mainly linked to migration and cellular morphodynamics but has

also been found to play a significant role in ERK-mediated cell differentiation (Kim et al., 2013; Nakakuki et al., 2010). Regardless of the HRG concentration, it has been found that activation of ErbB2/ErbB3 heterodimers enhances cellular motility. A process necessary to guarantee cellular motility, cellular scattering, has been linked to ErB3-mediated ERK-activation. Scattering of cells and the subsequent migration have been induced by concentrations equal to and higher than 20ng/mL of HRG (Chang et al., 2013; Keely and Barrett, 1999, p. 3; Okoshi et al., 2013). This concentration threshold has also been found crucial to achieving direct activation of ErbB2. Once activated, ErbB2 engages in dimerization with other members of the ErbB receptor family . Interestingly, concentrations ranging from 25ng/mL up to 400ng/mL have been found to activate transcription factors mediated by ERK that result in cell differentiation (Cedervall et al., 2013; Houlihan et al., 2010; Kim et al., 2013). HRG-induced cell differentiation has been linked to the activation of the ErbB2 receptor (Negro et al., 2004).

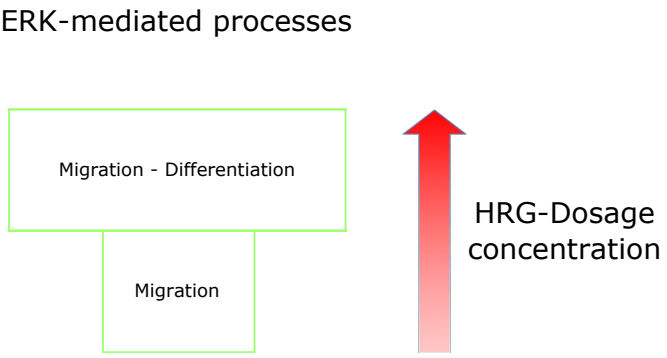

Figure 2. ERK-mediated process diversity dependency with HRG concentration

According to model predictions, unlike EGF, HRG-induced ERK activation speed increases steeply as HRG concentration increases (Birtwistle et al., 2007; Masunaga et al., 2017). Interestingly EGF and HRG both activate a protein that can be considered a central node of the cell's signaling network, Protein Kinase B. This protein, also known as AKT is a set of three kinases that, in its inactive form, is located in the cytosol; once activated, it translocates to the plasma membrane (Ersahin et al., 2015). Thus greatly enhancing cellular morphodynamics. AKT also plays an anti-apoptotic role by blocking the above-mentioned caspase 9 activation (Liu et al., 2008;

Mohammad et al., 2015). It has been linked to cellular differentiation due to its effect on cellular-cycle-related triggering proteins such as cyclin-dependent kinases (Chen et al., 2012; Worster et al., 2012; Ye et al., 2014). Despite ERK-related interactions and AKT-related interactions being complementary cell signaling networks, the effect of HRG and EGF concentrations show distinct behaviors. AKT shows a slow climbing, wide-range concentration-dependent response to HRG and a steep concentration-dependent response to EGF (Birtwistle et al., 2007; Masunaga et al., 2017). Our results also showed that EGF-induced ERK-dynamics and HRG-induced ERK-dynamics do not differ significantly in the peak activity. On the other hand, HRG-induced AKT activity is much more significant and sustained than its EGF-induced counterpart (Brüggemann et al., 2021). It has also been reported that at lower concentrations of EGF and HRG, the reactions involved in AKT-activation compete over the ErbB dimers with the ERK-activation reactions (Birtwistle et al., 2007; Kawamoto et al., 2015; Kim et al., 2013).

1.5 ERK temporal patterns and cell-fate decisions

The complexity of ERK's signaling network not only acts as a guarantor of its robustness. Paradoxically, this complexity also difficults its study, especially when it comes to dynamic studies (Bruggeman et al., 2009; Pérez Millán and Turjanski, 2015). The cellular environment comprises a myriad of constantly occurring mechanochemical temporal patterns that convey information to the cell. Thus, cellular responses are increasingly being considered as the integration of cellular history rather than a one-input one-output process (Chen et al., 2012). There is mounting evidence on the effect of the frequency and amplitude of growth factor temporal patterns on cell-fate decisions. It should also be considered that the growth factor itself is bound to the signaling network it activates, which is a determinant for cell-fate decisions (Brüggemann et al., 2021; De Donatis et al., 2008; Freed et al., 2017; Grecco et al., 2011; Moran et al., 1990; Muthuswamy et al., 1999; Stallaert et al., 2018; Stanoev et al., 2018; Wagner et al., 2013). However, in the case of ERK, it has been found that the growth factor, the duration of the ERK-activation, and the frequency of active-ERK peaks determine the outcome of cellular processes (Blüthgen, 2015;

Hiratsuka et al., 2020; Kuchenov et al., 2016; Nguyen et al., 2010; Raina et al., 2022; Ryu et al., 2015). In in-vitro cells, sustained ERK activation led to cell proliferation, whereas short-lived ERK peaks favored cell differentiation (Albeck et al., 2013; Chen et al., 2012; Johnson and Toettcher, 2019; Ryu et al., 2015; Worster et al., 2012). Thus, the same ligand can trigger different cellular processes depending on the ERK temporal pattern it creates.

Additionally, ERK dynamics have also been found to be correlated to cellular shape modifications by mechanical stress . Sustained mechanical stress has been negatively correlated with ERK signal amplitude (Shankaran et al., 2009). However, the frequencies embedded in ERK dynamics have been found indifferent to this condition. Similarly, high cellular densities have also been strongly linked to the shortening of growth-factor-induced-ERK peaks duration and overall have a significant effect on ERK dynamics (Yang et al., 2018). In contrast, acute mechanical stress, such as membrane deformations by neighboring cell protrusions, triggers ERK pulses which drive local protrusions (Johnson and Toettcher, 2019). These local protrusions allow cells to extend their boundaries and sense any possible mechano-chemical signal in their neighborhood. Although the detailed mechanism has not been elucidated, it has been reported that specific frequencies and magnitudes of acute mechanical promoted cell ERK-mediated proliferation (Yan et al., 2012). Regardless of the lack of a consensus on the time scale at which they correspond, cellular morphodynamics and ERK dynamics appear intrinsically connected.

1.6 Protein dynamics tracking by fluorophores

Compared to other biochemical analyses that represent the system's behavior at one specific time-point, live cell imaging with fluorophores gives researchers the ability to record the behavior of the studied complex during the entire experiment. Using the proper sampling time, molecular tracking reveals traits of the signaling dynamics that carry information about the fast-occurring molecular interactions. Moreover, live cell imaging with fluorophores can also convey information regarding the spatial distribution of a molecule. Combining these two traits makes it possible to

construct a distribution of spatiotemporal activity of the cell signaling network component. The selection of the proper fluorophore and its monitoring technique is critical for extracting the desired information from the cell. In this research, we used high-resolution confocal live cell microscopy with a cytoplasmic Förster resonance energy transfer (FRET) sensor.

1.6.1 FRET sensors

Fluorophores are essential to tracking proteins and protein dynamics in living cells. Substances are designed to emit photons with a defined wavelength range after exposure to a specific light frequency. The spectrum of a fluorophore illustrates at which light frequency the energy it absorbs would cause a radiative transition or a non-radiative transition. Non-radiative transitions indicate the absorption of energy that leads to molecular reconfigurations that do not involve the emission of photons. In contrast, the radiative transition describes the absorption of energy that takes the electron of the fluorescent protein to an excited state and the subsequent emission of photons once the electrons relax back to their ground state.

The dynamics of specific proteins, such as ERK, can depend on conditions other than their location. Specifically, ERKs phosphorylation temporal pattern relies on the information of its activity. Thus, sensors that can track this type of conformational change within a molecule convey crucial details of its dynamics. These types of sensors are called FRET sensors. FRET is a radiationless energy transmission phenomenon that occurs between two fluorophores separated by short distances that usually ranges between 1e-9 and 1e-8 m (Marx, 2017). One of the fluorophores acts as an energy donor, and the other as an acceptor. When the electrons of the donor jump from the ground state (So) to an excited state (S2), they transition within pico-seconds to the lowest vibrational state (S1).This movement of electrons is illustrated by its associated Jablonski diagram (Lakowicz, 2006) in Figure 3. At FRET conditions, instead of solely decaying back to So and emitting photons, a portion of the energy of these electrons is transferred to the electrons of the acceptor.

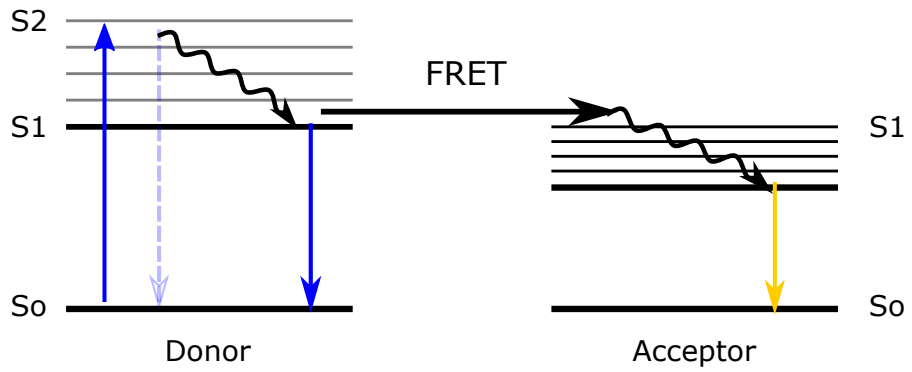

Figure 3. Electron transition during FRET
This Jablonski diagram shows the nonradiative transference of energy by Förster resonance from the electron of the donor fluorophore after coming down from the excited state S2 to the acceptor's electron that reaches the excited stage S1.

The electrons of the acceptor fluorophore achieve excitation, get to the lowest vibrational level (S1), emit light, and subsequently go back to the ground state (So). This dipole-dipole coupling leads to the non-radiative exchange of energy. In summary, when FRET occurs, the donor emits less light, and the equivalent in energy is added to the intensity of the acceptor. FRET sensors composed of two fluorophores are designed to have a "low-FRET" conformation that switches to a "High-FRET" configuration when a specific conformational change, such as phosphorylation, occurs in the target molecule. We used an ERK-substrate-based FRET biosensor equipped with a nuclear export sequence (EKAREV-NES) (Fritz et al., 2013). This EKAREV-NES is a second-generation RAC-1 biosensor composed of 2 fluorophores, a teal fluorescent protein (mTFP1) as a donor and a circular permutation of the fluorophore Venus as an acceptor. A WW binding domain links these fluorophores. The WW domain senses the loading status of a 10-amino acid Cdc25C ERK phosphorylation substrate attached to the acceptor (Figure 4).

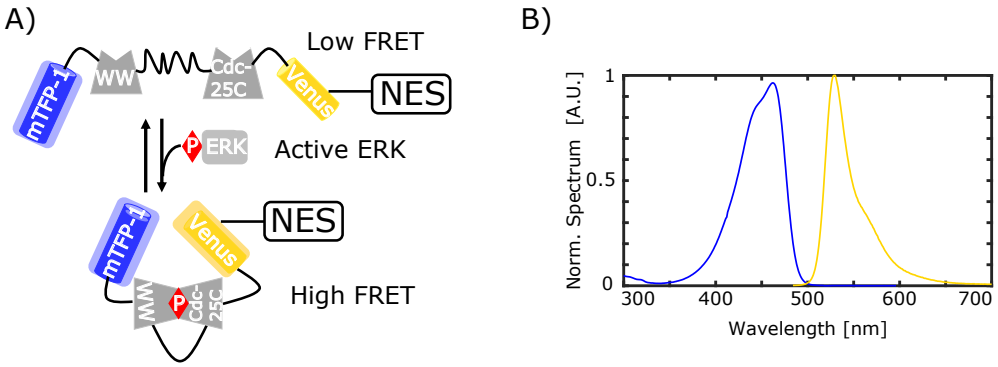

Figure 4. Principles of FRET fluorescence
(A) Schematic representation of the phosphorylated-ERK-substrate-based biosensor EKAREV-2G1. Upon the presence of active ERK, The reconfiguration between the WW (phosphoserine- and phosphothreonine-binding domain) and the Cdc25C (10-amino-acid ERK phosphorylation substrate peptide) induces high FRET between the mTFP1 and the Venus fluorophores. **(B)** Absorption (blue) and emission (orange) spectrum of the EKAREV 2g1 sensor

1.6.2 Confocal microscopy

Confocal microscopy relies on using a light source that passes through a pinhole and excites a specific specimen section. The emitted light passes through another pinhole in an optically conjugated plane placed in front of a light detector. The portion of emitted light that reaches the detector is that produced very close to the focal plane. Despite the fact that the pinhole blocks a significant portion of the emitted light, this technique yields high-resolution images. Consequently, the sensitivity of the detector is crucial for a confocal microscope. When working with two or more fluorophores, in addition to the limitations of the technique, overlapping the spectral distributions of the fluorophores must be considered when designing a microscopy experiment. Accidental photoactivation and bleed-through can be avoided using adequate activation wavelength, detecting range, and filters when available.

Furthermore, increasing the time of light exposure or higher laser intensity can compensate for the emitted light blocked by the pinhole and consequently improve the signal-to-noise ratio. However, cells can suffer from phototoxicity, and fluorophores can be bleached. Fluorophore bleaching leads to a decrease in the signal and reduces

the dynamic range. Naturally, to track fast-occurring molecular events, the frequency of image acquisition should be sufficiently high. Thus, more extended periods of light exposure can also lead to undersampling molecular dynamics.

Once the protocol has been established and the balance between dynamic range, cell viability, and sampling rate has been achieved, the data can be processed. The molecular dynamics recorded as time series can be analyzed to draw a hypothesis from the studied complex and its role within the signaling network.

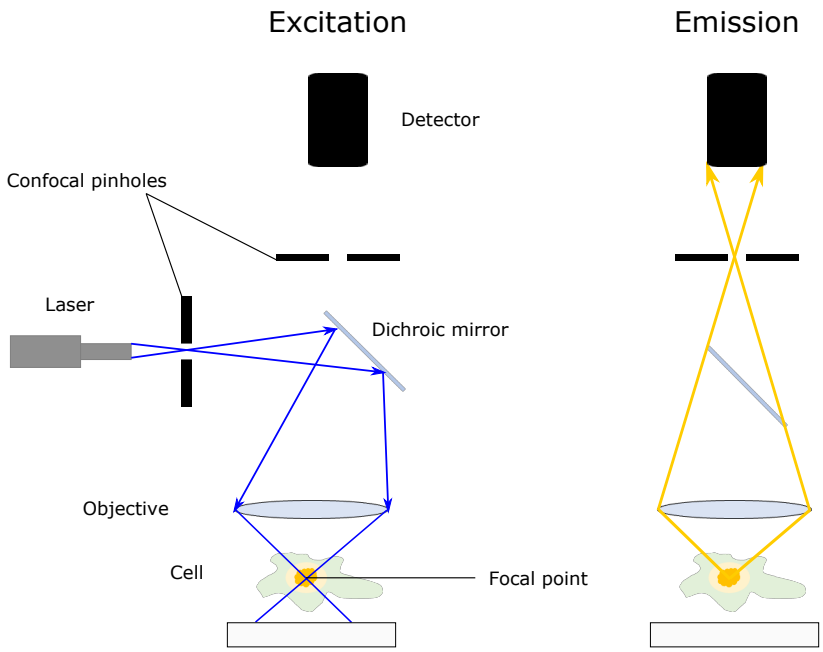

Figure 5. Schematic representation of confocal microscopy
Excitation: the blue light comes from the source (laser) and gets reflected into the cell by the dichroic mirror. The reflected light is aimed at the focal point (inside the cell) by the objective. **Emission:** the light emitted by the sample is conveyed by the dichroic mirror through the focal pinhole. The light from the co-focal plane reaches the detector.

1.7 Quantification of cellular morphodynamics

Cellular morphodynamics is crucial to understanding cellular behavior. The modification of the cellular cytoskeleton is an extension of molecular interactions. It has also been found that there is a relationship between molecular reactions and morphological modifications in cells on minute time scales (Tsukada et al., 2008). This

relationship hints at the fact that cellular morphodynamics and molecular dynamics are inseparable. These morphological modifications were quantified as global cellular deformations that were caused by a global stimulus on the cell signaling network. Intending to prove the connection on a smaller time scale and extend this relationship to continuously occurring communication between the cell signaling network and cellular morphodynamics by monitoring ERK, a central node of the signaling network, we probe a general quantification of the cellular shape. We applied a metric introduced by (Ming-Kuei Hu, 1962). Hu invariant moments have been used to characterize images robustly due to their resistance to geometrically distorted images, their sensitivity to picking up subtle modifications in images, and value consistency for images whose resolution is similar to the one we use in this research (Gornale et al., 2020; Zhang et al., 2021; Zhihu Huang and Jinsong Leng, 2010).

Furthermore, analyzing trends and frequencies embedded in Hu moments has been implemented to identify chronic morphological changes in cellular structures(Gornale et al., 2020; Monge-Alvarez et al., 2019). This research further corroborates the role of Hu invariant moments in quantifying time-dependent tissue modifications. Based on previous research, the resistance to noise is evident in the lower moments. In contrast, the higher moments are more able to distinguish structural modifications in the image (Zhihu Huang and Jinsong Leng, 2010). The Hu moment invariant number 3 has been reported by (Zhihu Huang and Jinsong Leng, 2010) as an optimal reporter to avoid noise. Consequently, we will utilize it as the morphodynamics quantifier because we are focusing on analyzing fast membrane movements that could be related to local-molecular interactions of the signaling network.

1.8 Recurrence analysis

Having exposed the complexity of ERK dynamics, its time dependence, the different time scales embedded within, and its connection to cellular morphodynamics, its sensitivity should also be explored. It has been found that activating one section of the signaling network enhances the sensitivity of other sections to become active (Agell et al., 2002; Fábián et al., 2014; Pinsino et al., 2011). In other words, stimulating

one signaling network would cause another signaling network becomes active by a sub-threshold stimulus present within its neighborhood, propagating the influence of the original stimulus. Considering how signals can permeate through different sections of the signaling network, masking direct interactions between molecules by a global perturbation of the network is expected upon stimulation with growth factors (Bastiaens et al., 2015; Blüthgen and Herzel, 2003; Meyer, 1991; Meyer and Teruel, 2003; Miranti and Brugge, 2002). Moreover, this effect is predicted to progress from one cellular signaling network to another and create an interconnected global cellular signaling network.

Studying such a complex system requires a multidimensional approach. As described in the literature and our previous results, the study of multidimensional recurrences sheds light on otherwise imperceptible events within the constraints of our three-dimensional space perception (Brick et al., 2017; Gavriljuk et al., 2021; Marwan, 2008; Marwan et al., 2007). Recurrences rely on the concept of pattern recognition, and their quantification can be used to characterize cellular processes and reveal connections between dynamic processes. Despite the recent mathematical definition of pattern recognition, recognizing patterns is a natural trait of humans. In humans, observing enough iterations of the same phenomenon, even if the phenomenon is part of a highly dynamic system, leads to predicting a particular event. Patter recognition relies on the perennial repetition of a phenomenon and the consistency in which this phenomenon occurs. That is the basis of recurrence. Recurrence is a concept first described by Poincare in 1890. In his work, Poincare focused on using Newton's law of universal gravitation to describe the motion of three interacting bodies. Poincare noticed that despite the chaotic behavior of the orbits of the celestial bodies, the system recurred to its initial state at Infinitum. However, it was not until 1987 that recurrence visualization and quantification were possible. Eckmann developed recurrence plots as a method to visualize the recurrences present in dynamic systems (Eckmann et al., 1987). Recurrence plots are Boolean matrices that compare the states of a system at different time points. The method relies on using the phase-state trajectories of a system and defining a recurrent state as the event when one state j is approximately at the same state as a former state i. In these matrices, recurrent states are shown with a 1, and non-recurrent states with a 0.

When studying nonlinear dynamics, especially in systems that contain events that occur at different time scales, the use of a recurrence plot is of great help, for it enables researchers to find trends in systems that might appear random and allows the characterization of the system by quantifying their recurrences. However, the difficulty of calculating their associated recurrence plot is reconstructing their phase space. Highly dynamic systems can exhibit a rather complex time dependency. Considering that m variables can define a system x, the contribution of each of the m parameters is contained within x behavior at any given time point t. As shown by Takens (Sauer et al., 1991; Takens, 1981), by comparing the original time series of x against itself a certain number of times (N), with a specific time delay (τ), the dynamics of the m parameters coupled to x can be reconstructed. In this research, we combined the Average mutual information function (AMI) and the false Nearest Neighbor function (FNN) to calculate the time delay (τ) and the number of embedding dimensions (N) (Wallot and Mønster, 2018). By guaranteeing Takens' theorem, the reconstructed attractor of x and its theoretical attractor is recognized as the representation of the same dynamical system.

The definition of a recurrent state depends on the method for measuring the distance between the states present in the space phase and the threshold for the distance (Marwan et al., 2007). The following expression defines the recurrence plot:

$$M_{i,j} = \theta(\varepsilon - \left|x_i - x_j\right|)$$

The distance between two states can be expressed as the L1 norm, the Euclidean norm of the L-infinity norm. We use the Euclidean norm to calculate the distances in the system because of its balanced neighbor-detecting properties. The detecting areas of the three norms are presented in Figure 6.

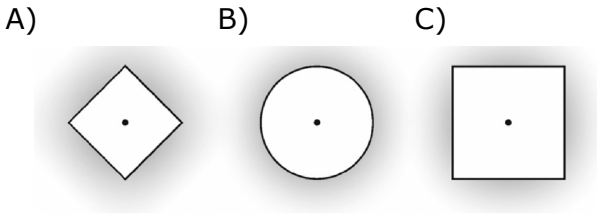

Figure 6. Three different definitions of neighborhoods:
Two-dimensional representation of norms used for the calculations of recurrence plots with the same radius around a state (dot). **(A)** L1 norm, **(B)** Euclidean norm, **(C)** L-infinity norm. Adapted and reprinted from (Marwan et al., 2007) with permission from Elsevier, Copyright © 2007.

The selection of the threshold ε is what ultimately transforms the matrix of distances into the quantifiable recurrence plot. A very small e increases the number of false negative errors and does not yield enough recurrence states to characterize the system. On the contrary, a very big ε increases the number of false positive errors and faulty records the systems recurrences. Although the selection of the value of ε is empirical, there are suggestions regarding its maximal value. In this research, we estimated ε as the standard deviation of the trajectories of the time-series reconstructed space state. As suggested by (Marwan et al., 2007), we corroborated that with this ε , the number of recurrent states did not exceed 10% of the total states of the system.

As an example of the recurrence characterization, four systems with different dynamics with their corresponding recurrence plots and space states can be observed below.

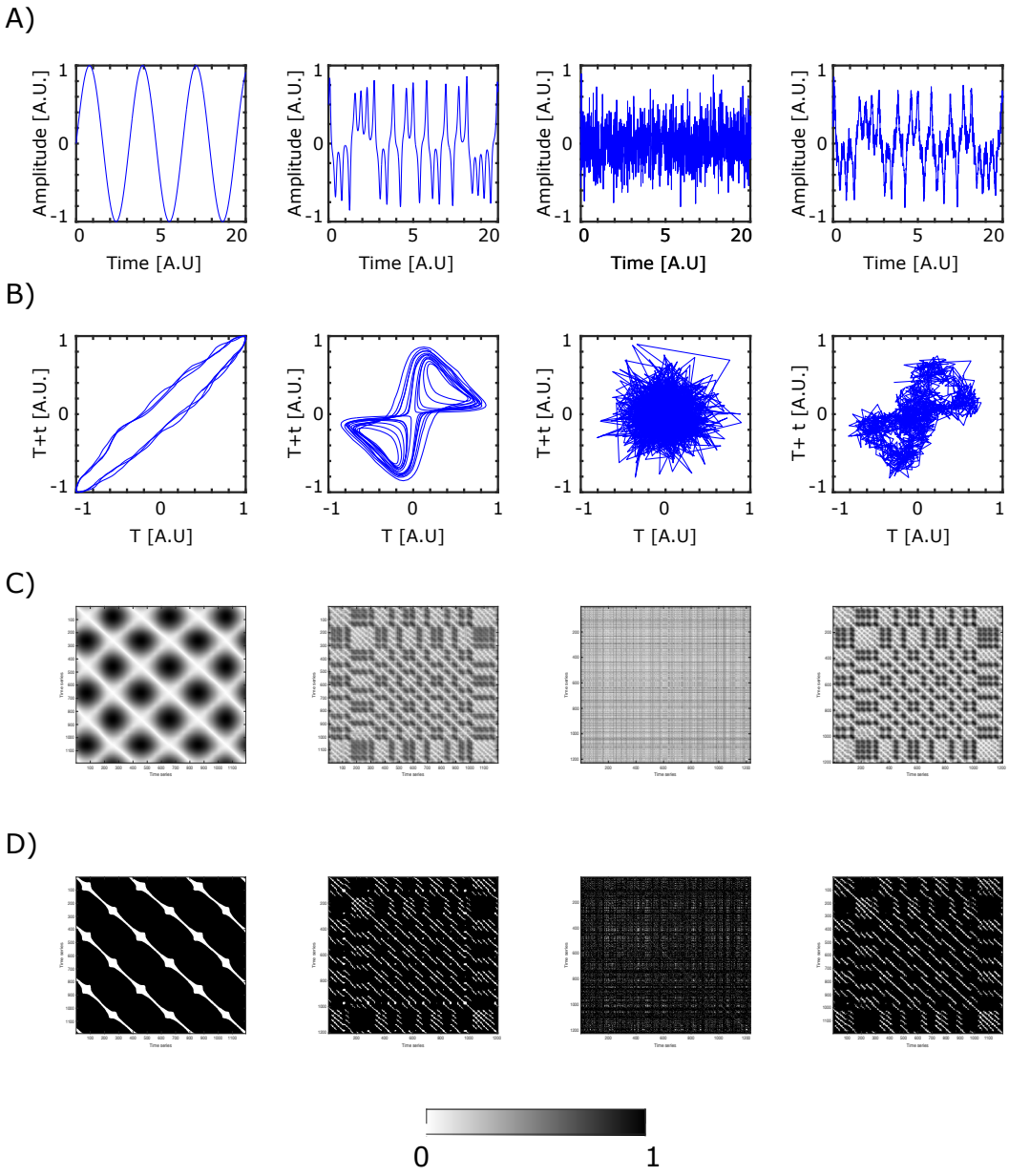

Figure 7. Dynamic characterization of 4 different systems
(A) Time series of, from left to right: a sine function, the x component of the Lorenz chaotic attractor, white noise, and the x component of the Lorenz chaotic attractor with white noise
(B) 2-D projections of the corresponding space states of the systems presented above.
(C) Unthresholded versions of the recurrence plot of each system, using the euclidean norm.
(D) Thresholded recurrence plots of each system using an e that guarantees a maximal recurrence rate of 10% of all the system's states
On panels **(C)** and **(D)**, “white” represents high recurrence.

As we move diagonally on the recurrence plot, we move in time for a specific system state. Thus, diagonally connected recurrences are a sign of the deterministic behavior of the system. Conversely, vertical distances between diagonal lines correspond to periods of oscillation. The recurrence plot of the white noise consists of disconnected single black points. As suggested by Eckmann (Eckmann et al., 1987), isolated recurrent states imply randomness and shorter diagonal lines, a less predictable system. In order to quantify the dynamic behavior of each system, measures based on the diagonal lines were developed. We focused on the maximal length of the diagonal lines, which is a measure of the persistence of a recurrence in the system, and the Shannon entropy of the diagonal lines' length distribution which is a measure of the diversity of recurrences in the system.

An extension of RP was developed to study the dependencies between two systems x and y (Brick et al., 2017; Marwan and Kurths, 2002; Zbilut et al., 1998).These are called cross-recurrence plots because they are considered a generalized linear cross-correlation between two time series. The cross-recurrence matrix is defined as follows:

$$M_{i,j} = \theta(\varepsilon - \left|x_i - y_j\right|)$$

As mentioned above, to calculate the cross-recurrence matrix of a system it is necessary to reconstruct its phase space. It should be considered that if the time-delay embedding parameters calculated for both systems differ, the higher embedding should be chosen. In case the time series differ in the order of magnitude, they should be normalized before calculating the cross-recurrence matrix. Contrary to the recurrence matrix, the main diagonal is not necessarily one. However, all the above statements regarding the diagonal lines and recurrence quantifications apply to cross-recurrence plots.

1.9 Objectives

In this thesis, we focused on revealing the presence of traits of cellular communication in ERK dynamics and cellular morphodynamics. By monitoring the ERK response in cells, we found an effect of the cellular environment on the ERK activation pattern. However, considering cellular communication as a continuous process, we proceeded to elucidate if this effect was limited to ERK's activation process or if it extended to its dynamics. We hypothesized that any information relevant to the cellular environment could be masked by global stimulation, such as exposure to a growth factor. Thus, we extracted the high-frequency components embedded in ERK dynamics and cellular morphodynamics. We used recurrence analysis to find patterns in ERK dynamics and cellular morphodynamics prior to growth factor stimulation. We found that these patterns were congruent, thus suggesting a continuous relationship between ERK dynamics and cellular morphodynamics. Finally, we compared the recurrences between neighboring and non-neighboring cells. We found that neighboring cells had a higher level of synchronization in ERK dynamics and cellular morphodynamics at specific conditions than non-neighboring cells. Stimulation with low concentrations of EGF proved to be an effective channel for neighboring cells to communicate.

2 Materials and methods

2.1 Cell culture, transfection, and growth factor stimulation

MCF-7 cells (ATCC, HTB-22) were grown in 8-well chambered glass slides (Lab-Tek, Thermo-Fisher Scientific, Waltham, United States) in DMEM (Dulbecco's modified Eagle's medium, Sigma Aldrich), enriched with 10% FBS (Fetal bovine serum), 10 mM L-glutamine and 1% non-essential amino acids, at 37 °C under a 5% CO2 atmosphere. According to the manufacturer's protocol, cells were transfected 24h prior to growth factor stimulation experiments with Fugene6 (Roche Diagnostics, Mannheim, Germany). Cells were serum-starved in DMEM without phenol red for at least two hours prior to growth factor exposition and subsequently stimulated with EGF or HRG-b at a final concentration of either 20 or 100 ng/mL. Erk Inhibition in cells was induced by 10um PD0325901 exposure. Erlotinib treatment consisted establishing a concentration of 10 μM of the EGFR-inhibitor immediately prior to imaging. For growth factor stimulation and subsequent growth-factor-induced response inhibition, the following reagents were used: EGF (Peprotech, Cat#AF-100-15 Hamburg, Germany) diluted to a concentration of 250 ng/mL in PBS + 0.1% BSA and stored at -20°C; HRG-b (Merck Millipore, Cat#01-201) diluted to a concentration of 250 ng/mL in PBS + 0.1% BSA, stored at -20°C; PD0325901 (Cell Signaling Technology, Catalog - 800153) diluted to a concentration of 1mM in DMSO and stored at -20°C. Erlotinib (Selleckchem, Catalog – No S7786) diluted to a concentration of 10mM in DMSO and stored at -20°C.

2.2 Plasmid

The plasmid encoding the EKAREV-NES, ERK activity reporter (EKAR2G1), was a gift from Olivier Pertz (Addgene plasmid #39835; http://n2t.net/addgene:39835; RRID: Addgene_39835)(Fritz et al., 2013).

2.3 Confocal microscopy

The images were taken with a Leica TCS SP8 DMI800 confocal microscopy (Leica microsystems, Wetzlar, Germany) equipped with: an incubator (Life Imaging Services, Switzerland) maintained at 37°C, a CO2 compressor maintained at 5%, and an HC PL APO 63x/1.2NA motCORR water objective (Leica microsystems, Wetzlar, Germany). The donor protein of the EKAREV2G1 construct (mTFP1) was excited with a 442 nm diode laser. The emitted light was measured with HyD SMD detectors for the donor channel: mTFP1 (460-508 nm) and the acceptor channel: Venus (525 – 575 nm). The pinhole was set at 5.8 airy units, and 12-bit 512x512 images were taken sequentially, between lines, with a 2x frame averaging at a rate of 1 image per 3.108 seconds.

2.4 Cell masking

The average background fluorescence was obtained from a cell-free area and subtracted from all images. The masks of the cells were modelled in FIJI (https://fiji.sc/) by applying a Gaussian filter (sigma=2.0) and thresholding the images accordingly. In order to obtain the cytoplasm section of the mask, an independent mask of the nucleus was made following the same processing than for the cell mask with a different threshold. The mask of the nucleus was subtracted from the full-cell mask and the resulting in the cytoplasm mask of the cells.

2.5 ERK's activity quantification

The algorithm used to read the images based on the masks and the subsequent calculation of the ERK activity was developed in the version 9.10.0.1649659 (R2021a) Update:1 of Matlab (https://www.mathworks.com). The nucleus-excluded masks were used to analyze the donor and acceptor time-series images. The ERK activity was calculated as the ratio of the average measured fluorescence per mask of the acceptor. At the same time, the donor is excited over the average measured fluorescence per mask of the donor while the donor is excited (IA/ID FRET).

2.6 Cellular morphodynamics quantification

The metric to quantify cellular morphodynamics, based on the full-cell masks, was the third Hu invariant moment. The algorithms used to calculate the Hu invariant moment were developed in the version 9.10.0.1649659 (R2021a) Update:1 of Matlab (https://www.mathworks.com). The Hu moment used in this research is the third rotation invariant moment defined in (Ming-Kuei Hu, 1962). First, the coordinate system is normalized:

$$\hat{x} = x - m_x$$
$$\hat{y} = y - m_y$$

x and y are the coordinates of each pixel that belongs to a cell mask. $\hat{x}$ and $\hat{y}$ are the normalized coordinates for each pixel present in a cell mask. m_x and m_y represent the x and y coordinates of the cell mask center of mass. The corresponding central moments M_{pq} are calculated as follows:

$$M_{pq} = \sum_x \sum_y (x - \hat{x})^p (y - \hat{y})^q f(x, y)$$

Where p and q are whole non-negative numbers between 0 and 3. And $f(x, y)$ is a boolean matrix with value 1 for pixels that belong to the cell mask. Finally, the Hu moment was calculated according to the following equation:

$$Hu_3 = (M_{30} - 3M_{12})^2 + (M_{03} - 3M_{21})^2$$

2.7 High frequency component extraction

The main trend associated to each time series was calculated using the built-in function “movmean” in the version 9.10.0.1739362 (R2021a) Update:5 of Matlab (https://www.mathworks.com). Moving means were calculated using a sliding window

of 7 neighboring elements. The means were subtracted from the original time series, and the resulting values were reported as the high frequency components and subsequently used for recurrence analysis.

2.8 Recurrence plots

The algorithm used calculate the recurrence plots, and its quantification was developed in the version 9.10.0.1649659 (R2021a) Update:1 of Matlab (https://www.mathworks.com). In order to guarantee Takens theorem (Sauer et al., 1991; Takens, 1981), the average mutual information (AMI), and the false nearest neighbor were calculated to estimate the time delay (Fraser and Swinney, 1986; Kantz and Schreiber, 2003; Wallot and Mønster, 2018) and the minimal dimensional embedding. The first local minimum of the AMI function was used as the time delay; the corresponding function is denoted as follows:

$$AMI(\tau) = \sum_{x(t_i),x(t_i+\tau)} P(x(t_i), x(t_i+\tau)) log_2 \left[\frac{P(x(t_i), x(t_i+\tau))}{P(x(t_i))P(x(t_i+\tau))} \right]$$

P denotes the probability of a value at a time point t_i of the time-series x of belonging to the same bin as the value of the time-series x at a delayed time point $t_i + \tau$. The minimal embedding dimension was calculated by minimizing the percentage of false nearest-neighbors (pFNN) method (Cao, 1997; Kennel et al., 1992; Wallot and Mønster, 2018). The criteria to rule the nearest neighbor in a time series as false is given by the following expression

$$R(t_i) = \frac{|x(t_i + n\tau) - x^{NN}(t_i + n\tau)|}{\left\| \sum_{n=0}^{d-1} [x(t_i + n\tau) - x^{NN}(t_i + n\tau)] \right\|} > 10$$

$$pFNN = \frac{\sum R(t_i)}{TNN}$$

TNN is the total amount of nearest neighbors in all the system's dimensions. x is the n embedded $t_i + \tau$ delayed time series. x^{NN} is the n dimension embedded τ delayed nearest neighbor. d is the maximal arbitrary dimension for the optimal embedding calculation.

The recurrence plot was calculated as the matrix of the Euclidian distances according to the formula:

$$M_{i,j} = \theta(\varepsilon - \left|x_i - x_j\right|)$$

$$\left|x_i - x_j\right| = \sqrt{(x_i - x_j)^2}$$

Where: $M_{i,j}$ is the element of the column j and the row i of the matrix M, θ is the Heaviside function, ε is the thresholding value, and x is the n-dimension-embedded τ delayed vector of the time series to study (ERK dynamics or cellular morphodynamics).

2.8.1 Cross recurrence plots

Similarly, the cross-recurrence plot was calculated as the matrix of the Euclidian distances according to the formula:

$$M_{i,j} = \theta(\varepsilon - \left|x_i - y_j\right|)$$

Where: $M_{i,j}$ is the element of the column j and the row i of the matrix M, θ is the Heaviside function, ε is the thresholding value, x and y are the n-dimension-embedded τ delayed vector of the ERK activity time series and cellular morphodynamics time series respectively. In contrast, for comparing neighboring cells, x and y, were simultaneously either ERK activity or cellular morphodynamics.The recurrence, and cross-recurrence, plots were thresholded according to (Marwan, 2008; Marwan et al., 2007). The cut-off value was set to the standard deviation of the space state distances when said values is smaller or equal to the 10% value of the

cumulative density function of the Euclidean distance distribution. Otherwise, the cut-off value was set to the distance that represents the 10% value of the cumulative density function of the Euclidean distance distribution.

2.9 Recurrence quantification

The maximal length of the diagonally connected recurrences was measured, and the distribution of diagonal recurrence line lengths was recorded. The distribution of recurrence lengths was used to calculate its associated Shannon's entropy (C. E. Shannon, 1948) which was used to quantify the diversity of recurrent states present in the time series (Marwan, 2008; Marwan et al., 2007; Webber, n.d.)

$$S_M = -\sum_{i=1}^{n} (p(l_i) log\ (p(l_i)))$$

Where S is the entropy associated to the recurrence plot M. p is the probability distribution of the recurrence lines l_i.

2.10 ERK's activity kinetic parameter

The algorithms to calculate the response time of the ERK activation, and the cells response delay were developed in the version 9.10.0.1649659 (R2021a) Update:1 of Matlab (https://www.mathworks.com). The time-series corresponding to the ratiometric IA/ID FRET (ERK activity quantification) signal of the EKAREV sensor was smoothed using a Savitzky-Golay ("sgolayfilt"). The time-series speed was calculated using a 5-point numerical derivative of the smoothed ERK activity time, and its maximum positive value reported. The reaction time was defined as the first time point when 10 out of the following 12 values of the time-series derivative showed non negative values. The stabilization time was defined as the fifth time point after the smoothed ERK activity time series' derivative reached a non-positive value after reaching its maximum.

2.11 Statistical analysis

The statistical inference related values were calculated using built-in functions (“kstest”, “mean”,” median”, “std”, “ranksum”) in the version 9.10.0.1649659 (R2021a) Update:1 of Matlab (https://www.mathworks.com). With a cut-off value of alpha=0.01, the One-sample Kolmogorov-Smirnov algorithm was used to evaluate the normality of the calculated distributions. The non-normal distributions were compared using the two-tailed Wilcox rank sum test, and their corresponding p-values presented. The normal distributions were compared using a one-way ANOVA test, and their corresponding values presented. The distributions average values results are expressed as mean ± SD.

2.12 Monotonal relationship estimation

The relationship between two distributions was calculated using the built-in function (“corr”) in the version 9.10.0.1649659 (R2021a) Update:1 of Matlab (https://www.mathworks.com). To assets a non-linear relationship we used the Spearman correlation coefficient [-1: decreasing monotonic,1: increasing monotonic]. To probe for a linear relationship, we used the Pearson correlation coefficient [-1: decreasing linear,1: increasing linear]. For both correlations we reported the p-value (ANOVA) associated to testing hypothesis of no correlation against the alternative hypothesis of significant correlation.

2.13 Distance between neighboring cells

The distance between neighboring cells was calculated applying the definition of the Euclidian distance between the centroids of the cellular masks in the version 9.10.0.1739362 (R2021a) Update:5 of Matlab (https://www.mathworks.com).

3 Results

In order to study ERK dynamics and cellular morphodynamics and their response to either EGF or HRG stimulation, we used MCF-7 cells. These are immortalized human breast cancer cells that express EGFR, and ErbB2/3 receptors, which have been reported to show ligand-specific ERK activity and morphodynamics responses.

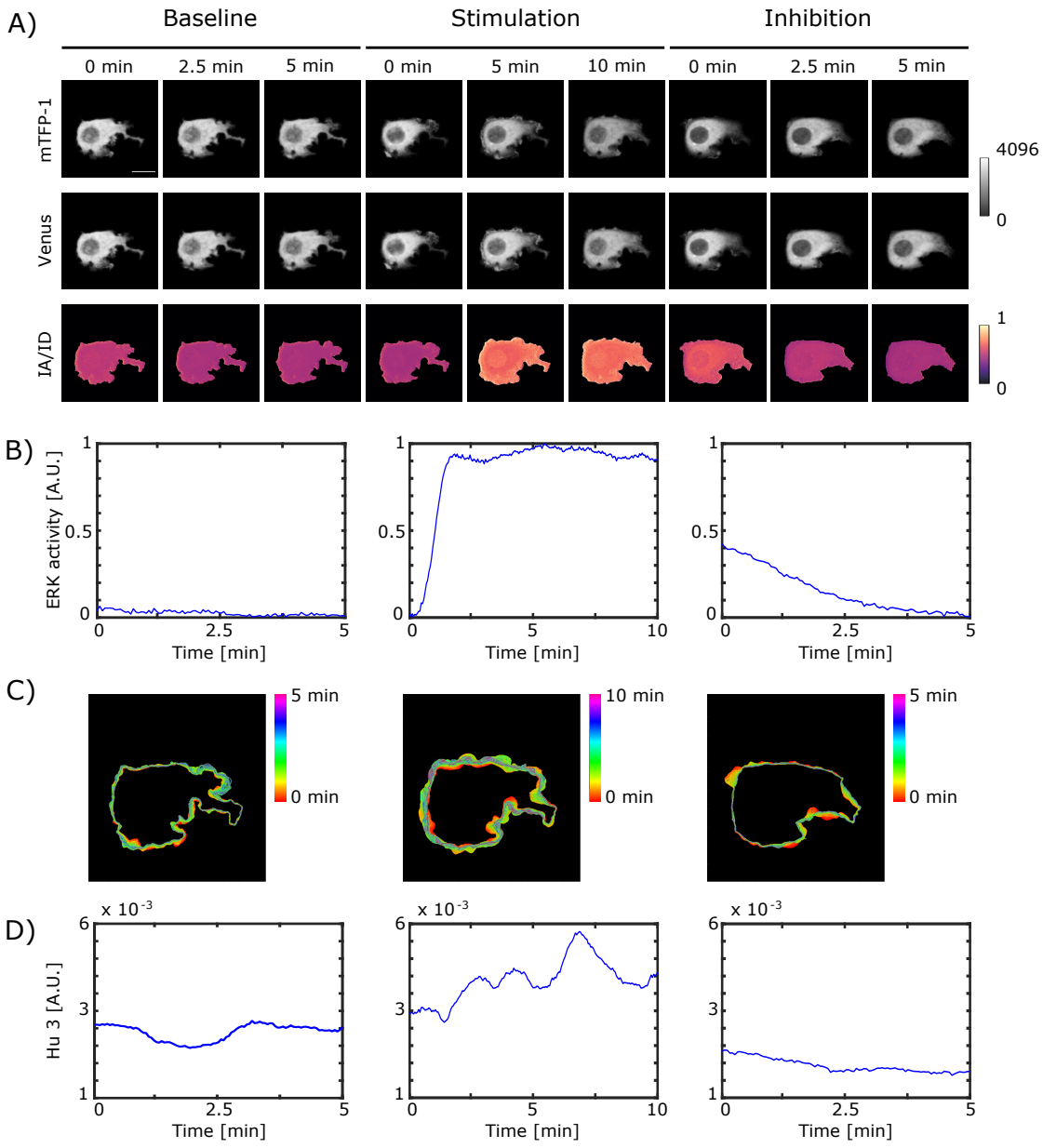

Figure 8. Quantification of ERK activity and cellular Morphodynamics
(A) Exemplary fluorescence images of an MCF-7 cell transfected with the EKAREV-2G1 sensor; prior to growth factor stimulation (Baseline – 2.5 min intervals), upon stimulation with 20ng/mL of EGF (stimulation – 5 min intervals), and after exposure to a 10uM concentration of PD0325901 (inhibition – 2.5 min intervals). Top row: fluorescence emitted by the donor after donor excitation (ID). Middle row: fluorescence emitted by the acceptor after donor excitation (IA). Bottom row: the ratiometric image of the quotient between IA and ID. **(B)** ERK activity time series of the cell presented in panel (A), quantified as the IA/ID ration left: "Baseline," center: "Stimulation," right: "Inhibition." **(C)** Exemplary contour traces of the cell presented in panel (A). Each contour represents one of 97 frames (3.108 s interval) for the "Baseline" condition, one of 194 frames for the "Stimulation" condition, and one of 87 frames for the "Inhibition condition." **(D)** Cellular morphodynamics quantified as the third Hu invariant moment of the cell presented in panel (A). Left: "Baseline," center: "Stimulation," right: "Inhibition."

As shown in Figure 8, cells before stimulation show limited membrane activity and ERK phosphorylation. It can be observed on the stable value of the morphodynamics activity and steadily low ERK activity. After growth factor exposure, the cellular membrane is visibly extended, and the apparition of filopodia and lamellipodia is appreciable. Similarly, ERK activity steeply increases and stabilizes after reaching its peak. Inhibition of MEK induces an indirect inhibition of ERK. During this stage, ERK activity slowly but continuously decreases. Simultaneously, exposure to the MEK inhibitor causes retraction of the cellular membrane and a diminishment of its activity. The experimental groups are conformed by n=35 cells exposed to 100mg/mL of EGF, n=24 cells exposed to 20ng/mL of EGF, n=22 cells exposed to 100 ng/mL of HRG, and n=26 cells exposed to 20ng/mL of HRG. The Baseline group comprises all the cells imaged prior to growth factor stimulation n=107 cells.Following our definition of neighboring cells, detailed in the “Methods” section, the group of cells stimulated with 100ng/mL of EGF comprises n=31 neighboring cells, the group stimulated with 20ng/mL of EGF n=19, the group stimulated with 100ng/mL of HRG n=23, and the group stimulated with 20ng/mL of HRG n=14.

3.1 Effect of cellular local environment on ERK’s response to growth factor stimulation

By overlaying the ERK response curves of all the experimental conditions, a visual trend regarding the speed with which ERK activity rises, the time it takes cells

to respond to a growth factor stimulus, and consequently, the time after which cells show a stabilized ERK activity became apparent.

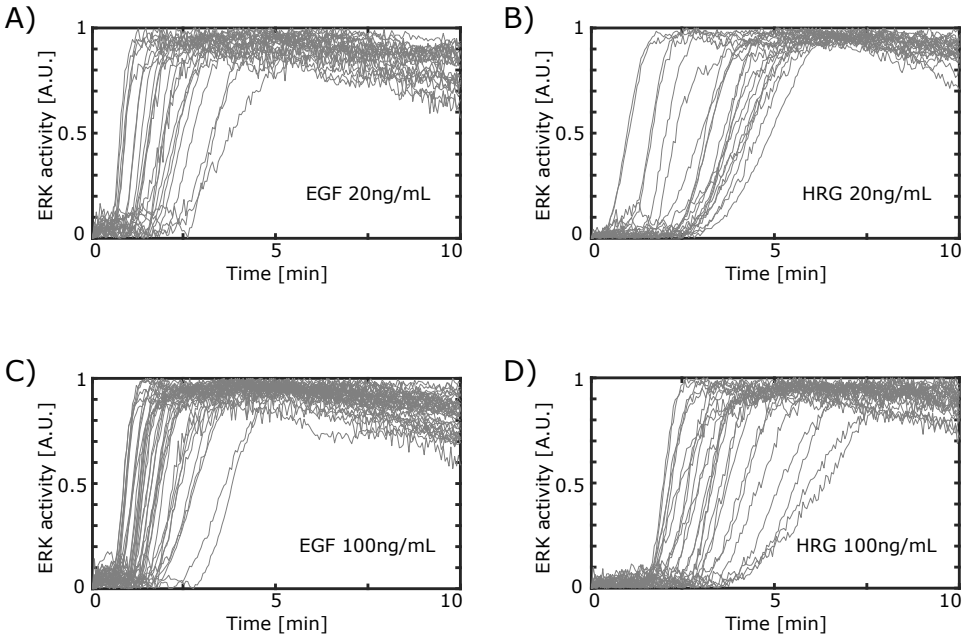

Figure 9. Overlaid ERK responses to different experimental conditions
(A) Stimulation with 20ng/mL of EGF. **(B)** Stimulation with 20ng/mL of HRG. **(C)** Stimulation with 100ng/mL of EGF. **(D)** Stimulation with 100ng/mL of HRG

Thus, we defined the three following kinetic parameters to characterize ERK activity behavior.

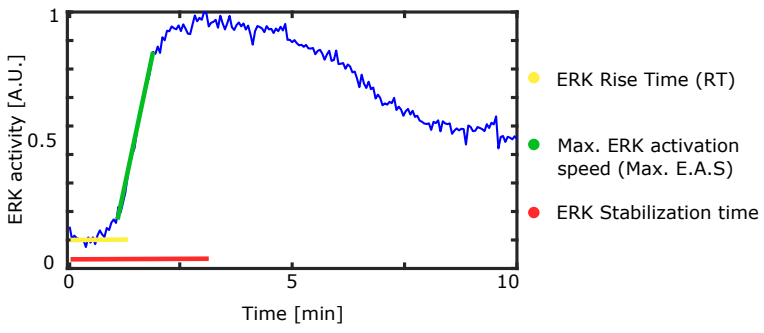

Figure 10. Kinetic parameters for ERK characterization
Exemplary ERK activity time series (blue line) with the graphic representation of the definitions of the "Rise Time" (yellow), "Max. ERK activation speed" (green), and the "ERK stabilization time" (red).

The average values for the maximal ERK activation speed showed no concentration dependency. However, stimulation with EGF yielded a higher maximal ERK activation speed than HRG.

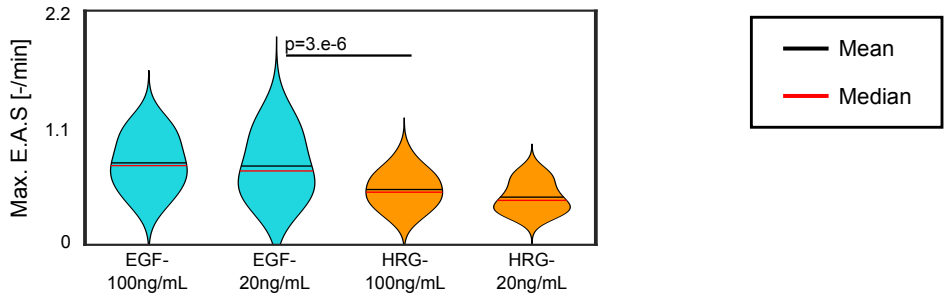

Figure 11. Max. ERK activation speed comparison between EGF and HRG stimulated cells
Violin distributions for the Max. E.A.S [-/min] of cells stimulated with either 20ng/mL or 100 ng/mL of either EGF (cyan) or HRG (orange).

Table 1. Max. ERK activation speed average values for growth factor stimulated cells

Max. E.A.S [-/min]	EGF 100 ng/mL	EGF 20 ng/mL	HRG 100 ng/mL	HRG 20 ng/mL
Mean +/- SD	1.22 +/- 0.40	1.18 +/- 0.48	0.83 +/-0.27	0.71+/-0.23

Similarly, despite the fact that EGF-stimulated cells showed a shorter ERK rise time than HRG-stimulated cells, there was no apparent difference regarding the concentration of the corresponding growth factor.

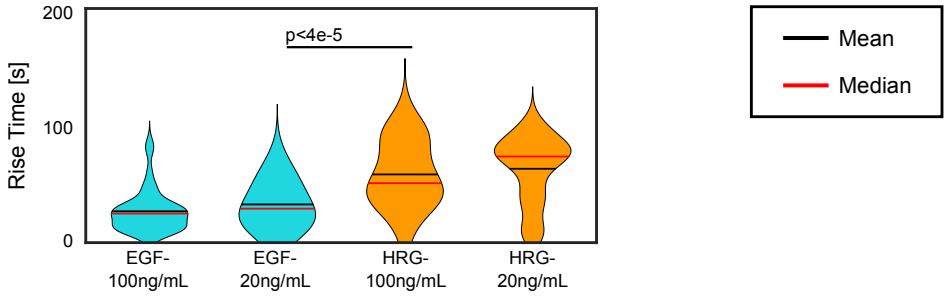

Figure 12. Rise Time comparison between EGF and HRG stimulated cells.
Violin distributions for the RT [s] of cells stimulated with either 20ng/mL or 100 ng/mL of either EGF (cyan) or HRG (orange).

Table 2. Rise Time average values for growth factor stimulated cells.

R.T [s]	EGF 100 ng/mL	EGF 20 ng/mL	HRG 100 ng/mL	HRG 20 ng/mL
Mean +/- SD	40.16 +/- 26.57	48.95 +/- 29.98	87.38 +/-42 96	94.65+/-43.19

Consequently, the stabilization time was calculated to be longer on HRG-stimulated cells than in EGF cells without a significant difference regarding the concentration used for the stimulus.

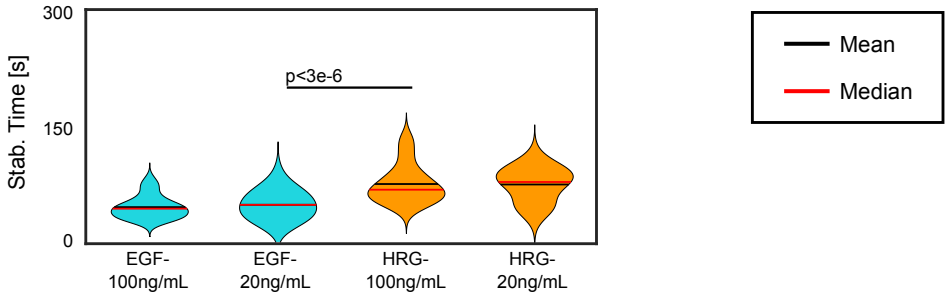

Figure 13. Stabilization time comparison between EGF and HRG stimulated cells. Violin distributions for the Stab. Time [s] of cells stimulated with either 20ng/mL or 100 ng/mL of either EGF (cyan) or HRG (orange).

Table 3. Stabilization time average values for growth factor stimulated cells.

Stab. Time [s]	EGF 100 ng/mL	EGF 20 ng/mL	HRG 100 ng/mL	HRG 20 ng/mL
Mean +/- SD	58.64 +/- 19.36	62.58 +/- 22.59	96.77 +/-31.94	97.57+/-27.93

Interestingly, by doing a correlation test, we found a clear relationship between the Maximal ERK activation speed and the ERK rise time for EGF-stimulated cells and cells stimulated with 20ng/mL of HRG. Furthermore, this relationship yields more statistically significant (Pearson's r and Spearman's ρ) and higher R^2 values for the lower concentrations of growth factor stimulation.

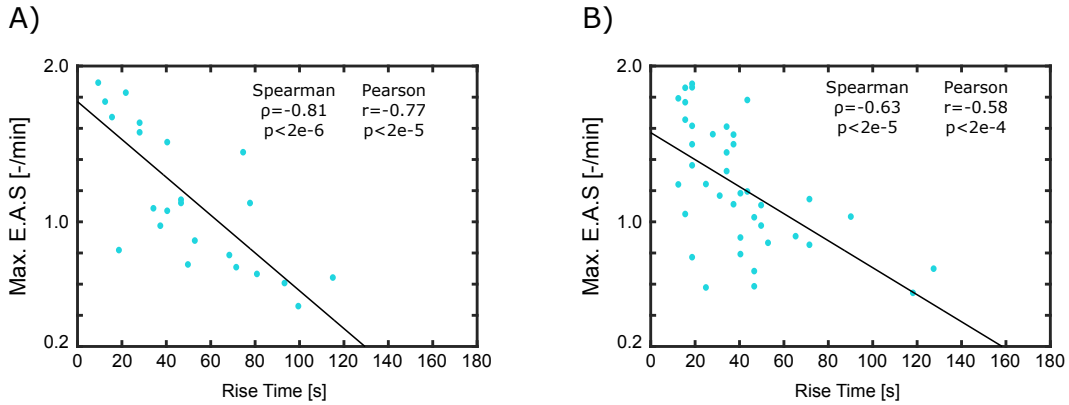

Figure 14. Relationship between Maximal ERK activation speed and Rise Time for EGF-stimulated cells

(A) Values were obtained from the time series of cells stimulated with 20ng/mL of EGF. The p values presented reject the null hypothesis of the distributions not being linearly dependent (Pearson) nor non-linearly dependent (Spearman). **(B)** Values were obtained from the time series of cells stimulated with 100ng/mL of EGF. The p values presented reject the null hypothesis of the distributions not being linearly dependent (Pearson) nor non-linearly dependent (Spearman).

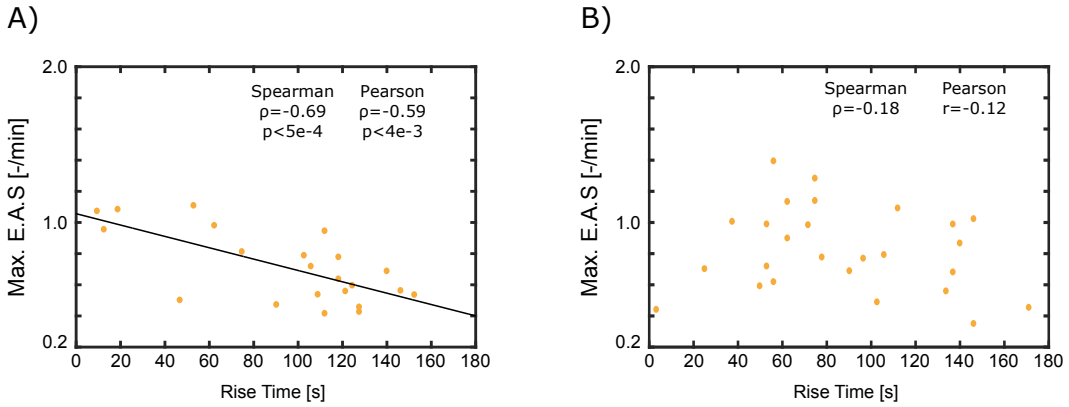

Figure 15. Relationship between Maximal ERK activation speed and Rise Time for HRG-stimulated cells

(A) Values were obtained from the time series of cells stimulated with 20ng/mL of HRG. The p values presented reject the null hypothesis of the distributions not being linearly dependent (Pearson) nor non-linearly dependent (Spearman). **(B)** Values were obtained from the time series of cells stimulated with 100ng/mL of HRG. No significant relationship between the distributions was found.

Table 4. Linear fitting parameters and goodness of fit for the "Max. E.A.S.= m (R.T.) + b" trend lines

Experimental condition	m	b	R^2
EGF 100 ng/mL	-0.00866	1.572	0.33
EGF 20 ng/mL	-0.01214	1.771	0.59
HRG 100 ng/mL	-	-	-
HRG 20 ng/mL	-0.00364	1.056	0.47

In order to probe for the effect of the local environment over ERK's rise time and the maximal ERK activation speed, we calculated the difference between these values for neighboring and non-neighboring cells.

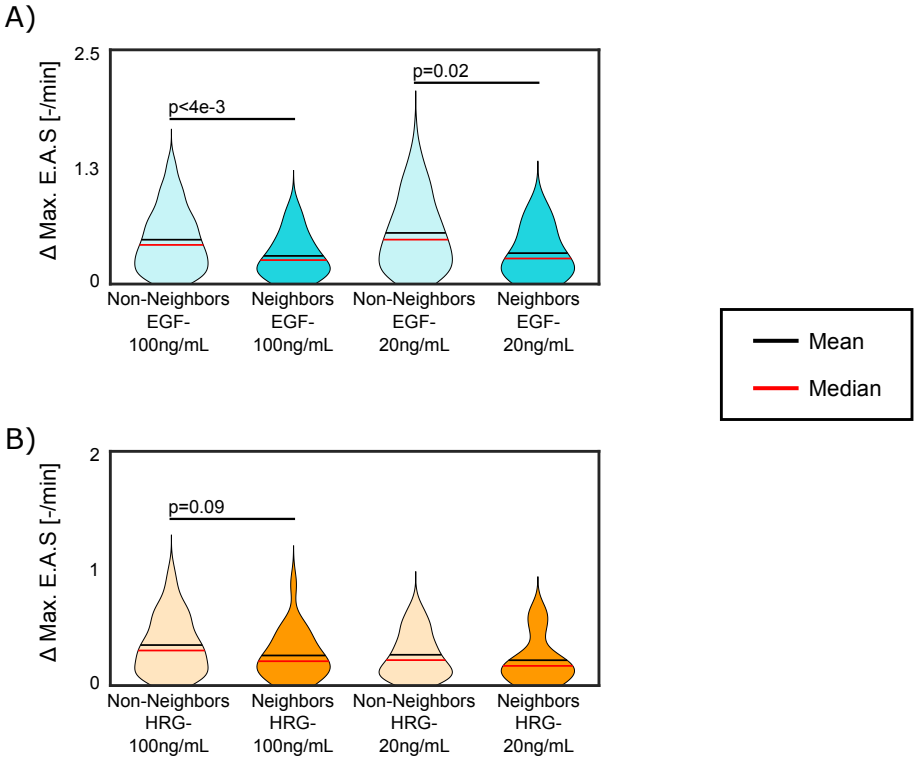

Figure 16. Comparison of the Max. ERK activation speed difference between neighboring and non-neighboring cells.
(A) Distributions calculated from the Max. EAS of non-neighboring cells (light cyan) and neighboring cells (cyan) stimulated with either 20ng/mL or 100ng/mL of EGF. **(B)** Distributions calculated from the Max. EAS of non-neighboring cells (light orange) and neighboring cells (orange) stimulated with either 20ng/mL or 100ng/mL of HRG

Table 5. Average difference in Max. ERK activation speed between neighboring and (*) non-neighboring cells

ΔMax E.A.S [-/min]	EGF 100 ng/mL *	EGF 100 ng/mL	EGF 20 ng/mL *	EGF 20 ng/mL	HRG 100 ng/mL *	HRG100 ng/mL	HRG 20 ng/mL *	HRG 20 ng/mL
Mean +/- SD	0.47+/- 0.33	0.30 +/- 0.22	0.55 +/- 0.39	0.33+/- 0.26	0.35+/- 0.25	0.27 +/- 0.20	0.26+/- 0.19	0.22+/- 0.20

As shown in Figure 16 and table xx, in neighboring cells, the values for ERK activation speed were more similar for neighboring cells than for non-neighboring cells. However, a more significant effect was observed on EGF-stimulated cells. Compared to their non-neighboring counterparts, neighboring cells stimulated with 100ng/mL and 20ng/mL of EGF had 36% and 40% more similar speeds.

A similar trend was observed when comparing the rise time between neighboring and non-neighboring cells. Under all conditions, all neighboring cells showed a higher synchronization on their ERK rise times than their non-neighboring counterparts.

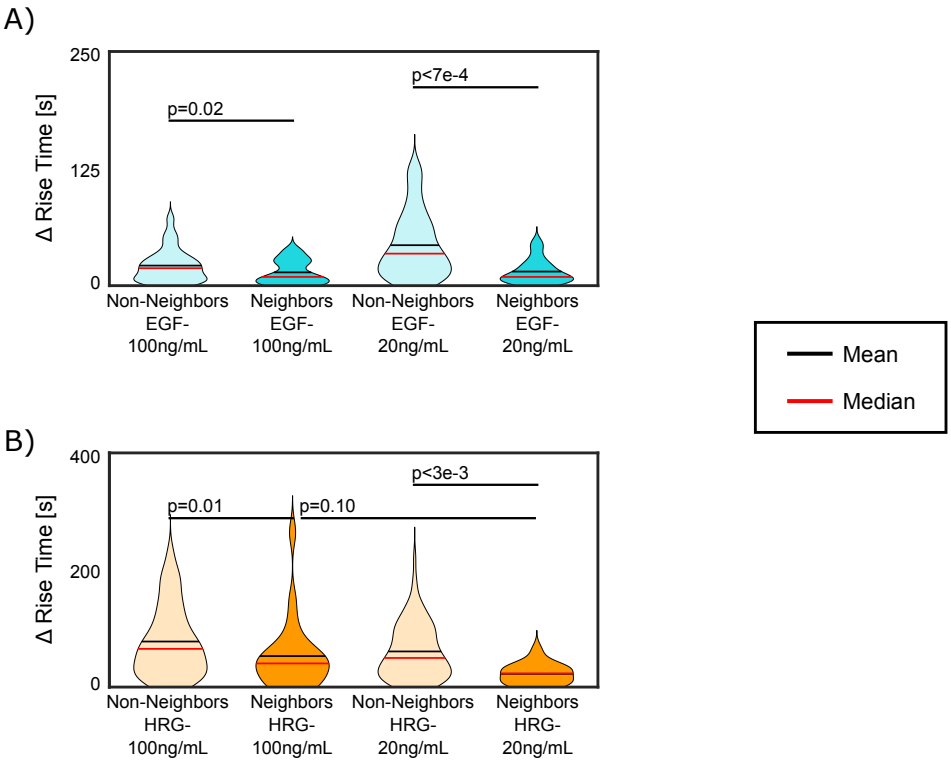

Figure 17. Comparison of the Rise Time difference between neighboring and non-neighboring cells.
(A) Distributions were calculated from the RT of non-neighboring cells (light cyan), and neighboring cells (cyan) stimulated with either 20ng/mL or 100ng/mL of EGF. **(B)** Distributions were calculated from the RT of non-neighboring cells (light orange), and neighboring cells (orange) stimulated with either 20ng/mL or 100ng/mL of HRG.

Table 6. Average difference in Rise time between neighboring and (*) non-neighboring cells

Δ RT [s]	EGF 100 ng/mL *	EGF 100 ng/mL	EGF 20 ng/mL *	EGF 20 ng/mL	HRG 100 ng/mL *	HRG100 ng/mL	HRG 20 ng/mL *	HRG 20 ng/mL
Mean +/- SD	21.43+/- 17.42	14.19+/ 12.46	43.20 +/- 34.26	15.05+/- 12.87	77.81+/- 59.29	52.97+/- 58.97	60.86+/- 46.36	22.64+/- 17.09

However, more similar ERK Rise Times were achieved under the neighboring condition after being stimulated with 20ng/mL of either EGF or HRG. Compared to their non-neighboring counterparts, both groups showed a relative reduction of over 60% in the difference in ERK rise times.

3.2 ERK dynamics recurrences strengthening upon growth factor stimulation

In order to study the local occurring ERK recurrences, we extracted the high-frequency components of ERK dynamics. Subsequently, we focused our analysis on the behavior of ERK after the stability time described in the previous section was reached. Figure 18 presents an exemplary extraction of the high-frequency, Figure 19 and 20 components and the resulting distribution of optimal time delays and minimal embedded dimensions.

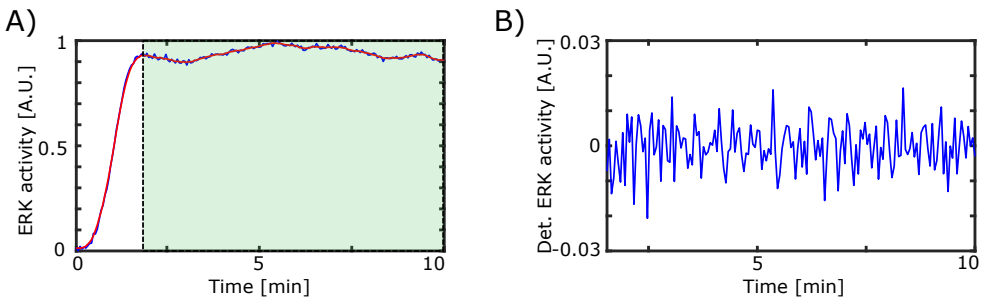

Figure 18. Extraction of the ERK dynamics high-frequency components
(A) Exemplary ERK dynamics line, calculated from the fluorescence images (blue line), its associated smoothed trend-line (red line), and the post-stabilization time (Stab. time) time series used for the recurrence analysis (green rectangle). **(B)** Exemplary high-frequency components extracted from the time series presented in panel (A).

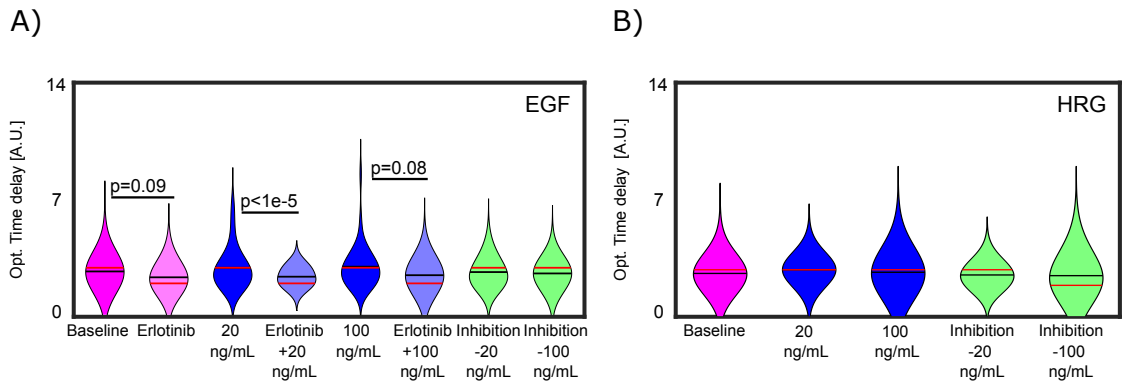

Figure 19. ERK dynamics's optimal time delay
(A) Violin distributions of the time delay were calculated using the AMI function. Except for the Baseline group (magenta) and Erlotinib group (light magenta), all the presented cell groups were treated with either 20ng/mL or 100ng/mL of EGF. **(B)** Violin distributions of the time delay were calculated using the AMI function. Except for the Baseline group (magenta), all the presented cell groups were treated with either 20ng/mL or 100ng/mL of HRG.

Table 7. Average optimal time delay for EGF-induced ERK dynamics

$Opt. Time\ delay$ [A.U.]	Baseline	Erlotinib	EGF 20ng/mL	Erlotinib+ EGF 20ng/mL	EGF 100ng/mL	Erlotinib+ EGF 100ng/mL	Inhibition – 20ng/mL EGF	Inhibition – 100ng/mL EGF
Mean +/- SD	2.9+/- 0.6	2.4 +/-0.6	3.0 +/-1.0	2.4 +/- 0.5	3.1+/- 1.0	2.5+/- 0.6	2.7+/- 1.0	2.6+/- 0.8

Table 8. Average optimal time delay for HRG-induced ERK dynamics

$Opt. Time\ delay$ [A.U.]	Baseline	HRG 20ng/mL	HRG 100ng/mL	Inhibition – 20ng/mL HRG	Inhibition – 100ng/mL HRG
Mean +/- SD	2.9+/- 0.6	3.0 +/-0.6	3.0+/- 0.7	2.7+/- 0.7	2.7+/- 0.9

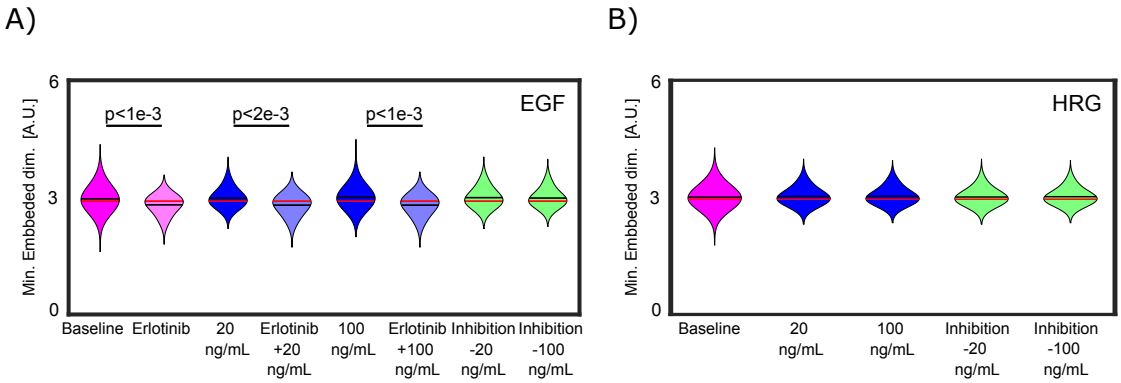

Figure 20. ERK dynamics' minimal number of embedded dimensions
(A) Violin distributions of the number of embedded dimensions were calculated using the FNN function. Except for the Baseline group (magenta) and Erlotinib group (light magenta), all the presented cell groups were treated with either 20ng/mL or 100ng/mL of EGF. **(B)** Violin distributions of the number of embedded dimensions were calculated using the FNN function. Except for the Baseline group (magenta), all the presented cell groups were treated with either 20ng/mL or 100ng/mL of HRG.

Table 9. Average minimal number of embedded dimensions for EGF-induced ERK dynamics

$Min.\ Emb.dim.$ [A.U.]	Baseline	Erlotinib	EGF 20ng/mL	Erlotinib + EGF 20ng/mL	EGF 100ng/mL	Erlotinib+ EGF 100ng/mL	Inhibition – 20ng/mL EGF	Inhibition – 100ng/mL EGF
Mean +/- SD	3.1+/-0.4	2.8 +/-0.4	3.1 +/-0.4	2.8+/- 0.4	3.2+/- 0.5	2.8+/- 0.4	3.1+/- 0.4	3.1+/- 0.4

Table 10. Average minimal number of embedded dimensions for HRG-induced ERK dynamics

$Min.\ Emb.dim.$ [A.U.]	Baseline	HRG 20ng/mL	HRG 100ng/mL	Inhibition – 20ng/mL HRG	Inhibition – 100ng/mL HRG
Mean +/- SD	2.9+/- 0.6	3.0 +/-0.6	3.0+/- 0.7	2.7+/- 0.7	2.7+/- 0.9

As shown in figures 19 and 20, except for the Erlotinib treated cells, ERK dynamics showed a consistent time delay and number of embedded dimensions through the studied conditions. A slight variation in the optimal time delay is appreciable after the indirect inhibition of ERK. Following Takens' theorem, with these

two values calculated, a space state that represents ERK can be faithfully reconstructed.

The corresponding reconstructions of the space state for the studied conditions are shown below in Figure 21.

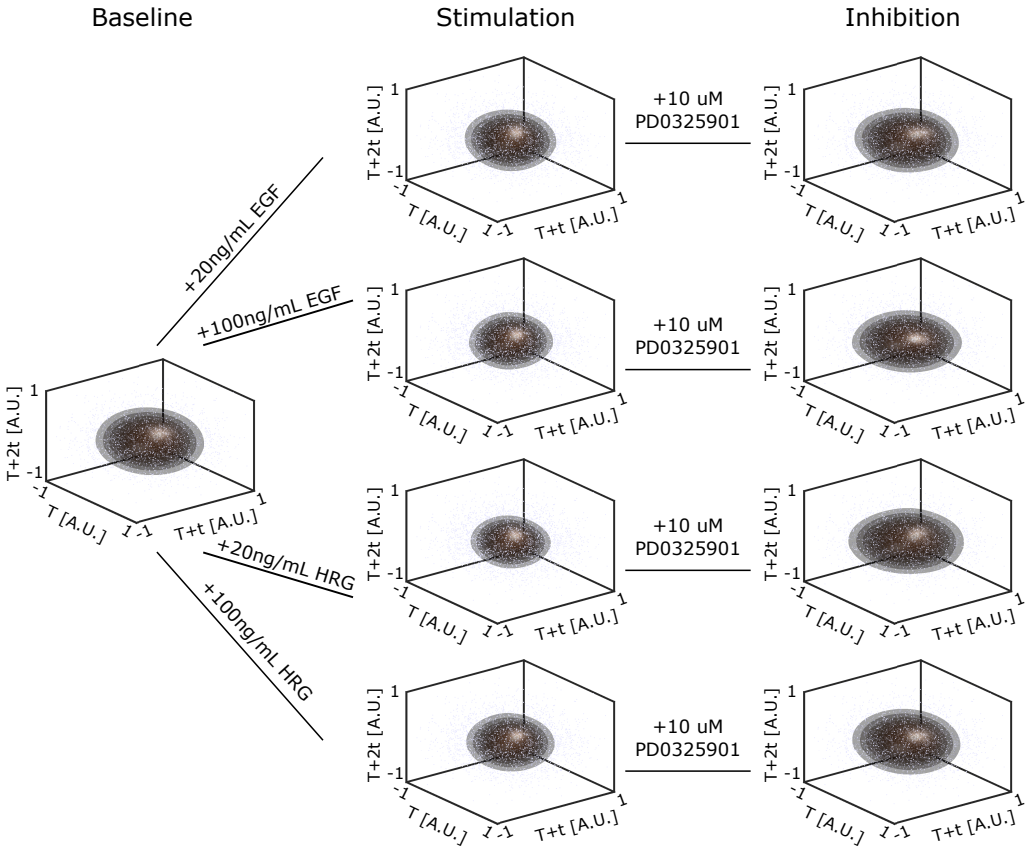

Figure 21. Space state visualization of ERK dynamics
Three-dimensional representation of ERK's dynamics space state, using the optimal time delay and the minimal number of embedded dimensions. Each axis represents the normalized embedded ERK's activity values of the original time series (T), normalized embedded ERK's activity values with one-time delay (T+t), and normalized embedded ERK's activity values with two-time delays (T+2t). The surfaces in the space state represent cumulous recurrence states with the same probability density.

By constructing the recurrence plots of ERK dynamics, we were able to confirm the presence of recurrence patterns in all the experimental groups. To provide a means of visualization, we calculated average un-thresholded averagerecurrence plots (Figure 22).

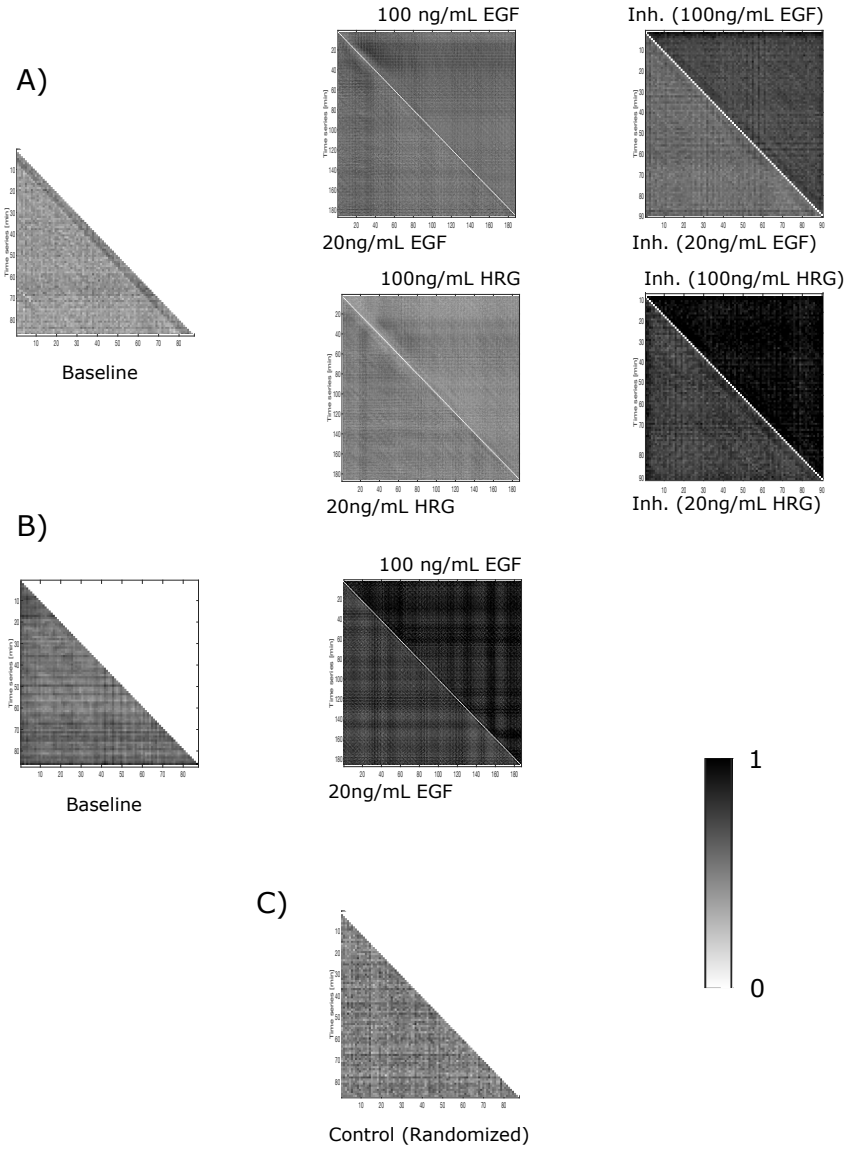

Figure 22. ERK dynamics' Unthresholded recurrence plots
(A) Unthresholded average recurrence plot (normalized Euclidean distance) associated with ERK dynamics time series prior to growth factor stimulation (left),) with the ERK dynamics time series after either 20ng/mL or 100 ng/mL of EGF stimulation (center top), with the ERK dynamics time series after either 20ng/mL or 100 ng/mL of HRG stimulation (center bottom), with the ERK dynamics time series of an either 20ng/mL or 100ng/mL EGF-stimulated cell after PD0325901 exposure (right-top), and with the ERK dynamics time series of an either 20ng/mL or 100ng/mL HRG-stimulated cell after PD0325901 exposure (right bottom). **(B)** Unthresholded average recurrence plot (normalized Euclidean distance) associated with ERK dynamics time series of cells treated with Erlotinib prior to growth factor stimulation (left) and after either 20ng/mL or 100 ng/mL of EGF stimulation post-Erlotinib exposure (center).
(C) Unthresholded average recurrence plot (normalized Euclidean distance) associated with a randomized time series of ERK dynamics of cells prior to growth factor stimulation. This group is defined as the control.

The recurrence lines (dark diagonal lines) present in the baseline become more apparent and persistent after growth factor stimulation. As expected, it slowly faded away after inhibiting ERK activity with the MEK inhibitor PD0325901. Similarly, once cells were exposed to the EGFR-inhibitor Erlotinib, the recurrences slowly disappeared. Furthermore, exposure to Erlotinib blocked the appearance of recurrence lines after stimulation with either 20ng/mL (n=21) or 100 ng/mL (n=21) of EGF. As a control, we randomly permutated a group of time ERK activity time series (n=35) and calculated its associated recurrence plot. In order to quantify the observed recurrences, we applied the threshold to the individual recurrence plots. We measured recurrence lines by counting the number of diagonally connected non-zero elements. We used the maximal recurrence length as a reporter for ERK recurrence persistence (Lmax). As a measure of the de-localization of recurrences on the space state, we calculated the Shannon's entropy associated with the distribution of our recurrence line lengths.

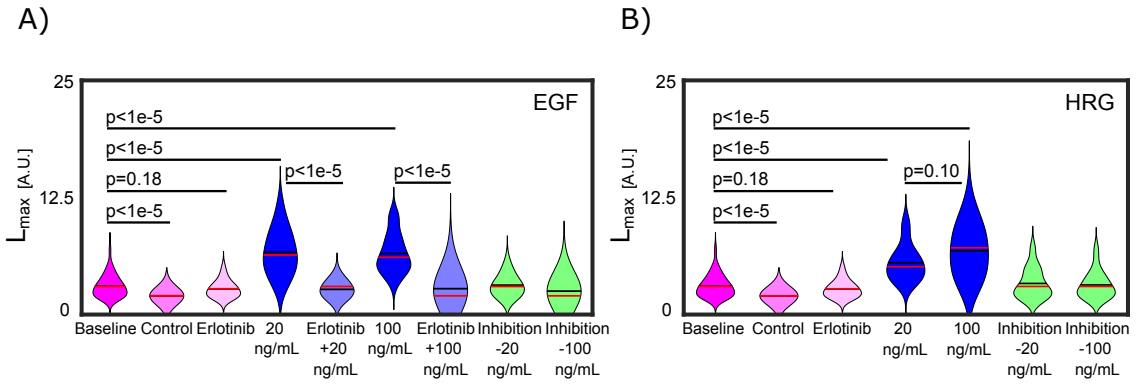

Figure 23. ERK dynamics' maximal recurrence length
(A) Violin distributions of the maximal recurrence length were measured from thresholded recurrence plots. Except for the Baseline group (magenta), control group (light magenta), and Erlotinib group (lighter magenta), all the presented cell groups were treated with either 20ng/mL or 100ng/mL of EGF. **(B)** Violin distributions of the maximal recurrence length were measured from thresholded recurrence plots. Except for the Baseline group (magenta), control group (light magenta), and Erlotinib group (lighter magenta), all the presented cell groups were treated with either 20ng/mL or 100ng/mL of HRG.

Table 11. Average maximal recurrence length for EGF-induced ERK dynamics

L_{max} [A.U.]	Baseline	Control	Erlotinib	EGF 20ng/mL	Erlotinib+ EGF 20ng/mL	EGF 100ng/mL	Erlotinib+ EGF 100ng/mL	Inhibition – 20ng/mL EGF	Inhibition – 100ng/mL EGF
Mean +/- SD	3.04+/- 1.14	2.00+/- 1.24	2.74 +/-0.87	6.64 +/-2.32	2.69+/- 0.74	6.52+/- 2.07	2.76+/- 1.17	3.13+/- 1.12	2.50+/- 0.84

Table 12. Average maximal recurrence length for HRG-induced ERK dynamics

L_{max} [A.U.]	Baseline	Control	Erlotinib	HRG 20ng/mL	HRG 100ng/mL	Inhibition – 20ng/mL HRG	Inhibition – 100ng/mL HRG
Mean +/- SD	3.04+/- 1.14	2.00+/- 1.24	2.74 +/-0.87	5.53 +/-1.88	6.82+/- 2.63	3.32+/- 1.54	3.16+/- 1.40

After growth factor stimulation, the maximal recurrence length increased for all the tested concentrations. Despite a slightly smaller value recorded on cells stimulated with 20ng/mL of HRG, there was no significant difference between the persistence of ERK recurrences between the rest of the growth factor stimulated cells. After ERK inhibition, the maximal recurrence lengths decreased on all growth-factor stimulated cells. Interestingly, in the case of cells exposed to 100ng/mL of EGF, the maximal recurrence length decreased to values below the calculated for the baseline. The randomized ERK dynamics (negative control group) showed the shortest maximal recurrence lengths. Cells exposed to just Erlotinib showed longer maximal recurrences lengths than the negative control group but shorter than the untreated cells. Additionally, Erlotinib prevented cells exposed to either 20ng/mL or 100 ng/mL of EGF from developing more persistent ERK recurrences.

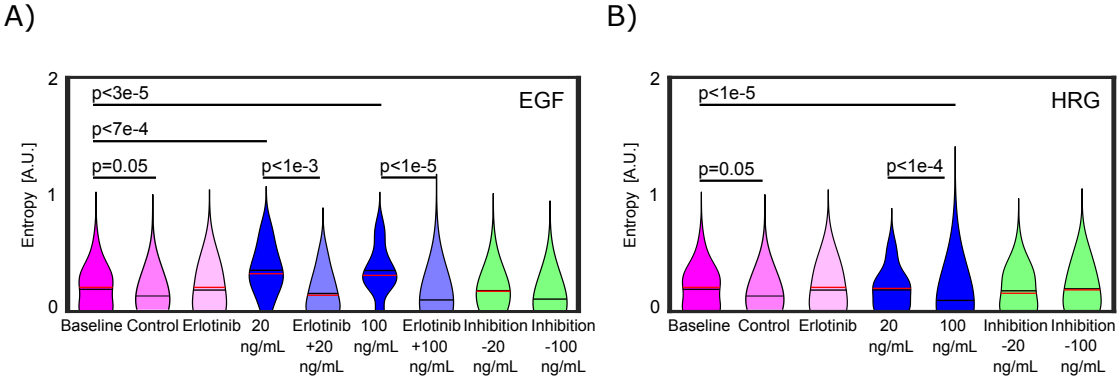

Figure 24. ERK dynamics's recurrence entropy
(A) Violin distributions of the recurrence entropy were calculated from the recurrence length distributions of thresholded recurrence plots. Except for the Baseline group (magenta), control group (light magenta), and Erlotinib group (lighter magenta), all the presented cell groups were treated with either 20ng/mL or 100ng/mL of EGF. **(B)** Violin distributions of the recurrence entropy were calculated from the recurrence length distributions of thresholded recurrence plots. Except for the Baseline group (magenta), control group (light magenta), and Erlotinib group (lighter magenta), all the presented cell groups were treated with either 20ng/mL or 100ng/mL of HRG.

Table 13. Average recurrence entropy for EGF-induced ERK dynamics

$Entr.$ [A.U.]	Baseline	Control	Erlotinib	EGF 20ng/mL	Erlotinib+ EGF 20ng/mL	EGF 100ng/mL	Erlotinib+ EGF 100ng/mL	Inhibition – 20ng/mL EGF	Inhibition – 100ng/mL EGF
Mean +/- SD	0.19+/- 0.17	0.15+/- 0.17	0.18+/- 0.19	0.35+/- 0.20	0.15+/- 0.17	0.35+/- 0.20	0.11+/- 0.14	0.17+/- 0.16	0.11+/- 0.13

Table 14. Average recurrence entropy for HRG-induced ERK dynamics

$Entr.$ [A.U.]	Baseline	Control	Erlotinib	HRG 20ng/mL	HRG 100ng/mL	Inhibition – 20ng/mL HRG	Inhibition – 100ng/mL HRG
Mean +/- SD	0.19+/- 0.17	0.15+/- 0.17	0.18+/- 0.19	0.19+/- 0.20	0.11+/- 0.17	0.17+/- 0.20	0.19+/- 0.14

The Shannon entropy of ERK recurrences showed no significant difference between Erlotinib-treated and untreated cells. However, these two groups have higher entropy than the negative control group. Stimulating cells with EGF resulted in an entropy increase, in a statistically indistinguishable value for both concentrations. Similarly to what was observed with the maximal recurrence lengths, cells treated with Erlotinib showed no significant change in entropy after exposure to either 20ng/mL or 100 ng/mL of EGF. Interestingly, stimulation with HRG showed no significant effect on the recurrence entropy of ERK. After PD0325901 exposure, the entropies of all groups decreased to values similar to that calculated for the baseline.

3.3 Growth factor stimulation increases cellular morphodynamics diversity

In order to compare the behavior of morphodynamics to ERK dynamics, we studied the recurrences of fast-occurring cellular structural changes. Similar to the previous section, we extracted the high-frequency components of the morphodynamics reporter Hu3 moment. Consistently, we focused our analysis on the time points that came after the stabilization time calculated for each cell (Figure 25). The associated optimal time delay and minimal embedded dimensions are shown below in Figure 26 and 27.

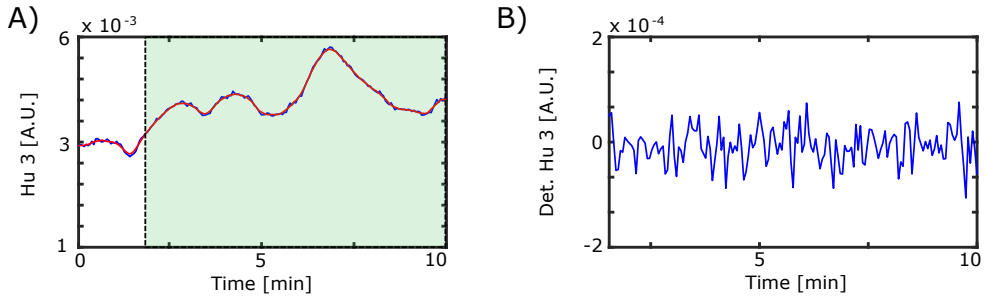

Figure 25. Extraction of the cellular morphodynamics high-frequency components
(A) Exemplary Hu 3 time series, calculated from the fluorescence images (blue line), its associated smoothed trend-line (red line), and the post-stabilization time (Stab. time) time series used for the recurrence analysis (green rectangle). **(B)** Exemplary high-frequency components extracted from the time series presented in panel (A).

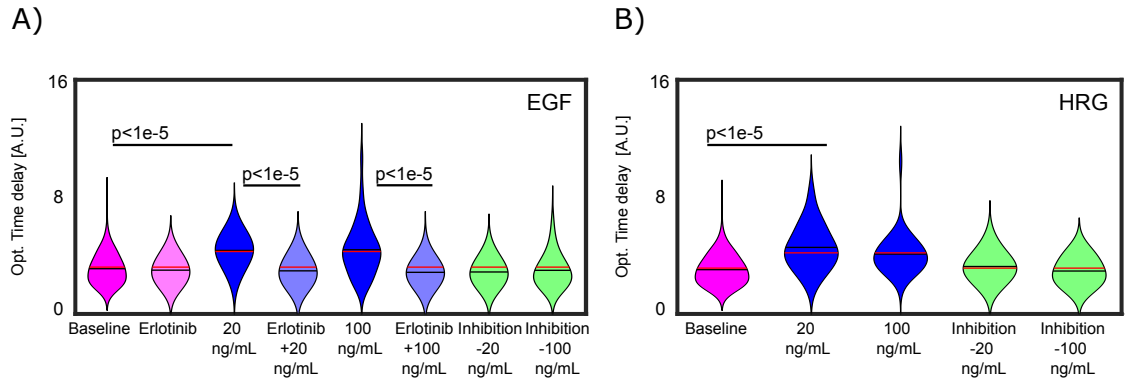

Figure 26. Cellular morphodynamics optimal time delay
(A) Violin distributions of the time delay were calculated using the AMI function. Except for the Baseline group (magenta) and Erlotinib group (light magenta), all the presented cell groups were treated with either 20ng/mL or 100ng/mL of EGF. **(B)** Violin distributions of the time delay were calculated using the AMI function. Except for the Baseline group (magenta), all the presented cell groups were treated with either 20ng/mL or 100ng/mL of HRG.

Table 15. Average optimal time delay for EGF-induced cellular morphodynamics

$Opt.\ Time\ delay$ [A.U.]	Baseline	Erlotinib	EGF 20ng/mL	Erlotinib+ EGF 20ng/mL	EGF 100ng/mL	Erlotinib+ EGF 100ng/mL	Inhibition – 20ng/mL EGF	Inhibition – 100ng/mL EGF
Mean +/- SD	2.9+/- 0.9	2.8 +/-0.7	4.1 +/-1.0	2.8+/- 0.8	4.1+/- 1.2	2.7+/- 0.7	2.7+/- 1.5	2.8+/- 1.0

Table 16. Average optimal time delay for HRG-induced cellular morphodynamics

$Opt.\ Time\ delay$ [A.U.]	Baseline	HRG 20ng/mL	HRG 100ng/mL	Inhibition – 20ng/mL HRG	Inhibition – 100ng/mL HRG
Mean +/- SD	2.9+/- 0.9	4.3 +/-1.2	4.0+/- 1.3	3.1+/- 0.9	2.8+/- 0.8

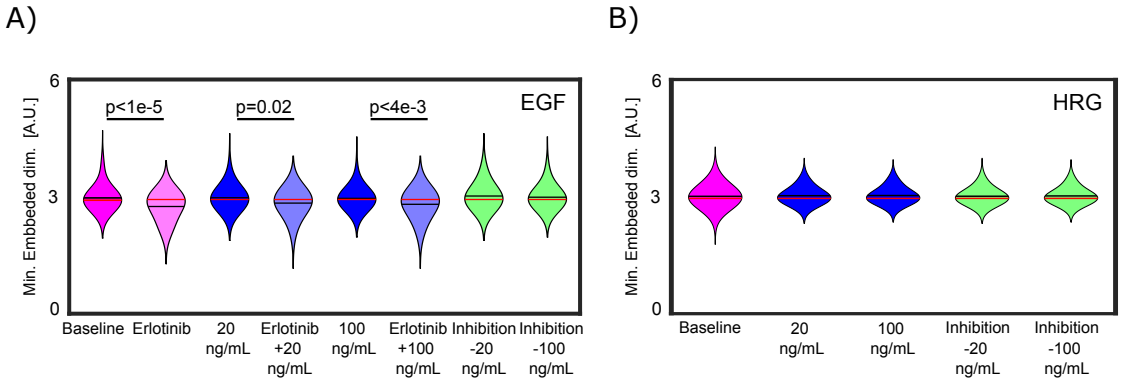

Figure 27. Cellular morphodynamics minimal number of embedded dimensions
(A) Violin distributions of the number of embedded dimensions were calculated using the FNN function. Except for the Baseline group (magenta) and Erlotinib group (light magenta), all the presented cell groups were treated with either 20ng/mL or 100ng/mL of EGF. **(B)** Violin distributions of the number of embedded dimensions were calculated using the FNN function. Except for the Baseline group (magenta), all the presented cell groups were treated with either 20ng/mL or 100ng/mL of HRG.

Table 17. Average minimal number of embedded dimensions for EGF-induced cellular morphodynamics

$Min. Emb. dim.$ [A.U.]	Baseline	Erlotinib	EGF 20ng/mL	Erlotinib+ EGF 20ng/mL	EGF 100ng/mL	Erlotinib+ EGF 100ng/mL	Inhibition – 20ng/mL EGF	Inhibition – 100ng/mL EGF
Mean +/- SD	3.1+/-0.3	2.7 +/-0.5	3.1 +/-0.3	2.9+/-0.4	3.1+/-0.2	2.8+/-0.4	3.1+/-0.4	3.1+/-0.3

Table 18. Average minimal number of embedded dimensions for HRG-induced cellular morphodynamics

$Min. Emb. dim.$ [A.U.]	Baseline	HRG 20ng/mL	HRG 100ng/mL	Inhibition – 20ng/mL HRG	Inhibition – 100ng/mL HRG
Mean +/- SD	3.1+/-0.3	3.1 +/-0.3	3.1+/-0.2	3.1+/-0.3	3.1+/-0.3

In contrast to what was observed in ERK dynamics, cellular morphodynamics showed a longer optimal time delay after growth factor treatment. Upon inhibition, the optimal time delay regressed to the mean value observed in the baseline. However, the calculated number of minimal embedded dimensions was uniform across all the experimental conditions, consistent with the results obtained for ERK dynamics. Once again, the space state of cellular morphodynamics can be reconstructed with the number of minimal embedded dimensions and the optimal time delay for all cellular conditions (Figure 28)

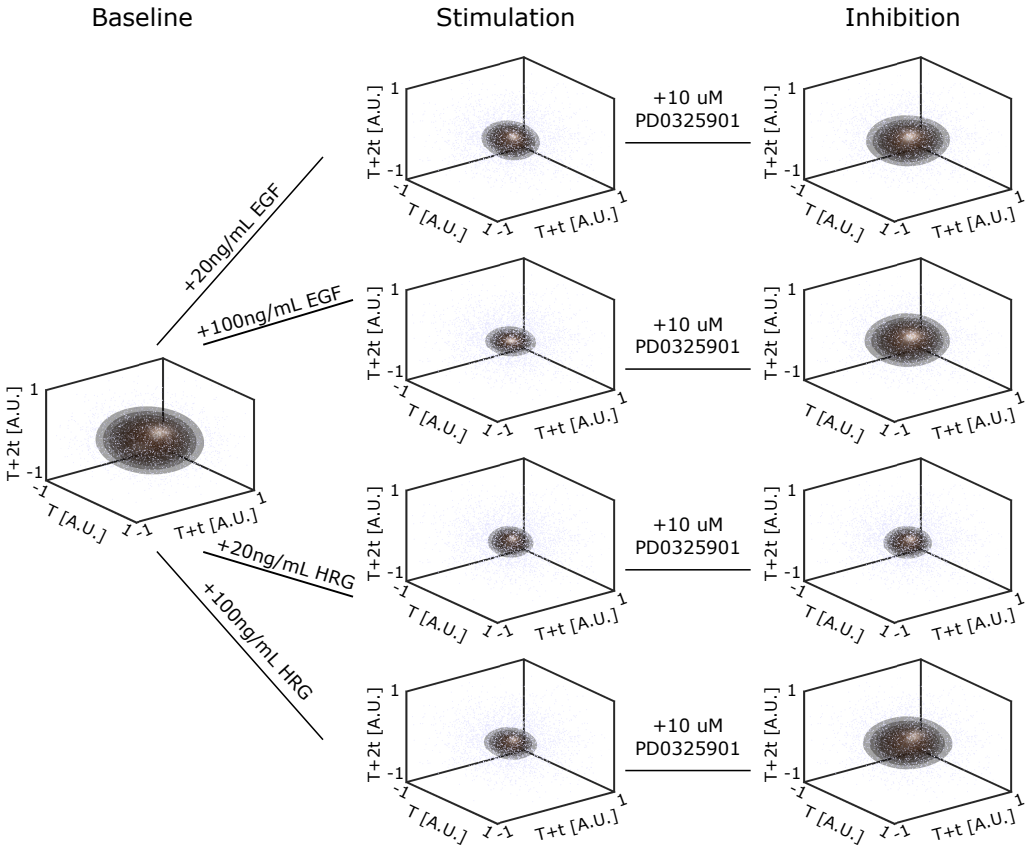

Figure 28. Space state visualization of cellular morphodynamics
Three-dimensional representation of cellular morphodynamics's space state, using the optimal time delay and the minimal number of embedded dimensions. Each axis represents the normalized embedded Hu 3 values of the original time series (T), normalized embedded Hu 3 values with one-time delay (T+t), and normalized embedded Hu 3 values with two-time delays (T+2t). The surfaces in the space state represent cumulous recurrence states with the same probability density.

Coinciding with ERK dynamics, the morphodynamics recurrence plots reveal the presence of recurrence lines prior to growth factor stimulation. These lines also increase in length upon either EGF or HRG exposure and fade out towards the last time points of the ERK-inhibition stage of the experiments. As expected, the negative control shows the loss of recurrence lines. The effect of Erlotinib treatment on recurrences is congruent with the tendency observed in ERK dynamics. After being exposed to Erlotinib, cells showed a decrease in recurrence lines. In addition, further exposure to either 20ng/mL or 100ng/mL of EGF to these groups of cells stopped the prolonging of said recurrence lines (Figure 29).

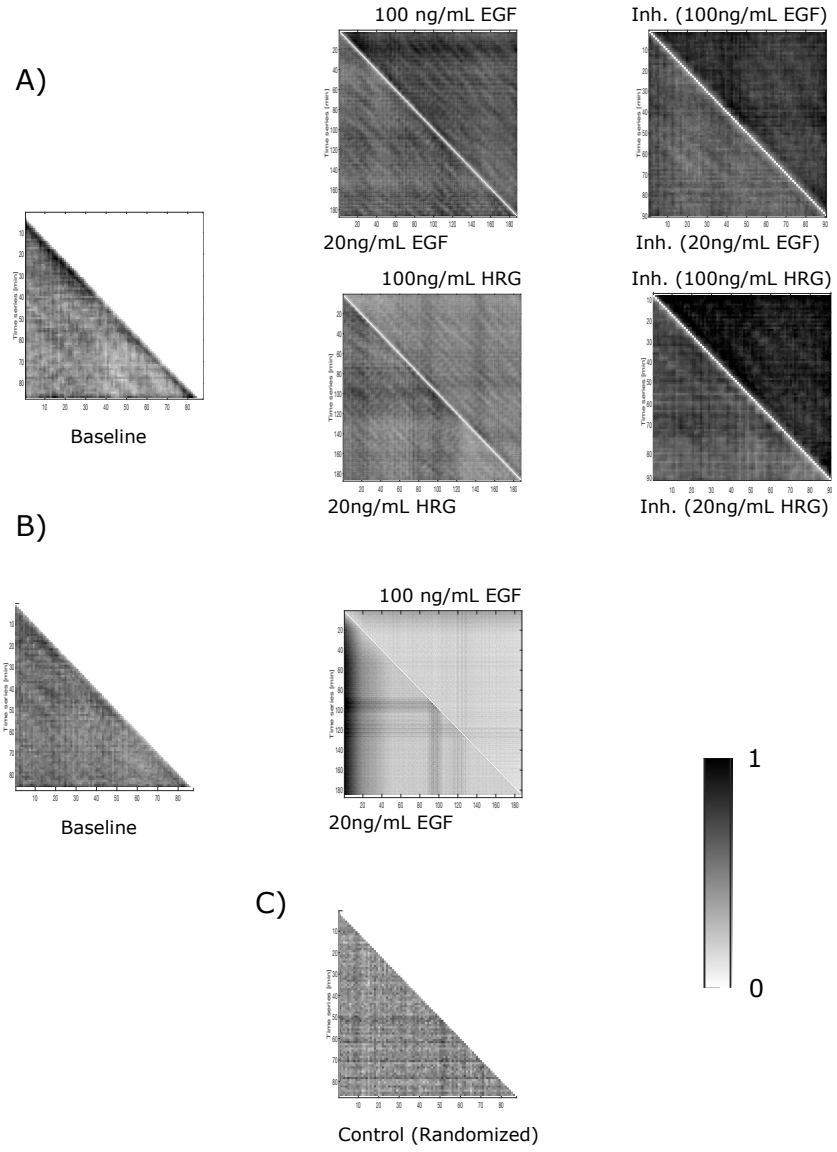

Figure 29. Cellular morphodynamics unthresholded recurrence plots
(A) Unthresholded average recurrence plot (normalized Euclidean distance) associated with cellular morphodynamics' time series prior to growth factor stimulation (left),) with the cellular morphodynamics' time series after either 20ng/mL or 100 ng/mL of EGF stimulation (center top), with the cellular morphodynamics' time series after either 20ng/mL or 100 ng/mL of HRG stimulation (center bottom), with the cellular morphodynamics' time series of an either 20ng/mL or 100ng/mL EGF-stimulated cell after PD0325901 exposure (right-top), and with the cellular morphodynamics' time series of an either 20ng/mL or 100ng/mL HRG-stimulated cell after PD0325901 exposure (right bottom). **(B)** Unthresholded average recurrence plot (normalized Euclidean distance) associated with cellular morphodynamics' time series of cells treated with Erlotinib prior to growth factor stimulation (left) and after either 20ng/mL or 100 ng/mL of EGF stimulation post-Erlotinib exposure (center). **(C)** Unthresholded average recurrence plot (normalized Euclidean distance) associated with a randomized time series of the cellular morphodynamics of cells prior to growth factor stimulation. This group is defined as the control.

After thresholding the individual recurrence plots, we used the same recurrence quantifiers to characterize the dynamics stage of cellular morphodynamics at each experimental condition. Maximal recurrence length to quantify morphodynamics recurrence persistence and Shannon's entropy for the de-localization of recurrence states on the morphodynamics space state.

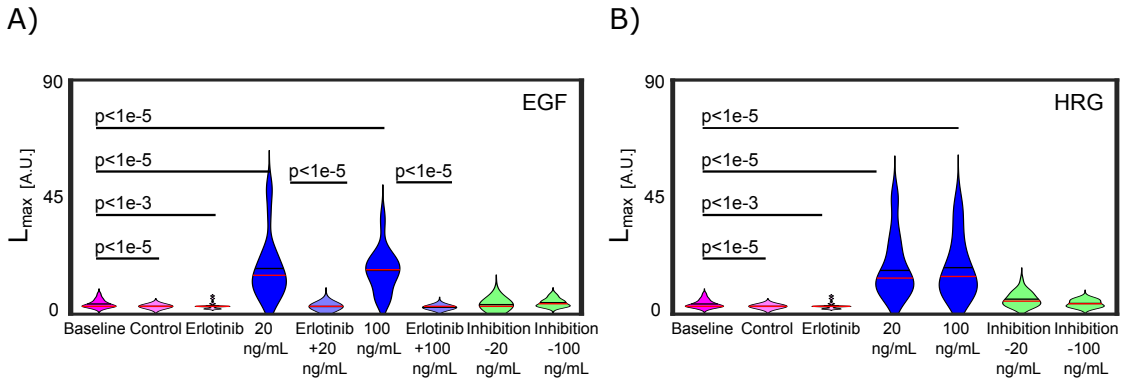

Figure 30. Cellular morphodynamics' maximal recurrence length
(A) Violin distributions of the maximal recurrence length were measured from thresholded recurrence plots. Except for the Baseline group (magenta), control group (light magenta), and Erlotinib group (and lighter magenta), all the presented cell groups were treated with either 20ng/mL or 100ng/mL of EGF. **(B)**Violin distributions of the maximal recurrence length were measured from thresholded recurrence plots. Except for the Baseline group (magenta), control group (light magenta), and Erlotinib group (and lighter magenta), all the presented cell groups were treated with either 20ng/mL or 100ng/mL of HRG.

Table 19. Average maximal recurrence length for EGF-induced cellular morphodynamics

L_{max} [A.U.]	Baseline	Control	Erlotinib	EGF 20ng/mL	Erlotinib+ EGF 20ng/mL	EGF 100ng/mL	Erlotinib+ EGF 100ng/mL	Inhibition – 20ng/mL EGF	Inhibition – 100ng/mL EGF
Mean +/- SD	3.9+/- 1.5	3.0+/- 0.5	3.3+/- 1.3	17.6+/- 12.1	2.9+/- 0.7	16.8+/- 8.3	2.6+/- 0.7	3.7+/- 1.4	4.4+/- 1.6

Table 20. Average maximal recurrence length for HRG-induced cellular morphodynamics

L_{max} [A.U.]	Baseline	Control	Erlotinib	HRG 20ng/mL	HRG 100ng/mL	Inhibition – 20ng/mL EGF	Inhibition – 100ng/mL EGF
Mean +/- SD	3.9+/- 1.5	3.0+/- 0.5	3.3+/- 1.3	16.8+/- 13.4	17.9+/- 11.4	5.8+/- 2.6	4.1+/ - 1.4

Compared to the negative control, both Erlotinib treated and untreated cells showed longer maximal recurrence lengths. Consistently, cells exposed to Erlotinib had shorter maximal recurrence lengths than the untreated group. Regardless of the concentration, exposure to either EGF or HRG led to a 3-fold increase, on average, in the maximal recurrence length. Morphodynamics recurrence persistence decreased in a practically equivalent quantity after cells were exposed to the MEK-inhibitor. Interestingly, the group of cells exposed to the inhibitor after being stimulated with either EGF or HRG showed longer maximal recurrence lengths than the cells pre-treated with Erlotinib that were later exposed to either 20ng/mL or 100ng/mL of EGF.

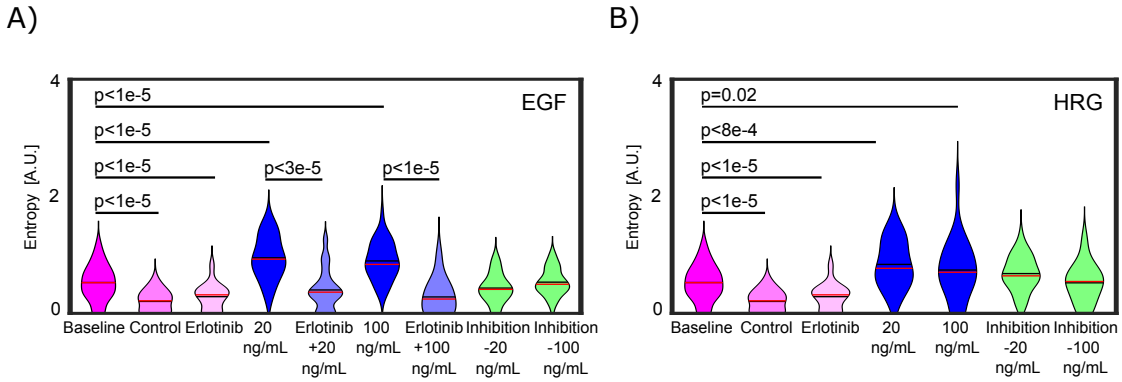

Figure 31. Cellular morphodynamics' recurrence entropy
(A) Violin distributions of the recurrence entropy were calculated from the recurrence length distributions of thresholded recurrence plots. Except for the Baseline group (magenta), control group (light magenta), and Erlotinib group (and lighter magenta), all the presented cell groups were treated with either 20ng/mL or 100ng/mL of EGF. **(B)** Violin distributions of the recurrence entropy were calculated from the recurrence length distributions of thresholded recurrence plots. Except for the Baseline group (magenta), control group (light magenta), and Erlotinib group (and lighter magenta), all the presented cell groups were treated with either 20ng/mL or 100ng/mL of HRG.

Table 21. Average recurrence entropy for EGF-induced cellular morphodynamics

$Entr.$ [A.U.]	Baseline	Control	Erlotinib	EGF 20ng/mL	Erlotinib+ EGF 20ng/mL	EGF 100ng/mL	Erlotinib+ EGF 100ng/mL	Inhibition – 20ng/mL EGF	Inhibition – 100ng/mL EGF
Mean +/- SD	0.53+/- 0.30	0.20+/- 0.18	0.29+/- 0.22	0.95+/- 0.35	0.40+/- 0.35	0.90+/- 0.31	0.29+/- 0.30	0.43+/- 0.25	0.53+/- 0.24

Table 22. Average recurrence entropy for HRG-induced cellular morphodynamics

$Entr.$ [A.U.]	Baseline	Control	Erlotinib	HRG 20ng/mL	HRG 100ng/mL	Inhibition – 20ng/mL HRG	Inhibition – 100ng/mL HRG
Mean +/- SD	0.53+/- 0.30	0.20+/- 0.18	0.29+/- 0.22	0.84+/- 0.38	0.74+/- 0.50	0.68+/- 0.29	0.52+/- 0.33

The morphodynamics of cells treated with Erlotinib showed a slightly higher recurrence entropy than the negative control group. However, untreated cells showed a 2-fold higher entropy. Interestingly, the recurrence entropy of cells treated with Erlotinib increased after exposure to 20ng/mL of EGF. Nonetheless, this increase resulted in an entropy lower than the calculated for untreated cells. Once the latter group of cells was exposed to growth factors, their entropy increased up to 79% on average for cells exposed to 20ng/mL of EGF and 70% for cells exposed to 100ng/mL of EGF. Surprisingly, despite being associated with strong cellular structural modifications, stimulation with HRG increased the entropy of untreated cells in smaller percentages than EGF. 100ng/mL of HRG caused 40% higher entropies, whereas treating cells with 20ng/mL of HRG resulted in 58% higher entropies. After being exposed to PD0325901, the morphodynamics recurrence entropy decreased to values similar to those calculated for untreated cells, except for cells stimulated with 20ng/mL of HRG. This group of cells retained an average entropy 28% higher than the untreated cells.

3.4 ERK dynamics and cellular morphodynamics connection remains unmodified upon growth factor stimulation

In order to test whether the high-frequency components embedded in ERK dynamics are related to the fast-occurring morphodynamic events, we studied their cross-recurrences. Their associated cross recurrence plots were calculated based on the time delay embedding calculations presented in sections 3.2 and 3.3 and, as in the previous sections, following the procedure described on (Marwan et al., 2007). The Figure 32, which contains the recurrence plots, is presented on the next page.

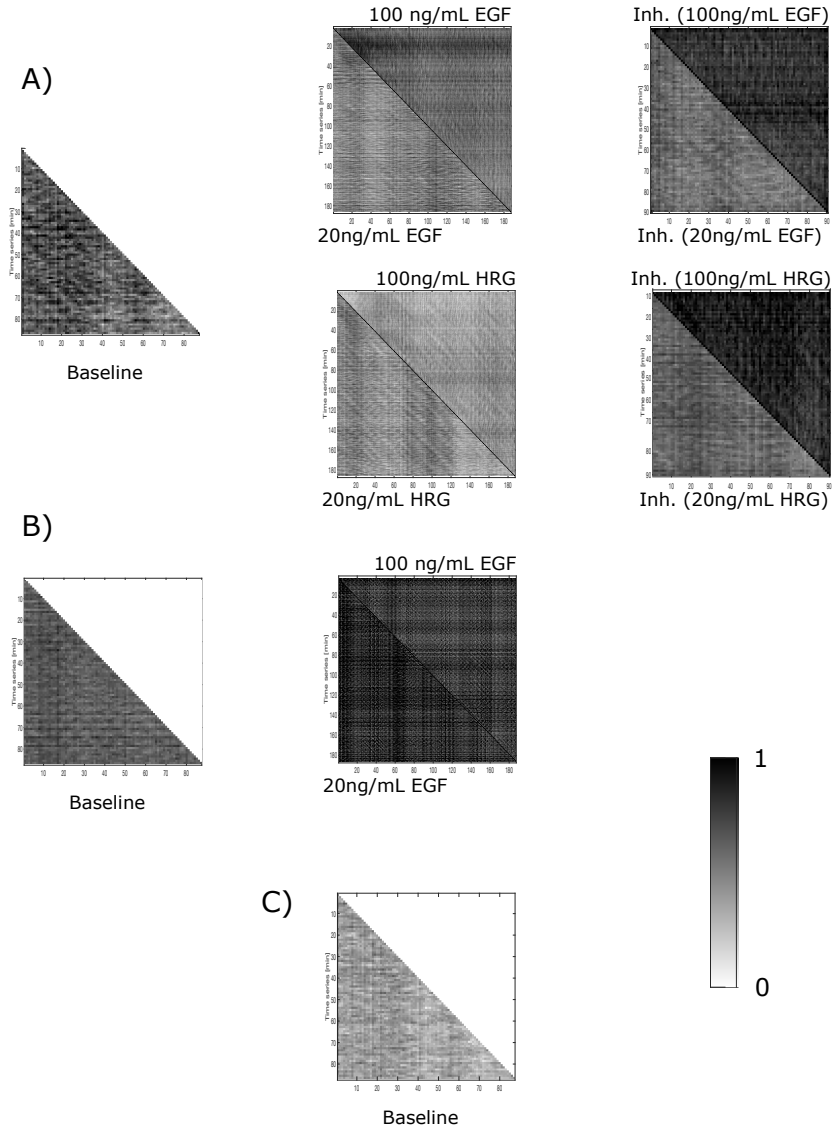

Figure 32. ERK dynamics - cellular morphodynamics unthresholded cross-recurrence plots

(A) Unthresholded average cross-recurrence plot (normalized Euclidean distance) associated with the cellular morphodynamics' and ERK dynamics time series prior to growth factor stimulation (left),) with the cellular morphodynamics' and ERK dynamics time series after either 20ng/mL or 100 ng/mL of EGF stimulation (center top), with the cellular morphodynamics' and ERK dynamics time series after either 20ng/mL or 100 ng/mL of HRG stimulation (center bottom), with the cellular morphodynamics' and ERK dynamics time series of either 20ng/mL or 100ng/mL EGF-stimulated cells after PD0325901 exposure (right-top), and with the cellular morphodynamics' and ERK dynamics time series of either 20ng/mL or 100ng/mL HRG-stimulated cells after PD0325901 exposure (right bottom). **(B)** Unthresholded average cross-recurrence plot (normalized Euclidean distance) associated with the cellular morphodynamics' and ERK dynamics time series of cells treated with Erlotinib prior to growth factor stimulation (left) and after either 20ng/mL or 100 ng/mL of EGF stimulation post-Erlotinib exposure (center). **(C)** Unthresholded average cross-recurrence plot (normalized Euclidean distance) associated with randomized cellular morphodynamics' and ERK dynamics time series of cells prior to growth factor stimulation. This group is defined as the control.

Interestingly, ERK dynamics and cellular morphodynamics showed coinciding recurrences prior to growth factor stimulation. In contrast, cells treated with Erlotinib showed a more random and discontinuous arrangement of recurrences. Similarly, the negative control group shows isolated recurrences. As was the case for the individual recurrences of ERK dynamics and cellular morphodynamics, the cross-recurrences between these two trends increase in persistence, as can be observed by longer recurrence lines. Upon exposure to the MEK inhibitor PD032951, the recurrence lines fade away towards the end of the imaging time. In addition, cells pre-treated with Erlotinib showed no change in their recurrence line distributions upon exposure to either 20ng/mL or 100 ng/mL of EGF. As in the previous sections, the recurrence plots were thresholded for each cellular condition. The maximal recurrence length and the recurrence entropy distributions are presented below.

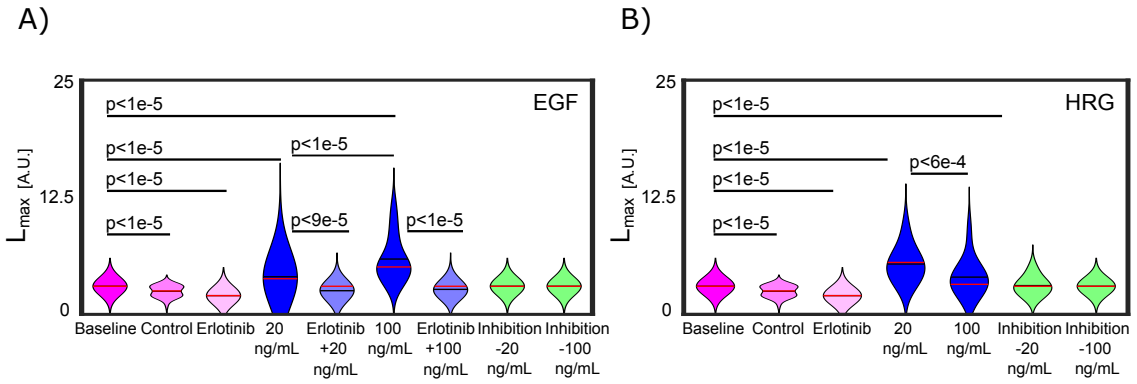

Figure 33. Cellular morphodynamics' and ERK dynamics maximal cross recurrence length
(A) Violin distributions of the maximal cross recurrence length were measured from thresholded recurrence plots. Except for the Baseline group (magenta), control group (light magenta), and Erlotinib group (and lighter magenta), all the presented cell groups were treated with either 20ng/mL or 100ng/mL of EGF. **(B)** Violin distributions of the maximal cross recurrence length were measured from thresholded recurrence plots. Except for the Baseline group (magenta), control group (light magenta), and Erlotinib group (and lighter magenta), all the presented cell groups were treated with either 20ng/mL or 100ng/mL of HRG.

Table 23. Average maximal cross-recurrence length for EGF-induced ERK dynamics - cellular morphodynamics recurrences

L_{max} [A.U.]	Baseline	Control	Erlotinib	EGF 20ng/mL	Erlotinib+ EGF 20ng/mL	EGF 100ng/mL	Erlotinib+ EGF 100ng/mL	Inhibition – 20ng/mL EGF	Inhibition – 100ng/mL EGF
Mean +/- SD	3.0+/- 0.7	2.4+/- 0.5	2.0+/- 0.6	4.2+/- 1.2	2.5+/- 0.8	5.9+/- 2.3	2.6+/- 0.6	3.0+/- 0.7	3.0+/- 1.4

Table 24. Average maximal cross-recurrence length for HRG-induced ERK dynamics - cellular morphodynamics recurrences

L_{max} [A.U.]	Baseline	Control	Erlotinib	HRG 20ng/mL	HRG 100ng/mL	Inhibition – 20ng/mL HRG	Inhibition – 100ng/mL HRG
Mean +/- SD	3.0+/- 0.7	2.4+/- 0.5	2.0+/- 0.6	5.4+/- 1.7	4.0+/- 1.9	3.0+/- 0.9	3.0+/- 0.6

Randomizing the time series (negative control) and treating cells with Erlotinib resulted in the shortening of the maximal recurrence length. The maximal recurrence length of cells pre-treated with Erlotinib increased in length on a similar scale once exposed to either 20 ng/mL or 100 ng/mL of EGF. However, the maximal average increase of 30% between Erlotinib-treated and Erlotinib-treated + 100ng/mL EGF resulted in shorter maximal recurrence lengths than the untreated (baseline) cells. Exposure to EGF showed a concentration dependency; 20ng/mL of EGF increased the maximal recurrence lengths by 40%, whereas 100ng/mL of EGF led to almost a fold increase of the baseline maximal recurrence lengths. In contrast, the concentration dependency observed in HRG showed a decreasing trend. Compared to the baseline cells, 20ng/mL of HRG increased the length of the recurrence lines by an average of 80%. However, 100ng/mL had an average elongating effect of recurrence lines of 33%. Inhibiting ERK dynamics shortened the recurrence lines to values indistinguishable from the baseline condition.

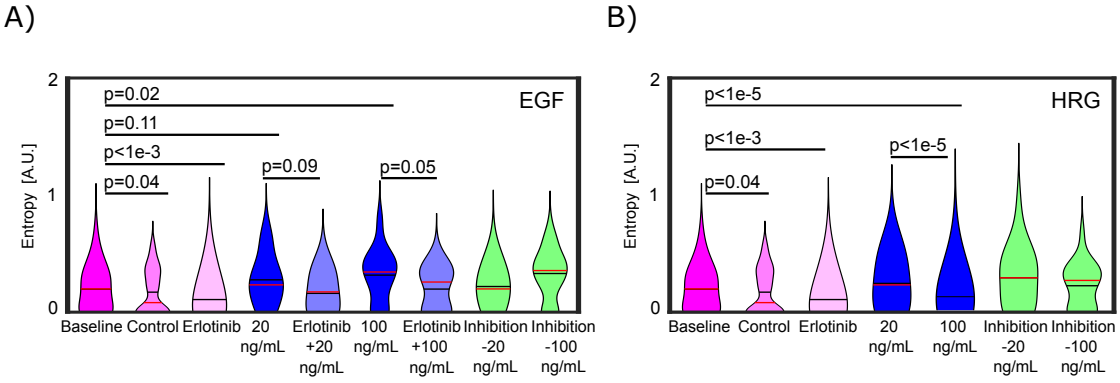

Figure 34. Cellular morphodynamics' and ERK dynamics cross-recurrence entropy **(A)** Violin distributions of the cross-recurrence entropy were calculated from the recurrence length distributions of thresholded cross-recurrence plots. Except for the Baseline group (magenta), control group (light magenta), and Erlotinib group (and lighter magenta), all the presented cell groups were treated with either 20ng/mL or 100ng/mL of EGF. **(B)**Violin distributions of the cross-recurrence entropy were calculated from the recurrence length distributions of thresholded cross-recurrence plots. Except for the Baseline group (magenta), control group (light magenta), and Erlotinib group (and lighter magenta), all the presented cell groups were treated with either 20ng/mL or 100ng/mL of HRG.

Table 25. Average cross-recurrence entropy for EGF-induced cellular morphodynamics

$Entr.$ [A.U.]	Baseline	Control	Erlotinib	EGF 20ng/mL	Erlotinib+ EGF 20ng/mL	EGF 100ng/mL	Erlotinib+ EGF 100ng/mL	Inhibition – 20ng/mL EGF	Inhibition – 100ng/mL EGF
Mean +/- SD	0.20+/- 0.19	0.17+/- 0.19	0.10+/- 0.16	0.28+/- 0.22	0.16+/- 0.16	0.32+/- 0.22	0.18+/- 0.18	0.22+/- 0.17	0.33+/- 0.21

Table 26. Average cross-recurrence entropy for HRG-induced cellular morphodynamics

$Entr.$ [A.U.]	Baseline	Control	Erlotinib	HRG 20ng/mL	HRG 100ng/mL	Inhibition – 20ng/mL HRG	Inhibition – 100ng/mL HRG
Mean +/- SD	0.20+/- 0.19	0.17+/- 0.19	0.10+/- 0.16	0.25+/- 0.23	0.15+/- 0.21	0.26+/- 0.25	0.23+/- 0.19

Treating cells with Erlotinib resulted in 50% smaller recurrence entropies than the baseline condition. The randomized time series showed recurrence entropies higher than the Erlotinib treated cells but 20% smaller than the baseline condition. Interestingly stimulating cells with 100ng/mL of HRG resulted in recurrence entropies smaller than the untreated cells. In contrast, stimulating cells with 20ng/mL of EGF, 100ng/mL of EGF, and 20ng/mL of HRG led to 40%, 60%, and 25% average increased recurrence entropies respectively. Contrary to the trends observed in the previous sections, Exposing cells to PD0325901 did not cause an overall decrease in the recurrence entropies. Cells stimulated with 100ng/mL of EGF, or 20ng/mL of HRG showed no significantly different recurrence entropies when exposed to the inhibitor. The recurrence entropy of Cells stimulated with 20 ng/mL of EGF decreased to values similar to the baseline condition. Exposing cells stimulated with 100ng/mL of HRG to the inhibitor increased their associated recurrence entropy to the baseline value.

3.5 Effect of the local cellular environment on cellular communication

The results from section 3.1 suggest the existence of an effect of the local cellular environment on the response to a growth factor. We calculated the ERK dynamics cross-recurrence plots between neighboring cells and the morphodynamics recurrence plots between neighboring cells. As control groups, we randomly selected a group of non-neighboring cells, with the sample size for each cellular condition. We calculated the recurrences between neighboring cells for the Erlotinib-exposed and the subsequently EGF-stimulated cells and compared them to their untreated and stimulated equivalents.

3.5.1 EGF-induced ERK dynamics reveal local cellular communication

The recurrence plot of neighboring cells shows coinciding recurrence states on the baseline condition. As observed in the previous cases, stimulation with growth factors leads to recurrence line elongation and inhibition of ERK to a shortening of said lines. The cross-like structures on the recurrence plots are discontinuities between the cell's ERK dynamics. Despite the fact that these structures are present on the neighboring cells' recurrence plots, they are significantly more evident on the non-neighbors recurrence plots.

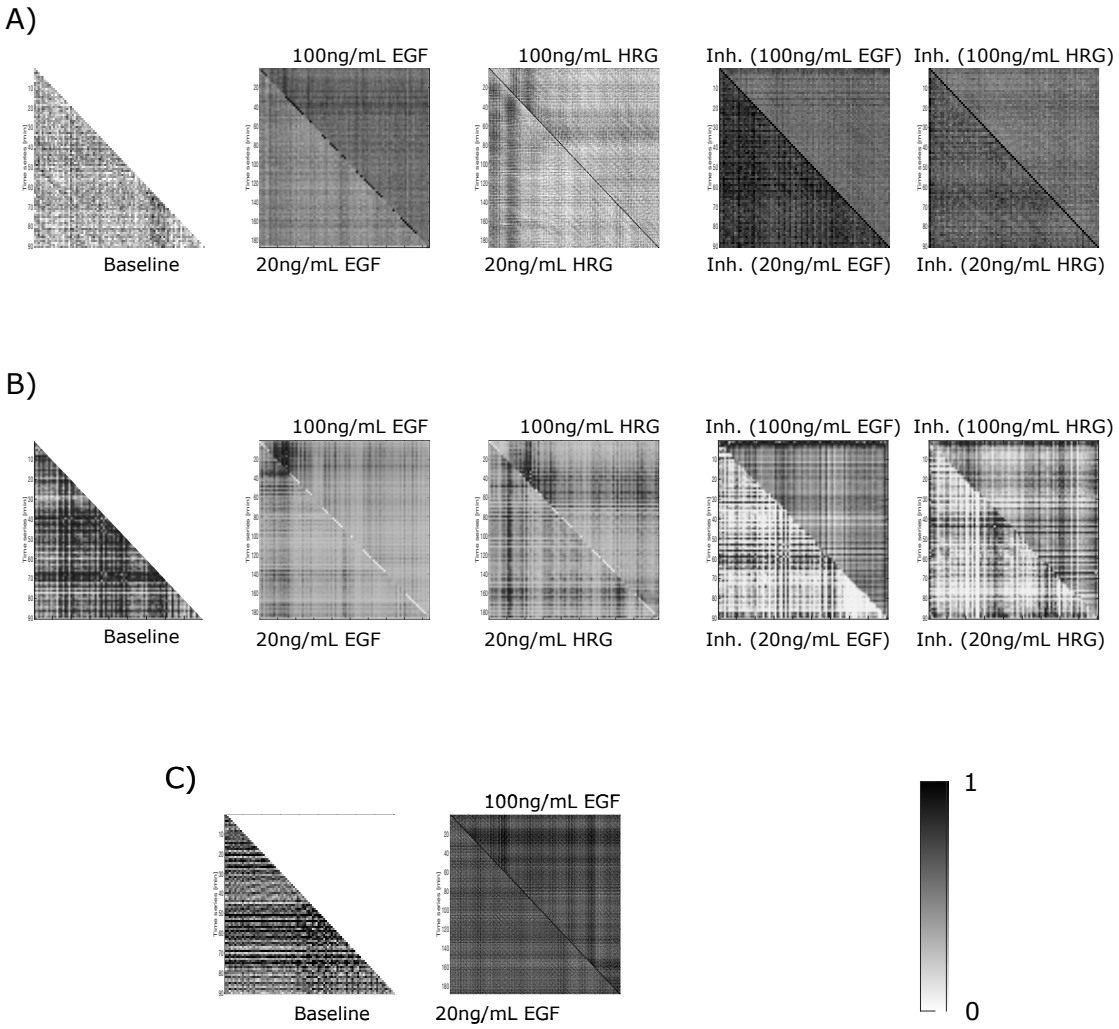

Figure 35. Neighboring and non-neighboring cells ERK dynamics cross-recurrence plots

(A) Unthresholded average cross-recurrence plot (normalized Euclidean distance) associated with the ERK dynamics time series between neighboring cells. From left to right: prior to growth factor stimulation (left), after either 20ng/mL or 100 ng/mL of EGF stimulation, after either 20ng/mL or 100 ng/mL of HRG stimulation (center bottom), after PD0325901 exposure post-stimulation with either 20ng/mL or 100ng/mL of EGF, and after PD0325901 exposure post-stimulation with either 20ng/mL or 100ng/mL of HRG. **(B)** Unthresholded average cross-recurrence plot (normalized Euclidean distance) to the ERK dynamics time series of non-neighboring cells. From left to right: prior to growth factor stimulation (left), after either 20ng/mL or 100 ng/mL of EGF stimulation, after either 20ng/mL or 100 ng/mL of HRG stimulation (center bottom), after PD0325901 exposure post-stimulation with either 20ng/mL or 100ng/mL of EGF, and after PD0325901 exposure post-stimulation with either 20ng/mL or 100ng/mL of HRG. **(C)** Unthresholded average cross-recurrence plot (normalized Euclidean distance) associated with the ERK dynamics time series between neighboring cells treated with Erlotinib prior to growth factor stimulation (left) and after either 20ng/mL or 100 ng/mL of EGF stimulation post-Erlotinib exposure (right).

The corresponding quantification of these recurrence plots is presented below.

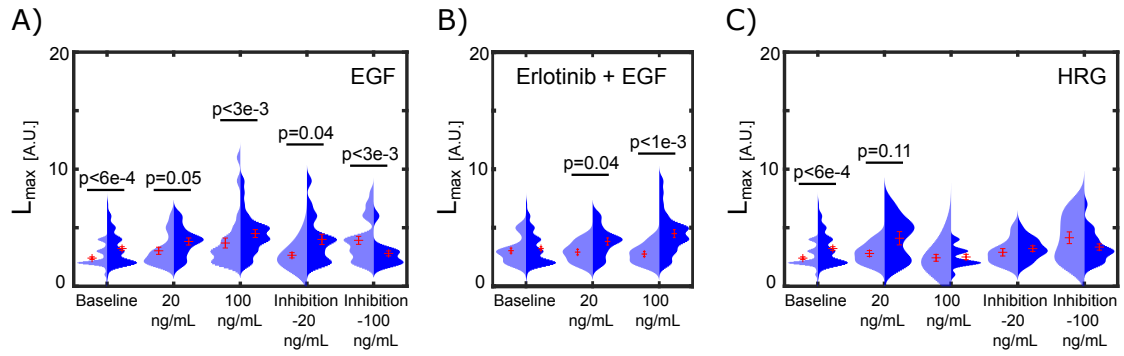

Figure 36. ERK dynamics cross-recurrence maximal length
(A) Composite violin distributions of the maximal cross-recurrence length were measured from thresholded cross-recurrence plots. The left side of the distribution is associated with the non-neighboring cells' maximal cross-recurrence length. The right side corresponds to neighboring cells' maximal cross-recurrence maximal length. Except for the Baseline, all the presented cell groups were treated with either 20ng/mL or 100ng/mL of EGF. **(B)** Composite violin distributions of the maximal cross-recurrence length were measured from thresholded cross-recurrence plots. The left side of the distribution is associated with Erlotinib-treated neighboring cells' maximal cross-recurrence length. The right side corresponds to Erlotinib-untreated neighboring cells' maximal cross-recurrence length. Except for the Baseline, all the presented cell groups were treated with either 20ng/mL or 100ng/mL of EGF. **(C)** Composite violin distributions of the maximal cross-recurrence length were measured from thresholded cross-recurrence plots. The left side of the distribution is associated with the non-neighboring cells' maximal cross-recurrence length. The right side corresponds to neighboring cells' maximal cross-recurrence maximal length. Except for the Baseline, all the presented cell groups were treated with either 20ng/mL or 100ng/mL of HRG.

Table 27. Average maximal cross-recurrence length for EGF-induced ERK dynamics recurrences between neighboring or (*) non-neighboring cells

L_{max} [A.U.]	Baseline *	Baseline	EGF 20ng/mL *	EGF 20ng/mL	EGF 100ng/mL *	EGF 100ng/mL	Inhibition - EGF 20ng/mL *	Inhibition - EGF 20ng/mL	Inhibition - EGF 100ng/mL *	Inhibition - EGF 100ng/mL
Mean +/- SD	2.4+/-1.0	3.3+/-1.3	3.0+/-1.3	3.8+/-1.2	3.6+/-2.2	4.5+/-1.7	4.0+/-1.9	2.6+/-0.9	2.8+/-1.2	3.9+/-1.7

Table 28.Average maximal cross-recurrence length for EGF-induced ERK dynamics recurrences between neighboring cells at Erlotinib-treated or Erlotinib-untreated conditions

L_{max} [A.U.]	Erlotinib Baseline	Baseline	Erlotinib EGF 20ng/mL	EGF 20ng/mL	Erlotinib EGF 100ng/mL	EGF 100ng/mL
Mean +/- SD	3.0+/- 1.0	3.3+/- 1.3	2.9+/- 0.8	3.8+/- 1.2	2.8+/- 0.8	4.5+/- 1.7

Table 29. Average maximal cross-recurrence length for EGF-induced ERK dynamics recurrences between neighboring or (*) non-neighboring cells

L_{max} [A.U.]	Baseline *	Baseline	HRG 20ng/mL *	HRG 20ng/mL	HRG 100ng/mL *	HRG 100ng/mL	Inhibition - HRG 20ng/mL *	Inhibition - HRG 20ng/mL	Inhibition - HRG 100ng/mL *	Inhibition - HRG 100ng/mL
Mean +/- SD	2.4+/- 1.0	3.3+/- 1.3	2.8+/- 0.8	4.1+/- 1.8	2.4+/- 1.1	2.5+/- 0.9	2.9+/- 1.0	3.2+/- 0.9	4.1+/- 1.9	3.3+/- 1.3

Compared to non-neighboring cells, untreated and growth factor stimulated neighboring cells showed longer maximal recurrence lengths. Interestingly, the local cellular environment showed no effect on the maximal cross-recurrence length of cells stimulated with 100ng/mL of HRG. As observed on the recurrence plots, stimulation with a growth factor increased the baseline cross-recurrence length of up to 24% for neighboring cells stimulated with 20ng/mL of HRG. Except for neighboring cells stimulated with 100ng/mL of EGF, inhibition of ERK led to maximal cross-recurrence lengths indistinguishable from the baseline condition. Treating cells with Erlotinib negated the effect of EGF stimulation on the cross-recurrence length between neighboring cells. The cross-recurrence persistence value calculated for Erlotinib treated cells was 10% smaller than that for the untreated neighboring cells.

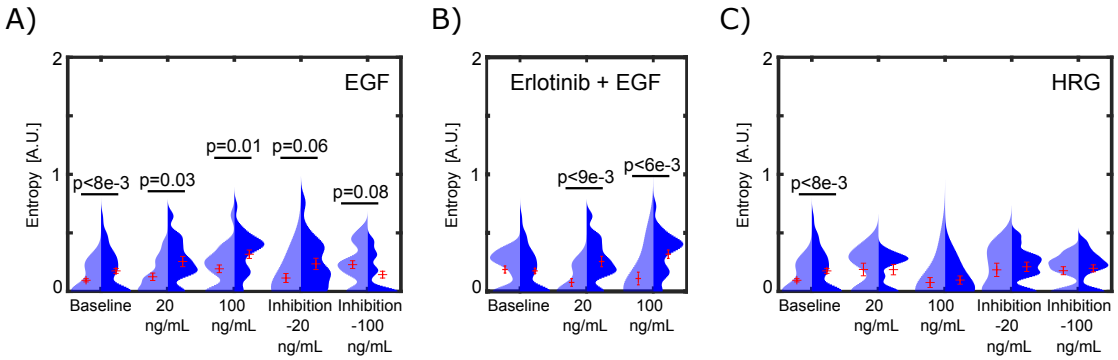

Figure 37. ERK dynamics cross-recurrence entropy
(A) Composite violin distributions of the cross-recurrence entropy were calculated from the recurrence length distribution of thresholded cross-recurrence plots. The left side of the distribution is associated with the cross-recurrence entropy calculated for non-neighboring cells. The right side corresponds to neighboring cells' cross-recurrence entropy. Except for the Baseline, all the presented cell groups were treated with either 20ng/mL or 100ng/mL of EGF. **(B)** Composite violin distributions of the cross-recurrence entropy were calculated from the recurrence length distribution of thresholded cross-recurrence plots. The left side of the distribution is associated with the cross-recurrence entropy calculated for Erlotinib-treated neighboring cells. The right side corresponds to Erlotinib-untreated neighboring cells' cross-recurrence entropy. Except for the Baseline, all the presented cell groups were treated with either 20ng/mL or 100ng/mL of EGF. **(C)** Composite violin distributions of the cross-recurrence entropy were calculated from the recurrence length distribution of thresholded recurrence plots. The left side of the distribution is associated with the cross-recurrence entropy calculated for non-neighboring cells. The right side corresponds to neighboring cells' cross-recurrence entropy. Except for the Baseline, all the presented cell groups were treated with either 20ng/mL or 100ng/mL of HRG.

Table 30. Average cross-recurrence entropy for EGF-induced ERK dynamics recurrences between neighboring or (*) non-neighboring cells

Entr. [A.U.]	Baseline *	Baseline	EGF 20ng/mL *	EGF 20ng/mL	EGF 100ng/mL *	EGF 100ng/mL	Inhibition - EGF 20ng/mL *	Inhibition - EGF 20ng/mL	Inhibition - EGF 100ng/mL *	Inhibition - EGF 100ng/mL
Mean +/- SD	0.09+/-0.11	0.18+/-0.18	0.13+/-0.13	0.26+/-0.18	0.19+/-0.16	0.32+/-0.18	0.11+/-0.16	0.24+/-0.21	0.23+/-0.17	0.14+/-0.16

Table 31. Average cross-recurrence entropy for EGF-induced ERK dynamics recurrences between neighboring cells at Erlotinib-treated or Erlotinib-untreated conditions

$Entr.$ [A.U.]	Erlotinib Baseline	Baseline	Erlotinib EGF 20ng/mL	EGF 20ng/mL	Erlotinib EGF 100ng/mL	EGF 100ng/mL
Mean +/- SD	0.18+/-0.14	0.18+/-0.18	0.08+/-0.11	0.26+/-0.18	0.11+/-0.18	0.32+/-0.18

Table 32. Average cross-recurrence entropy for HRG-induced ERK dynamics recurrences between neighboring or (*) non-neighboring cells

$Entr.$ [A.U.]	Baseline *	Baseline	HRG 20ng/mL *	HRG 20ng/mL	HRG 100ng/mL *	HRG 100ng/mL	Inhibition - HRG 20ng/mL *	Inhibition - HRG 20ng/mL	Inhibition - HRG 100ng/mL *	Inhibition - HRG 100ng/mL
Mean +/- SD	0.09+/-0.11	0.18+/-0.18	0.19+/-0.18	0.19+/-0.14	0.08+/-0.16	0.10+/-0.12	0.18+/-0.18	0.21+/-0.15	0.18+/-0.13	0.20+/-0.14

The local cellular environment also showed an effect on cross-recurrence entropy. However, this effect was only appreciable on untreated cells, and cells stimulated with EGF. Neighboring cells stimulated with HRG and neighboring cells exposed to PD0325901 post-HRG-stimulation showed indistinguishable values of cross-recurrence entropies when compared to their non-neighboring counterparts. In contrast, untreated neighboring cells had one-fold higher cross recurrence entropy values than untreated non-neighboring cells. Stimulation with 20ng/mL or 100ng/mL of EGF resulted in a cross-recurrence entropy increase for neighboring and non-neighboring cells. However, the cross-recurrence entropy of neighboring cells was one-fold higher than the non-neighboring cells for the 20ng/mL stimulated group. Similarly, neighboring cells stimulated with 100ng/mL of EGF showed cross-recurrence entropies approximately 60% higher than their non-neighboring counterparts. Treating cells with Erlotinib resulted in cross-recurrence entropy values

indistinguishable from the untreated neighboring cells group. Nonetheless, opposite to what was observed in untreated cells, stimulating Erlotinib-treated cells with EGF caused a reduction of the cross-recurrence entropy.

3.5.1 Cellular morphodynamical patterns reveal traits of local cellular communication upon stimulation with 20ng/mL of EGF

Similar to ERK dynamics, neighboring cells show cross-recurrences prior to growth factor stimulation. The morphodynamics cross-recurrence lines also become more apparent and elongated once cells are exposed to either EGF or HRG. Their recurrence lines, albeit appreciable shortly after cells are exposed to PD0325901, become dimmer as the exposure continues. The disappearing of recurrence lines implies the randomization of the morphodynamics cross-recurrences between neighboring cells. The discontinuities between neighboring cells' morphodynamics are less appreciable than in ERK dynamics. Similarly, the cross recurrence plots of non-neighboring cells also present fewer cross-like structures than their ERK dynamics counterpart. However, the discontinuities in the cross recurrence plots are more prevalent in the non-neighboring cell morphodynamics than in the neighboring cells.

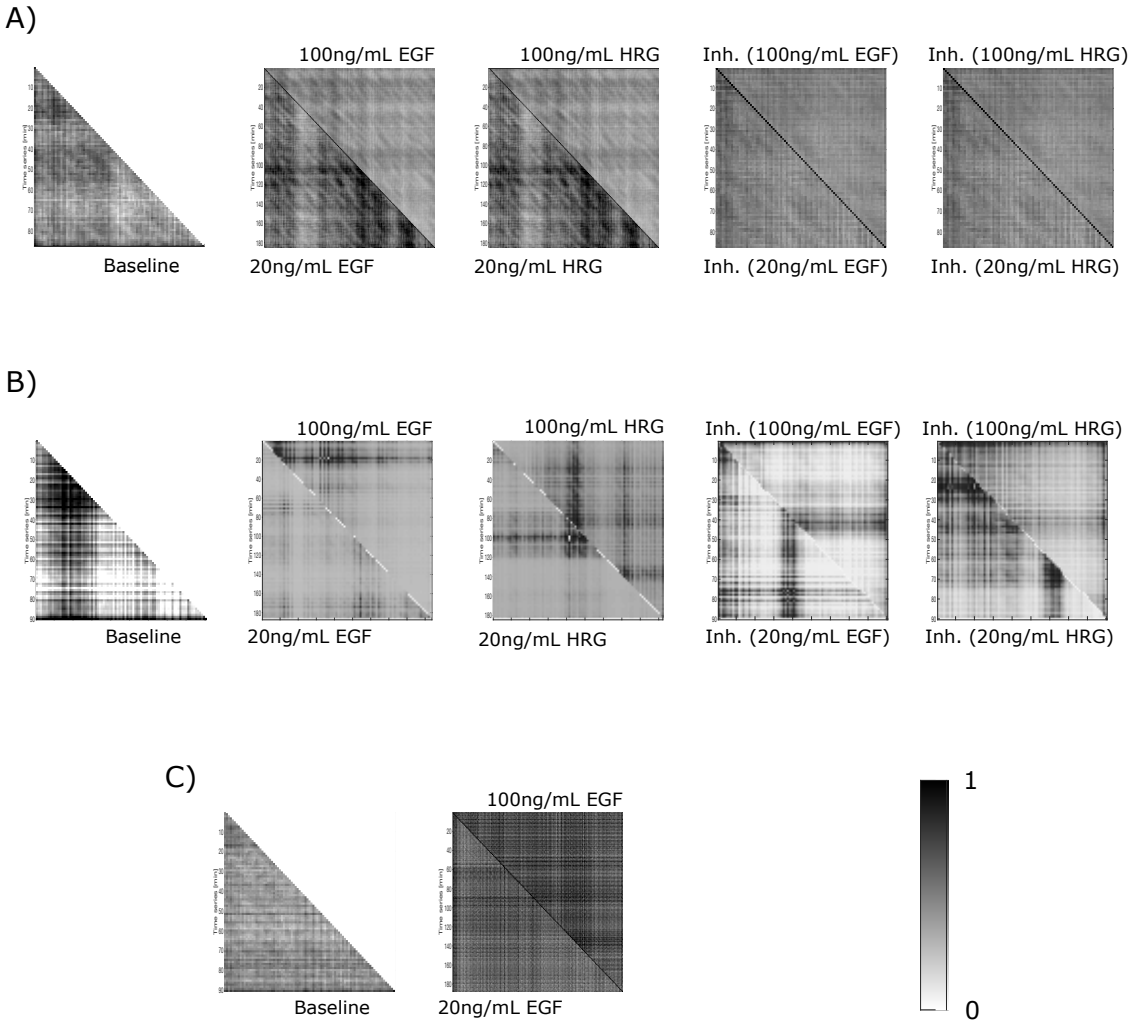

Figure 38. Neighboring and non-neighboring cells cellular morphodynamics cross-recurrence plots

(A) Unthresholded average cross-recurrence plot (normalized Euclidean distance) associated with the cellular morphodynamics time series between neighboring cells. From left to right: prior to growth factor stimulation (left), after either 20ng/mL or 100 ng/mL of EGF stimulation, after either 20ng/mL or 100 ng/mL of HRG stimulation (center bottom), after PD0325901 exposure post-stimulation with either 20ng/mL or 100ng/mL of EGF, and after PD0325901 exposure post-stimulation with either 20ng/mL or 100ng/mL of HRG. **(B)** Unthresholded average cross-recurrence plot (normalized Euclidean distance) to the cellular morphodynamics time series of non-neighboring cells. From left to right: prior to growth factor stimulation (left), after either 20ng/mL or 100 ng/mL of EGF stimulation, after either 20ng/mL or 100 ng/mL of HRG stimulation (center bottom), after PD0325901 exposure post-stimulation with either 20ng/mL or 100ng/mL of EGF, and after PD0325901 exposure post-stimulation with either 20ng/mL or 100ng/mL of HRG. **(C)** Unthresholded average cross-recurrence plot (normalized Euclidean distance) associated with the cellular morphodynamics time series between neighboring cells treated with Erlotinib prior to growth factor stimulation (left) and after either 20ng/mL or 100 ng/mL of EGF stimulation post-Erlotinib exposure (right).

The corresponding quantification of these recurrence plots is presented below.

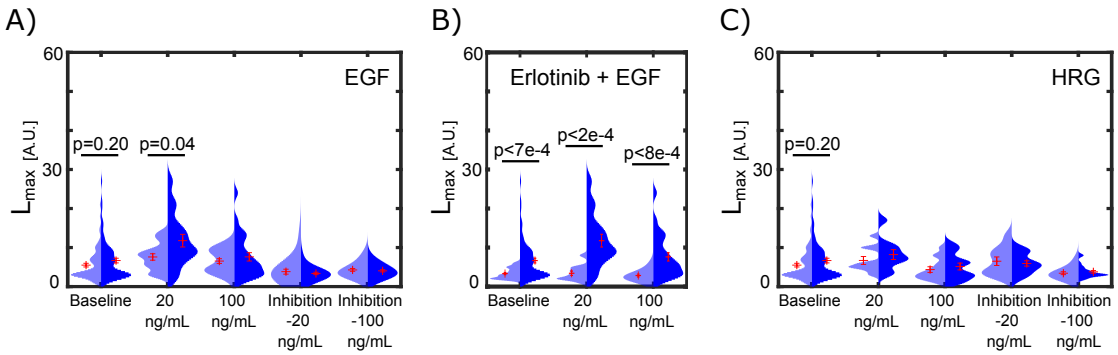

Figure 39. Cellular morphodynamics maximal cross-recurrence length
(A) Composite violin distributions of the maximal cross-recurrence length were measured from thresholded cross-recurrence plots. The left side of the distribution is associated with the non-neighboring cells' maximal cross-recurrence length. The right side corresponds to neighboring cells' maximal cross-recurrence maximal length. Except for the Baseline, all the presented cell groups were treated with either 20ng/mL or 100ng/mL of EGF. **(B)** Composite violin distributions of the maximal cross-recurrence length were measured from thresholded cross-recurrence plots. The left side of the distribution is associated with Erlotinib-treated neighboring cells' maximal cross-recurrence length. The right side corresponds to Erlotinib-untreated neighboring cells' maximal cross-recurrence length. Except for the Baseline, all the presented cell groups were treated with either 20ng/mL or 100ng/mL of EGF. **(C)** Composite violin distributions of the maximal cross-recurrence length were measured from thresholded cross-recurrence plots. The left side of the distribution is associated with the non-neighboring cells' maximal cross-recurrence length. The right side corresponds to neighboring cells' maximal cross-recurrence maximal length. Except for the Baseline, all the presented cell groups were treated with either 20ng/mL or 100ng/mL of HRG.

Table 33. Average maximal cross-recurrence length for EGF-induced cellular morphodynamics recurrences between neighboring or (*) non-neighboring cells

L_{max} [A.U.]	Baseline *	Baseline	EGF 20ng/mL *	EGF 20ng/mL	EGF 100ng/mL *	EGF 100ng/mL	Inhibition - EGF 20ng/mL *	Inhibition - EGF 20ng/mL	Inhibition - EGF 100ng/mL *	Inhibition - EGF 100ng/mL
Mean +/- SD	5.5+/- 4.0	6.7+/- 5.0	7.6+/- 3.4	11.8+/- 6.6	6.5+/- 3.0	7.6+/- 5.4	3.8+/- 2.6	3.4+/- 1.3	4.3+/- 1.8	4.0+/- 1.5

Table 34. Average maximal cross-recurrence length for EGF-induced cellular morphodynamics recurrences between neighboring cells at Erlotinib-treated or Erlotinib-untreated conditions

L_{max} [A.U.]	Erlotinib Baseline	Baseline	Erlotinib EGF 20ng/mL	EGF 20ng/mL	Erlotinib EGF 100ng/mL	EGF 100ng/mL
Mean +/- SD	3.3+/- 1.4	6.7+/- 5.0	3.4+/- 1.9	11.8+/- 6.6	2.8+/- 1.3	7.6+/- 5.4

Table 35. Average maximal cross-recurrence length for EGF-induced cellular morphodynamics recurrences between neighboring or (*) non-neighboring cells

L_{max} [A.U.]	Baseline *	Baseline	HRG 20ng/mL *	HRG 20ng/mL	HRG 100ng/mL *	HRG 100ng/mL	Inhibition - HRG 20ng/mL *	Inhibition - HRG 20ng/mL	Inhibition - HRG 100ng/mL *	Inhibition - HRG 100ng/mL
Mean +/- SD	5.5+/- 4.0	6.7+/- 5.0	6.7+/- 3.2	8.2+/- 4.0	4.4+/- 2.7	5.1+/- 3.3	6.5+/- 3.5	5.9+/- 2.5	3.4+/- 1.4	3.8+/- 1.7

Interestingly, non-neighboring and neighboring cells showed similar maximal cross-recurrence lengths on the baseline condition. Erlotinib-treated neighboring cells had a 50% shorter average maximal recurrence length than the untreated neighboring cells. Additionally, stimulation with 100ng/mL of HRG amount to a decrease in the maximal cross-recurrence length for neighboring and non-neighboring cells. In contrast, stimulation with growth factor, except for the former case, increased maximal cross-recurrence length. This increase ranged from 14% for neighboring cells stimulated with 100ng/mL of EGF to over 70% for neighboring cells stimulated with 20ng/mL of EGF. PD0325901 exposure decreased cross-recurrence maximal lengths in neighboring cells to values below that calculated for the baseline neighboring cells. For cellular morphodynamics, the local environment showed no effect over the maximal cross recurrence lengths on cells stimulated with any concentration of HRG nor on cells stimulated with 100ng/mL of EGF. However, neighboring cells stimulated with 20ng/mL showed maximal cross-recurrence lengths over 70% longer than their

non-neighboring counterparts. Consistent with the trend observed in ERK dynamics, treating cells with Erlotinbi caused the stagnation of the maximal cross-recurrence length. There was no significant change in the cross-recurrence length of neighboring cells treated with Erlotinib after exposure to either 20ng/mL or 100ng/mL of EGF.

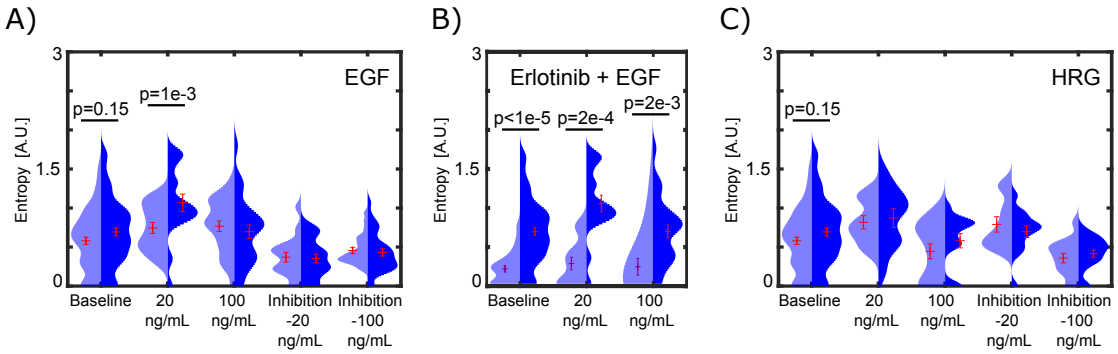

Figure 40. Cellular morphodynamics cross-recurrence entropy
(A) Composite violin distributions of the cross-recurrence entropy were calculated from the recurrence length distribution of thresholded cross-recurrence plots. The left side of the distribution is associated with the cross-recurrence entropy calculated for non-neighboring cells. The right side corresponds to neighboring cells' cross-recurrence entropy. Except for the Baseline, all the presented cell groups were treated with either 20ng/mL or 100ng/mL of EGF. **(B)** Composite violin distributions of the cross-recurrence entropy were calculated from the recurrence length distribution of thresholded cross-recurrence plots. The left side of the distribution is associated with the cross-recurrence entropy calculated for Erlotinib-treated neighboring cells. The right side corresponds to Erlotinib-untreated neighboring cells' cross-recurrence entropy. Except for the Baseline, all the presented cell groups were treated with either 20ng/mL or 100ng/mL of EGF. **(C)** Composite violin distributions of the cross-recurrence entropy were calculated from the recurrence length distribution of thresholded recurrence plots. The left side of the distribution is associated with the cross-recurrence entropy calculated for non-neighboring cells. The right side corresponds to neighboring cells' cross-recurrence entropy. Except for the Baseline, all the presented cell groups were treated with either 20ng/mL or 100ng/mL of HRG.

Table 36. Average cross-recurrence entropy for EGF-induced cellular morphodynamics recurrences between neighboring or (*) non-neighboring cells

Entr. **[A.U.]**	**Baseline ***	**Baseline**	**EGF 20ng/mL ***	**EGF 20ng/mL**	**EGF 100ng/mL ***	**EGF 100ng/mL**	**Inhibition - EGF 20ng/mL ***	**Inhibition - EGF 20ng/mL**	**Inhibition - EGF 100ng/mL ***	**Inhibition - EGF 100ng/mL**
Mean +/- SD	0.58+/-0.39	0.69+/-0.44	0.74+/-0.28	1.10+/-0.45	0.77+/-0.34	0.70+/-0.43	0.37+/-0.26	0.35+/-0.25	0.45+/-0.19	0.43+/-0.26

Table 37. Average cross-recurrence entropy for EGF-induced cellular morphodynamics recurrences between neighboring cells at Erlotinib-treated or Erlotinib-untreated conditions

$Entr.$ [A.U.]	Erlotinib Baseline	Baseline	Erlotinib EGF 20ng/mL	EGF 20ng/mL	Erlotinib EGF 100ng/mL	EGF 100ng/mL
Mean +/- SD	0.20+/-0.20	0.69+/-0.44	0.27+/-0.29	1.10+/-0.45	0.23+/-0.39	0.70+/-0.43

Table 38. Average cross-recurrence entropy for HRG-induced cellular morphodynamics recurrences between neighboring or (*) non-neighboring cells

$Entr.$ [A.U.]	Baseline *	Baseline	HRG 20ng/mL *	HRG 20ng/mL	HRG 100ng/mL *	HRG 100ng/mL	Inhibition - HRG 20ng/mL *	Inhibition - HRG 20ng/mL	Inhibition - HRG 100ng/mL *	Inhibition - HRG 100ng/mL
Mean +/- SD	0.58+/-0.39	0.69+/-0.44	0.82+/-0.27	0.87+/-0.38	0.44+/-0.36	0.58+/-0.34	0.80+/-0.31	0.70+/-0.28	0.36+/-0.23	0.42+/-0.21

Except for cells stimulated with 100ng/mL of HRG, growth factor exposure led to an overall increase in the cross-recurrence entropy. In this case, 100mg/mL of HRG led neighboring cells to have an approximately 15% smaller entropy than the baseline neighboring cells. Conversely, ERK-Inhibition via PD0325901 amounted to a decrease in cross-recurrence entropy. Interestingly, among all the experimental conditions, only neighboring cells stimulated with 20ng/mL of EGF had a significantly higher cross-recurrence entropy than their non-neighboring counterparts. Coincidently, the morphodynamics cross-recurrence entropy of untreated neighboring cells increased by approximately 60% after the stimulation with 20ng/mL of EGF. Stimulating cells with 20ng/mL of EGF resulted in the maximal increase in cross-recurrence entropy

compared to all experimental conditions. On the other hand, neighboring cells treated with Erlotinib had a cross-recurrence entropy over two-fold smaller than the neighboring cells at the baseline condition. Furthermore, stimulating Erlotinib-treated neighboring cells with 20 ng/mL or 100ng/mL had no significant effect on the cross-recurrence entropy value. In addition, the cross-recurrence entropy of these two groups was significantly smaller than their Erlotinib-untreated counterparts.

4 Discussion

There is an open argument about which components of the ERK signaling network are crucial for its robustness and what type of information is encrypted in its signal (Kochańczyk et al., 2017; Obatake et al., 2019; Ryu et al., 2015; Shankaran et al., 2009; Shankaran and Wiley, 2010; Waters et al., 2014). However, ERK dynamics and the different regularities embedded within these dynamics are widely used for cell-fate predictions. Furthermore, although cytoplasmic ERK comprises a richer dynamic behavior, nuclear ERK has been more widely described. However, according to the literature and our previous results (Brüggemann et al., 2021), cytoplasmic ERK can be used to track its ligand-specific behavior as well as different cell-fate decisions (Ryu et al., 2015; Shankaran et al., 2009). In addition, evidence on its ligand-specific behavior is still being gathered (Arkun and Yasemi, 2018; Kuchenov et al., 2016; Liu et al., 2011)

The difference in ERK rise time and maximal ERK activation speed between neighboring and non-neighboring cells suggests that the cellular environment has a significant effect on the reaction of cells to a global stimulus like growth factor stimulation. Considering the higher synchrony between neighboring sheds light on the possibility of continuous local communication between cells and how this process shapes the internal stage of the cellular signaling networks. Interestingly, stimulation with EGF had a more significant effect on the maximal ERK activation speed synchronization between neighboring cells. Coincidently, the existence of EGF-producing genes in MCF-7 cells has been reported. In contrast, HRG-producing genes have not been found on the same cells (Garnett et al., 2012; Klijn et al., 2015; Santos et al., 2015). The presence of endogenous EGF in the cellular environment could be a channel for local communication between MCF-7 cells.

The recurrence analysis of ERK high-frequency components revealed information concerning the cellular environment embedded within. Similarities between the optimal time delay and the minimal embedded dimensions imply a consequent dynamic behavior. Growth factor stimulation did not appear to modify ERK dynamic components significantly. In contrast, exposure to either Erlotinib caused a

slight reduction in the optimal time delay and the minimal embedded dimensions, which hints at the loss of dynamic components in ERK dynamics. The increase in the maximal ERK recurrence length results from more persistent recurrence states on ERK dynamics after growth factor stimulation. In addition, the increase in ERK recurrence entropy reveals a more uniformly distributed occurrence of recurrences. A higher persistence of ERK recurrences and more uniformly distributed recurrences suggest the coordination of ERK-mediated mechanisms towards cell-fate decisions.

Similarly, recurrence analysis also highlighted cellular environment relevant information embedded in cellular morphodynamics high-frequency components. The optimal time delay calculated for the fast-occurring events in ERK dynamics and cellular morphodynamics were insignificantly different for the unstimulated condition. Furthermore, they only differed in an average of one time-point for stimulated conditions. These similitudes suggest the existence of a fast-occurring nexus between cellular morphodynamics and ERK dynamics. The increase in cellular morphodynamics recurrence persistence combined with the higher optimal time delay calculated for growth factor-stimulated cells could result from the increased membrane activity observed in cells after exposure to either EGF or HRG. Moreover, the increased entropy confirms the presence of more uniformly distributed diverse membrane structural modifications upon stimulation. Interestingly, cells treated with PD0325901 after being stimulated with 20 ng/mL of HRG showed a significant membrane retraction which could be why this group had an entropy higher than the other cells exposed to the MEK-inhibitor.

Although the sporadic connection between ERK dynamics and cellular morphodynamics has been well documented, our results suggest the existence of a continuous link between these two dynamics. The congruence between cellular morphodynamic and ERK dynamic already exists in unstimulated cells, and its persistence increases upon growth factor stimulation. Perturbing ERK dynamics with the MEK-inhibitor decreased the stability of this congruence, whereas treating cells with Erlotinib fixated stopped the colocalization from strengthening. Intriguingly stimulating cells with 100ng/mL of HRG showed a decrease in the ERK dynamics - cellular dynamics cross recurrence, which could be attributed to the fact that HRG has been strongly linked with Akt activation. Based on our previous results, the EGF effect

on AKT is short-lived (Brüggemann et al., 2021). In contrast, HRG induces sustained activation of the protein. The recurrence entropy trend hints that stimulation with 20ng/mL of either HRG or EGF has little effect on the distribution of ERK dynamics - cellular morphodynamic entropies. This lack of change in cross-recurrence entropy suggests that lower growth factor concentrations have a less invasive effect on the pre-existing cellular processes.

Quantified by longer maximal cross-recurrence lengths, the cellular environment plays a significant role in the ERK dynamics synchronization cells. Neighboring cells at the baseline condition already show signs of higher synchronization when compared to their non-neighboring counterpart. This trend is maintained when cells are stimulated with either EGF or 20ng/mL of HRG. In contrast, compared to the baseline condition, treating cells with Erlotinib did not significantly affect the ability of neighboring cells to have synchronized ERK dynamics. Neighboring cells' ability to synchronize despite their exposure to Erlotinib could be related to the residual effect of the local environment on cells and the reaction time for Erlotinib's input to take full effect (Abdelgalil et al., 2020; Moyer et al., 1997). Nonetheless, Erlotinib effectively stopped the ability of neighboring cells to synchronize after EFG stimulation. ERK cross recurrence entropies are the quantification of the degree of cellular communication diversity. Compared to non-neighboring untreated cells, The higher values of ERK cross recurrence entropies between their neighboring counterparts imply a more diversified cellular communication. Furthermore, it suggests that cellular synchronization, and consequently cellular communication, is a continuous process intrinsic to cellular behavior. Stimulation with EGF did not impede nor hinder communication between neighboring cells. Thus, EGF appears to provide an effective channel for diverse local cellular communication.

Similarly, cross-recurrence analysis of neighboring cells' morphodynamics corroborated the importance of the local environment on cellular communication. This effect was less apparent on untreated cells than on cells exposed to growth factors, possibly due to the passivity of the cellular membrane. In contrast, Erlotinib treatment disturbed the local cellular communication even at the baseline condition. Once exposed to 20ng/mL of EGF, the synchronization between neighboring cells was significantly higher than the non-neighboring cells. Consistently, the morphodynamics

cross-recurrence entropy between neighboring cells stimulated with 20ng/mL of EGF showed significantly higher values than its non-neighboring equivalents. Thus, 20ng/mL of EGF appears to guarantee an effective means for morphodynamic synchronization between neighboring cells.

Extracting the high-frequency components from the original ERK dynamics and cellular morphodynamics time series effectively separated the global from the local stimulus. Furthermore, the results of our recurrence analysis confirmed the existence of biologically relevant information in the high-frequency components of ERK dynamics and cellular morphodynamics. The congruence of these recurrences suggests the inseparability of ERK dynamics from cellular morphodynamics. However, the cellular environment plays a significant role in cellular responses to growth factors. Nonetheless, this influence mainly prevails after stimulation with low concentrations of growth factors. Only low concentrations of EGF appear to allow effective cellular communication between neighboring cells.

5 Bibliography

Abdelgalil, A.A., Al-Kahtani, H.M., Al-Jenoobi, F.I., 2020. Erlotinib. Profiles Drug Subst. Excip. Relat. Methodol. 45, 93–117. https://doi.org/10.1016/bs.podrm.2019.10.004

Agell, N., Bachs, O., Rocamora, N., Villalonga, P., 2002. Modulation of the Ras/Raf/MEK/ERK pathway by Ca(2+), and calmodulin. Cell. Signal. 14, 649–654. https://doi.org/10.1016/s0898-6568(02)00007-4

Albanese, C., Johnson, J., Watanabe, G., Eklund, N., Vu, D., Arnold, A., Pestell, R.G., 1995. Transforming p21ras Mutants and c-Ets-2 Activate the Cyclin D1 Promoter through Distinguishable Regions (∗). J. Biol. Chem. 270, 23589–23597. https://doi.org/10.1074/jbc.270.40.23589

Albeck, J.G., Mills, G.B., Brugge, J.S., 2013. Frequency-modulated pulses of ERK activity transmit quantitative proliferation signals. Mol. Cell 49, 249–261. https://doi.org/10.1016/j.molcel.2012.11.002

Allan, L.A., Morrice, N., Brady, S., Magee, G., Pathak, S., Clarke, P.R., 2003. Inhibition of caspase-9 through phosphorylation at Thr 125 by ERK MAPK. Nat. Cell Biol. 5, 647–654. https://doi.org/10.1038/ncb1005

Arkun, Y., Yasemi, M., 2018. Dynamics and control of the ERK signaling pathway: Sensitivity, bistability, and oscillations. PLOS ONE 13, e0195513. https://doi.org/10.1371/journal.pone.0195513

Atkins, C.M., Selcher, J.C., Petraitis, J.J., Trzaskos, J.M., Sweatt, J.D., 1998. The MAPK cascade is required for mammalian associative learning. Nat. Neurosci. 1, 602–609. https://doi.org/10.1038/2836

Bakhoum, S.F., Cantley, L.C., 2018. The Multifaceted Role of Chromosomal Instability in Cancer and Its Microenvironment. Cell 174, 1347–1360. https://doi.org/10.1016/j.cell.2018.08.027

Balañá, M.E., Lupu, R., Labriola, L., Charreau, E.H., Elizalde, P.V., 1999. Interactions between progestins and heregulin (HRG) signaling pathways: HRG acts as mediator of progestins proliferative effects in mouse mammary adenocarcinomas. Oncogene 18, 6370–6379. https://doi.org/10.1038/sj.onc.1203028

Bastiaens, P., Birtwistle, M.R., Blüthgen, N., Bruggeman, F.J., Cho, K.-H., Cosentino, C., de la Fuente, A., Hoek, J.B., Kiyatkin, A., Klamt, S., Kolch, W., Legewie, S., Mendes, P., Naka, T., Santra, T., Sontag, E., Westerhoff, H.V., Kholodenko, B.N., 2015. Silence on the relevant literature and errors in implementation. Nat. Biotechnol. 33, 336–339. https://doi.org/10.1038/nbt.3185

Baumdick, M., Brüggemann, Y., Schmick, M., Xouri, G., Sabet, O., Davis, L., Chin, J.W., Bastiaens, P.I., 2015. EGF-dependent re-routing of vesicular recycling switches spontaneous phosphorylation suppression to EGFR signaling. eLife 4, e12223. https://doi.org/10.7554/eLife.12223

Baumdick, M., Gelléri, M., Uttamapinant, C., Beránek, V., Chin, J.W., Bastiaens, P.I.H., 2018. A conformational sensor based on genetic code expansion reveals an autocatalytic component in EGFR activation. Nat. Commun. 9, 3847. https://doi.org/10.1038/s41467-018-06299-7

Bergeron, J.J.M., Di Guglielmo, G.M., Dahan, S., Dominguez, M., Posner, B.I., 2016. Spatial and Temporal Regulation of Receptor Tyrosine Kinase Activation and Intracellular Signal Transduction. Annu. Rev. Biochem. 85, 573–597. https://doi.org/10.1146/annurev-biochem-060815-014659

Bertelsen, V., Stang, E., 2014. The Mysterious Ways of ErbB2/HER2 Trafficking. Membranes 4, 424–446. https://doi.org/10.3390/membranes4030424

Birtwistle, M.R., Hatakeyama, M., Yumoto, N., Ogunnaike, B.A., Hoek, J.B., Kholodenko, B.N., 2007. Ligand-dependent responses of the ErbB signaling network: experimental and modeling analyses. Mol. Syst. Biol. 3, 144. https://doi.org/10.1038/msb4100188

Blüthgen, N., 2015. Signaling output: it's all about timing and feedbacks. Mol. Syst. Biol. 11, 843. https://doi.org/10.15252/msb.20156642

Blüthgen, N., Herzel, H., 2003. How robust are switches in intracellular signaling cascades? J. Theor. Biol. 225, 293–300. https://doi.org/10.1016/s0022-5193(03)00247-9

Bonni, A., Brunet, A., West, A.E., Datta, S.R., Takasu, M.A., Greenberg, M.E., 1999. Cell Survival Promoted by the Ras-MAPK Signaling Pathway by Transcription-Dependent and -Independent Mechanisms. Science 286, 1358–1362. https://doi.org/10.1126/science.286.5443.1358

Bourguignon, L.Y.W., Gilad, E., Peyrollier, K., 2007. Heregulin-mediated ErbB2-ERK signaling activates hyaluronan synthases leading to CD44-dependent ovarian tumor cell growth and migration. J. Biol. Chem. 282, 19426–19441. https://doi.org/10.1074/jbc.M610054200

Brahmbhatt, A.A., Klemke, R.L., 2003. ERK and RhoA Differentially Regulate Pseudopodia Growth and Retraction during Chemotaxis*. J. Biol. Chem. 278, 13016–13025. https://doi.org/10.1074/jbc.M211873200

Brandman, O., Ferrell, J.E.J., Li, R., Meyer, T., 2005. Interlinked fast and slow positive feedback loops drive reliable cell decisions. Science 310, 496–498. https://doi.org/10.1126/science.1113834

Brick, T.R., Gray, A.L., Staples, A.D., 2017. Recurrence Quantification for the Analysis of Coupled Processes in Aging. J. Gerontol. B. Psychol. Sci. Soc. Sci. 73, 134–147. https://doi.org/10.1093/geronb/gbx018

Bruggeman, F.J., Blüthgen, N., Westerhoff, H.V., 2009. Noise management by molecular networks. PLoS Comput. Biol. 5, e1000506. https://doi.org/10.1371/journal.pcbi.1000506

Brüggemann, Y., Karajannis, L.S., Stanoev, A., Stallaert, W., Bastiaens, P.I.H., 2021. Growth factor–dependent ErbB vesicular dynamics couple receptor signaling to spatially and functionally distinct Erk pools. Sci. Signal. 14, eabd9943. https://doi.org/10.1126/scisignal.abd9943

Brumbaugh, J., Russell, J.D., Yu, P., Westphall, M.S., Coon, J.J., Thomson, J.A., 2014. NANOG Is Multiply Phosphorylated and Directly Modified by ERK2 and CDK1 In Vitro. Stem Cell Rep. 2, 18–25. https://doi.org/10.1016/j.stemcr.2013.12.005

Burdon, T., Stracey, C., Chambers, I., Nichols, J., Smith, A., 1999. Suppression of SHP-2 and ERK Signalling Promotes Self-Renewal of Mouse Embryonic Stem Cells. Dev. Biol. 210, 30–43. https://doi.org/10.1006/dbio.1999.9265

Bywater, M.J., Pearson, R.B., McArthur, G.A., Hannan, R.D., 2013. Dysregulation of the basal RNA polymerase transcription apparatus in cancer. Nat. Rev. Cancer 13, 299–314. https://doi.org/10.1038/nrc3496

C. E. Shannon, 1948. A mathematical theory of communication. Bell Syst. Tech. J. 27, 379–423. https://doi.org/10.1002/j.1538-7305.1948.tb01338.x

Cao, L., 1997. Practical method for determining the minimum embedding dimension of a scalar time series. Phys. Nonlinear Phenom. 110, 43–50. https://doi.org/10.1016/S0167-2789(97)00118-8

Cargnello, M., Roux, P.P., 2011. Activation and function of the MAPKs and their substrates, the MAPK-activated protein kinases. Microbiol. Mol. Biol. Rev. MMBR 75, 50–83. https://doi.org/10.1128/MMBR.00031-10

Carrière, A., Cargnello, M., Julien, L.-A., Gao, H., Bonneil, É., Thibault, P., Roux, P.P., 2008. Oncogenic MAPK Signaling Stimulates mTORC1 Activity by Promoting RSK-Mediated Raptor Phosphorylation. Curr. Biol. 18, 1269–1277. https://doi.org/10.1016/j.cub.2008.07.078

Case, L.B., Waterman, C.M., 2015. Integration of actin dynamics and cell adhesion by a three-dimensional, mechanosensitive molecular clutch. Nat. Cell Biol. 17, 955–963. https://doi.org/10.1038/ncb3191

Cedervall, J., Zhang, Y., Ringvall, M., Thulin, Å., Moustakas, A., Jahnen-Dechent, W., Siegbahn, A., Olsson, A.-K., 2013. HRG regulates tumor progression, epithelial to mesenchymal transition and metastasis via platelet-induced signaling in the

pre-tumorigenic microenvironment. Angiogenesis 16, 889–902. https://doi.org/10.1007/s10456-013-9363-8

Chang, Y.-T., Shu, C.-L., Fukui, Y., 2013. Activation of the MEK pathway is required for complete scattering of MCF7 cells stimulated with heregulin-β1. Biochem. Biophys. Res. Commun. 433, 311–316. https://doi.org/10.1016/j.bbrc.2013.02.103

Chen, J.-Y., Lin, J.-R., Cimprich, K.A., Meyer, T., 2012. A Two-Dimensional ERK-AKT Signaling Code for an NGF-Triggered Cell-Fate Decision. Mol. Cell 45, 196–209. https://doi.org/10.1016/j.molcel.2011.11.023

Chen, L., Willis, S.N., Wei, A., Smith, B.J., Fletcher, J.I., Hinds, M.G., Colman, P.M., Day, C.L., Adams, J.M., Huang, D.C.S., 2005. Differential Targeting of Prosurvival Bcl-2 Proteins by Their BH3-Only Ligands Allows Complementary Apoptotic Function. Mol. Cell 17, 393–403. https://doi.org/10.1016/j.molcel.2004.12.030

De Donatis, A., Comito, G., Buricchi, F., Vinci, M.C., Parenti, A., Caselli, A., Camici, G., Manao, G., Ramponi, G., Cirri, P., 2008. Proliferation Versus Migration in Platelet-derived Growth Factor Signaling. J. Biol. Chem. 283, 19948–19956. https://doi.org/10.1074/jbc.M709428200

Deschênes-Simard, X., Kottakis, F., Meloche, S., Ferbeyre, G., 2014. ERKs in Cancer: Friends or Foes? Cancer Res. 74, 412–419. https://doi.org/10.1158/0008-5472.CAN-13-2381

Deshpande, D., Toledo-Velasquez, D., Thakkar, D., Liang, W., Rojanasakul, Y., 1996. Enhanced cellular uptake of oligonucleotides by EGF receptor-mediated endocytosis in A549 cells. Pharm. Res. 13, 57–61. https://doi.org/10.1023/a:1016073132320

Dessauges, C., Mikelson, J., Dobrzyński, M., Jacques, M.-A., Frismantiene, A., Gagliardi, P.A., Khammash, M., Pertz, O., 2022. Optogenetic actuator - ERK biosensor circuits identify MAPK network nodes that shape ERK dynamics. Mol. Syst. Biol. 18, e10670. https://doi.org/10.15252/msb.202110670

Dhaliwal, N.K., Miri, K., Davidson, S., Tamim El Jarkass, H., Mitchell, J.A., 2018. KLF4 Nuclear Export Requires ERK Activation and Initiates Exit from Naive Pluripotency. Stem Cell Rep. 10, 1308–1323. https://doi.org/10.1016/j.stemcr.2018.02.007

Dinsmore, C.J., Soriano, P., 2018. MAPK and PI3K signaling: At the crossroads of neural crest development. Dev. Biol. 444 Suppl 1, S79–S97. https://doi.org/10.1016/j.ydbio.2018.02.003

Drosten, M., Dhawahir, A., Sum, E.Y.M., Urosevic, J., Lechuga, C.G., Esteban, L.M., Castellano, E., Guerra, C., Santos, E., Barbacid, M., 2010. Genetic analysis of

Ras signalling pathways in cell proliferation, migration and survival. EMBO J. 29, 1091–1104. https://doi.org/10.1038/emboj.2010.7

Eblen, S.T., Slack-Davis, J.K., Tarcsafalvi, A., Parsons, J.T., Weber, M.J., Catling, A.D., 2004. Mitogen-activated protein kinase feedback phosphorylation regulates MEK1 complex formation and activation during cellular adhesion. Mol. Cell. Biol. 24, 2308–2317. https://doi.org/10.1128/MCB.24.6.2308-2317.2004

Eckmann, J.-P., Kamphorst, S.O., Ruelle, D., 1987. Recurrence Plots of Dynamical Systems. Europhys. Lett. EPL 4, 973–977. https://doi.org/10.1209/0295-5075/4/9/004

Edlich, F., 2018. BCL-2 proteins and apoptosis: Recent insights and unknowns. Mitochondrial Dyn. 500, 26–34. https://doi.org/10.1016/j.bbrc.2017.06.190

Ersahin, T., Tuncbag, N., Cetin-Atalay, R., 2015. The PI3K/AKT/mTOR interactive pathway. Mol. Biosyst. 11, 1946–1954. https://doi.org/10.1039/c5mb00101c

Fábián, Z., Ramadurai, S., Shaw, G., Nasheuer, H.-P., Kolch, W., Taylor, C., Barry, F., 2014. Basic fibroblast growth factor modifies the hypoxic response of human bone marrow stromal cells by ERK-mediated enhancement of HIF-1α activity. Stem Cell Res. 12, 646–658. https://doi.org/10.1016/j.scr.2014.02.007

Fowler, T., Sen, R., Roy, A.L., 2011. Regulation of Primary Response Genes. Mol. Cell 44, 348–360. https://doi.org/10.1016/j.molcel.2011.09.014

Fraser, A.M., Swinney, H.L., 1986. Independent coordinates for strange attractors from mutual information. Phys. Rev. A 33, 1134–1140. https://doi.org/10.1103/PhysRevA.33.1134

Freed, D.M., Bessman, N.J., Kiyatkin, A., Salazar-Cavazos, E., Byrne, P.O., Moore, J.O., Valley, C.C., Ferguson, K.M., Leahy, D.J., Lidke, D.S., Lemmon, M.A., 2017. EGFR Ligands Differentially Stabilize Receptor Dimers to Specify Signaling Kinetics. Cell 171, 683-695.e18. https://doi.org/10.1016/j.cell.2017.09.017

Fritsche-Guenther, R., Witzel, F., Sieber, A., Herr, R., Schmidt, N., Braun, S., Brummer, T., Sers, C., Blüthgen, N., 2011. Strong negative feedback from Erk to Raf confers robustness to MAPK signalling. Mol. Syst. Biol. 7, 489. https://doi.org/10.1038/msb.2011.27

Fritz, R.D., Letzelter, M., Reimann, A., Martin, K., Fusco, L., Ritsma, L., Ponsioen, B., Fluri, E., Schulte-Merker, S., van Rheenen, J., Pertz, O., 2013. A Versatile Toolkit to Produce Sensitive FRET Biosensors to Visualize Signaling in Time and Space. Sci. Signal. 6. https://doi.org/10.1126/scisignal.2004135

Fuentealba, L.C., Eivers, E., Ikeda, A., Hurtado, C., Kuroda, H., Pera, E.M., De Robertis, E.M., 2007. Integrating Patterning Signals: Wnt/GSK3 Regulates the

Duration of the BMP/Smad1 Signal. Cell 131, 980–993. https://doi.org/10.1016/j.cell.2007.09.027

Garnett, M.J., Edelman, E.J., Heidorn, S.J., Greenman, C.D., Dastur, A., Lau, K.W., Greninger, P., Thompson, I.R., Luo, X., Soares, J., Liu, Q., Iorio, F., Surdez, D., Chen, L., Milano, R.J., Bignell, G.R., Tam, A.T., Davies, H., Stevenson, J.A., Barthorpe, S., Lutz, S.R., Kogera, F., Lawrence, K., McLaren-Douglas, A., Mitropoulos, X., Mironenko, T., Thi, H., Richardson, L., Zhou, W., Jewitt, F., Zhang, T., O'Brien, P., Boisvert, J.L., Price, S., Hur, W., Yang, W., Deng, X., Butler, A., Choi, H.G., Chang, J.W., Baselga, J., Stamenkovic, I., Engelman, J.A., Sharma, S.V., Delattre, O., Saez-Rodriguez, J., Gray, N.S., Settleman, J., Futreal, P.A., Haber, D.A., Stratton, M.R., Ramaswamy, S., McDermott, U., Benes, C.H., 2012. Systematic identification of genomic markers of drug sensitivity in cancer cells. Nature 483, 570–575. https://doi.org/10.1038/nature11005

Gavriljuk, K., Scocozza, B., Ghasemalizadeh, F., Seidel, H., Nandan, A.P., Campos-Medina, M., Schmick, M., Koseska, A., Bastiaens, P.I.H., 2021. A self-organized synthetic morphogenic liposome responds with shape changes to local light cues. Nat. Commun. 12, 1548. https://doi.org/10.1038/s41467-021-21679-2

Ghosh, A., Awasthi, S., Hamburger, A.W., 2013. ErbB3-binding protein EBP1 decreases ErbB2 levels via a transcriptional mechanism. Oncol. Rep. 29, 1161–1166. https://doi.org/10.3892/or.2012.2186

Ginzberg, M.B., Kafri, R., Kirschner, M., 2015. On being the right (cell) size. Science 348, 1245075. https://doi.org/10.1126/science.1245075

Good, M., Tang, G., Singleton, J., Reményi, A., Lim, W.A., 2009. The Ste5 scaffold directs mating signaling by catalytically unlocking the Fus3 MAP kinase for activation. Cell 136, 1085–1097. https://doi.org/10.1016/j.cell.2009.01.049

Gornale, S.S., Patravali, P.U., Hiremath, P.S., 2020. Automatic Detection and Classification of Knee Osteoarthritis Using Hu's Invariant Moments. Front. Robot. AI 7, 591827. https://doi.org/10.3389/frobt.2020.591827

Graves, L.M., Guy, H.I., Kozlowski, P., Huang, M., Lazarowski, E., Pope, R.M., Collins, M.A., Dahlstrand, E.N., Earp, H.S., Evans, D.R., 2000. Regulation of carbamoyl phosphate synthetase by MAP kinase. Nature 403, 328–332. https://doi.org/10.1038/35002111

Grecco, H.E., Schmick, M., Bastiaens, P.I.H., 2011. Signaling from the Living Plasma Membrane. Cell 144, 897–909. https://doi.org/10.1016/j.cell.2011.01.029

Guo, Y., Pan, W., Liu, S., Shen, Z., Xu, Y., Hu, L., 2020. ERK/MAPK signalling pathway and tumorigenesis (Review). Exp. Ther. Med. https://doi.org/10.3892/etm.2020.8454

Haq, R., Shoag, J., Andreu-Perez, P., Yokoyama, S., Edelman, H., Rowe, G.C., Frederick, D.T., Hurley, A.D., Nellore, A., Kung, A.L., Wargo, J.A., Song, J.S., Fisher, D.E., Arany, Z., Widlund, H.R., 2013. Oncogenic BRAF Regulates Oxidative Metabolism via PGC1α and MITF. Cancer Cell 23, 302–315. https://doi.org/10.1016/j.ccr.2013.02.003

Harding, A., Tian, T., Westbury, E., Frische, E., Hancock, J.F., 2005. Subcellular localization determines MAP kinase signal output. Curr. Biol. CB 15, 869–873. https://doi.org/10.1016/j.cub.2005.04.020

Herrero, A., Pinto, A., Colón-Bolea, P., Casar, B., Jones, M., Agudo-Ibáñez, L., Vidal, R., Tenbaum, S.P., Nuciforo, P., Valdizán, E.M., Horvath, Z., Orfi, L., Pineda-Lucena, A., Bony, E., Keri, G., Rivas, G., Pazos, A., Gozalbes, R., Palmer, H.G., Hurlstone, A., Crespo, P., 2015. Small Molecule Inhibition of ERK Dimerization Prevents Tumorigenesis by RAS-ERK Pathway Oncogenes. Cancer Cell 28, 170–182. https://doi.org/10.1016/j.ccell.2015.07.001

Herzig, S., Shaw, R.J., 2018. AMPK: guardian of metabolism and mitochondrial homeostasis. Nat. Rev. Mol. Cell Biol. 19, 121–135. https://doi.org/10.1038/nrm.2017.95

Hiratsuka, T., Bordeu, I., Pruessner, G., Watt, F.M., 2020. Regulation of ERK basal and pulsatile activity control proliferation and exit from the stem cell compartment in mammalian epidermis. Proc. Natl. Acad. Sci. U. S. A. 117, 17796–17807. https://doi.org/10.1073/pnas.2006965117

Hollenberg, M.D., Gregory, H., 1980. Epidermal growth factor-urogastrone: biological activity and receptor binding of derivatives. Mol. Pharmacol. 17, 314–320.

Houles, T., Gravel, S.-P., Lavoie, G., Shin, S., Savall, M., Méant, A., Grondin, B., Gaboury, L., Yoon, S.-O., St-Pierre, J., Roux, P.P., 2018. RSK Regulates PFK-2 Activity to Promote Metabolic Rewiring in Melanoma. Cancer Res. 78, 2191–2204. https://doi.org/10.1158/0008-5472.CAN-17-2215

Houlihan, L.M., Davies, G., Tenesa, A., Harris, S.E., Luciano, M., Gow, A.J., McGhee, K.A., Liewald, D.C., Porteous, D.J., Starr, J.M., Lowe, G.D., Visscher, P.M., Deary, I.J., 2010. Common Variants of Large Effect in F12, KNG1, and HRG Are Associated with Activated Partial Thromboplastin Time. Am. J. Hum. Genet. 86, 626–631. https://doi.org/10.1016/j.ajhg.2010.02.016

Huang, G., Yan, H., Ye, S., Tong, C., Ying, Q., 2014. STAT3 Phosphorylation at Tyrosine 705 and Serine 727 Differentially Regulates Mouse ESC Fates. Stem Cells 32, 1149–1160. https://doi.org/10.1002/stem.1609

Johnson, H.E., Toettcher, J.E., 2019. Signaling Dynamics Control Cell Fate in the Early Drosophila Embryo. Dev. Cell 48, 361-370.e3. https://doi.org/10.1016/j.devcel.2019.01.009

Kale, J., Osterlund, E.J., Andrews, D.W., 2018. BCL-2 family proteins: changing partners in the dance towards death. Cell Death Differ. 25, 65–80. https://doi.org/10.1038/cdd.2017.186

Kantz, H., Schreiber, T., 2003. Nonlinear Time Series Analysis, 2nd ed. Cambridge University Press, Cambridge. https://doi.org/10.1017/CBO9780511755798

Kawamoto, T., Ishige, K., Thomas, M., Yamashita-Kashima, Y., Shu, S., Ishikura, N., Ariizumi, S., Yamamoto, M., Kurosaki, K., Shoda, J., 2015. Overexpression and gene amplification of EGFR, HER2, and HER3 in biliary tract carcinomas, and the possibility for therapy with the HER2-targeting antibody pertuzumab. J. Gastroenterol. 50, 467–479. https://doi.org/10.1007/s00535-014-0984-5

Keely, S.J., Barrett, K.E., 1999. ErbB2 and ErbB3 receptors mediate inhibition of calcium-dependent chloride secretion in colonic epithelial cells. J. Biol. Chem. 274, 33449–33454. https://doi.org/10.1074/jbc.274.47.33449

Kennel, M.B., Brown, R., Abarbanel, H.D.I., 1992. Determining embedding dimension for phase-space reconstruction using a geometrical construction. Phys. Rev. A 45, 3403–3411. https://doi.org/10.1103/PhysRevA.45.3403

Kim, J., Jeong, H., Lee, Y., Kim, C., Kim, H., Kim, A., 2013. HRG-β1-driven ErbB3 signaling induces epithelial-mesenchymal transition in breast cancer cells. BMC Cancer 13, 383. https://doi.org/10.1186/1471-2407-13-383

Klemke, R.L., Cai, S., Giannini, A.L., Gallagher, P.J., Lanerolle, P. de, Cheresh, D.A., 1997. Regulation of Cell Motility by Mitogen-activated Protein Kinase. J. Cell Biol. 137, 481–492. https://doi.org/10.1083/jcb.137.2.481

Klijn, C., Durinck, S., Stawiski, E.W., Haverty, P.M., Jiang, Z., Liu, H., Degenhardt, J., Mayba, O., Gnad, F., Liu, J., Pau, G., Reeder, J., Cao, Y., Mukhyala, K., Selvaraj, S.K., Yu, M., Zynda, G.J., Brauer, M.J., Wu, T.D., Gentleman, R.C., Manning, G., Yauch, R.L., Bourgon, R., Stokoe, D., Modrusan, Z., Neve, R.M., de Sauvage, F.J., Settleman, J., Seshagiri, S., Zhang, Z., 2015. A comprehensive transcriptional portrait of human cancer cell lines. Nat. Biotechnol. 33, 306–312. https://doi.org/10.1038/nbt.3080

Kochańczyk, M., Kocieniewski, P., Kozłowska, E., Jaruszewicz-Błońska, J., Sparta, B., Pargett, M., Albeck, J.G., Hlavacek, W.S., Lipniacki, T., 2017. Relaxation oscillations and hierarchy of feedbacks in MAPK signaling. Sci. Rep. 7, 38244. https://doi.org/10.1038/srep38244

Koseska, A., Bastiaens, P.I., 2017. Cell signaling as a cognitive process. EMBO J. 36, 568–582. https://doi.org/10.15252/embj.201695383

Kuchenov, D., Laketa, V., Stein, F., Salopiata, F., Klingmüller, U., Schultz, C., 2016. High-Content Imaging Platform for Profiling Intracellular Signaling Network Activity in Living Cells. Cell Chem. Biol. 23, 1550–1559. https://doi.org/10.1016/j.chembiol.2016.11.008

Lai, S., Pelech, S., 2016. Regulatory roles of conserved phosphorylation sites in the activation T-loop of the MAP kinase ERK1. Mol. Biol. Cell 27, 1040–1050. https://doi.org/10.1091/mbc.E15-07-0527

Lakowicz, J., 2006. Lakowicz JR (2006) Principles of fluorescence spectroscopy, 3rd edn. Springer, New York, 2006.

Lavoie, H., Gagnon, J., Therrien, M., 2020. ERK signalling: a master regulator of cell behaviour, life and fate. Nat. Rev. Mol. Cell Biol. 21, 607–632. https://doi.org/10.1038/s41580-020-0255-7

Lavoie, H., Therrien, M., 2015. Regulation of RAF protein kinases in ERK signalling. Nat. Rev. Mol. Cell Biol. 16, 281–298. https://doi.org/10.1038/nrm3979

Lee, K.-M., Nam, K., Oh, S., Lim, J., Lee, T., Shin, I., 2015. ECM1 promotes the Warburg effect through EGF-mediated activation of PKM2. Cell. Signal. 27, 228–235. https://doi.org/10.1016/j.cellsig.2014.11.004

Lee, M.-Y., Jeong, W.-J., Oh, J.-W., Choi, K.-Y., 2009. NM23H2 inhibits EGF- and Ras-induced proliferation of NIH3T3 cells by blocking the ERK pathway. Cancer Lett. 275, 221–226. https://doi.org/10.1016/j.canlet.2008.10.018

Legewie, S., Schoeberl, B., Blüthgen, N., Herzel, H., 2007. Competing docking interactions can bring about bistability in the MAPK cascade. Biophys. J. 93, 2279–2288. https://doi.org/10.1529/biophysj.107.109132

Lemmon, M.A., Schlessinger, J., 2010. Cell signaling by receptor tyrosine kinases. Cell 141, 1117–1134. https://doi.org/10.1016/j.cell.2010.06.011

Li, P., Deng, Q., Liu, J., Yan, J., Wei, Z., Zhang, Z., Liu, H., Li, B., 2019. Roles for HB-EGF in Mesenchymal Stromal Cell Proliferation and Differentiation During Skeletal Growth. J. Bone Miner. Res. Off. J. Am. Soc. Bone Miner. Res. 34, 295–309. https://doi.org/10.1002/jbmr.3596

Liu, H.-X., Henson, B.S., Zhou, Y., D'Silva, N.J., Mistretta, C.M., 2008. Fungiform papilla pattern: EGF regulates inter-papilla lingual epithelium and decreases papilla number by means of PI3K/Akt, MEK/ERK, and p38 MAPK signaling. Dev. Dyn. Off. Publ. Am. Assoc. Anat. 237, 2378–2393. https://doi.org/10.1002/dvdy.21657

Liu, P., Kevrekidis, I.G., Shvartsman, S.Y., 2011. Substrate-Dependent Control of ERK Phosphorylation Can Lead to Oscillations. Biophys. J. 101, 2572–2581. https://doi.org/10.1016/j.bpj.2011.10.025

Liu, Y., Calmel, C., Desbois-Mouthon, C., Sobczak-Thépot, J., Karaiskou, A., Praz, F., 2020. Regulation of the EGFR/ErbB signalling by clathrin in response to various ligands in hepatocellular carcinoma cell lines. J. Cell. Mol. Med. 24, 8091–8102. https://doi.org/10.1111/jcmm.15440

Lopez, J., Hesling, C., Prudent, J., Popgeorgiev, N., Gadet, R., Mikaelian, I., Rimokh, R., Gillet, G., Gonzalo, P., 2012. Src tyrosine kinase inhibits apoptosis through the Erk1/2- dependent degradation of the death accelerator Bik. Cell Death Differ. 19, 1459–1469. https://doi.org/10.1038/cdd.2012.21

Lopez-Bergami, P., Lau, E., Ronai, Z., 2010. Emerging roles of ATF2 and the dynamic AP1 network in cancer. Nat. Rev. Cancer 10, 65–76. https://doi.org/10.1038/nrc2681

Lorenz, K., Schmitt, J.P., Schmitteckert, E.M., Lohse, M.J., 2009. A new type of ERK1/2 autophosphorylation causes cardiac hypertrophy. Nat. Med. 15, 75–83. https://doi.org/10.1038/nm.1893

Lu, H.-C., Tan, Q., Rousseaux, M.W.C., Wang, W., Kim, J.-Y., Richman, R., Wan, Y.-W., Yeh, S.-Y., Patel, J.M., Liu, X., Lin, T., Lee, Y., Fryer, J.D., Han, J., Chahrour, M., Finnell, R.H., Lei, Y., Zurita-Jimenez, M.E., Ahimaz, P., Anyane-Yeboa, K., Van Maldergem, L., Lehalle, D., Jean-Marcais, N., Mosca-Boidron, A.-L., Thevenon, J., Cousin, M.A., Bro, D.E., Lanpher, B.C., Klee, E.W., Alexander, N., Bainbridge, M.N., Orr, H.T., Sillitoe, R.V., Ljungberg, M.C., Liu, Z., Schaaf, C.P., Zoghbi, H.Y., 2017. Disruption of the ATXN1–CIC complex causes a spectrum of neurobehavioral phenotypes in mice and humans. Nat. Genet. 49, 527–536. https://doi.org/10.1038/ng.3808

Lukow, D.A., Sausville, E.L., Suri, P., Chunduri, N.K., Wieland, A., Leu, J., Smith, J.C., Girish, V., Kumar, A.A., Kendall, J., Wang, Z., Storchova, Z., Sheltzer, J.M., 2021. Chromosomal instability accelerates the evolution of resistance to anti-cancer therapies. Dev. Cell 56, 2427-2439.e4. https://doi.org/10.1016/j.devcel.2021.07.009

Maachi, H., Fergusson, G., Ethier, M., Brill, G.N., Katz, L.S., Honig, L.B., Metukuri, M.R., Scott, D.K., Ghislain, J., Poitout, V., 2020. HB-EGF Signaling Is Required for Glucose-Induced Pancreatic β-Cell Proliferation in Rats. Diabetes 69, 369–380. https://doi.org/10.2337/db19-0643

Marwan, N., 2008. A historical review of recurrence plots. Eur. Phys. J. Spec. Top. 164, 3–12. https://doi.org/10.1140/epjst/e2008-00829-1

Marwan, N., Carmenromano, M., Thiel, M., Kurths, J., 2007. Recurrence plots for the analysis of complex systems. Phys. Rep. 438, 237–329. https://doi.org/10.1016/j.physrep.2006.11.001

Marwan, N., Kurths, J., 2002. Nonlinear analysis of bivariate data with cross recurrence plots. Phys. Lett. A 302, 299–307. https://doi.org/10.1016/S0375-9601(02)01170-2

Marx, V., 2017. Probes: FRET sensor design and optimization. Nat. Methods 14, 949–953. https://doi.org/10.1038/nmeth.4434

Masunaga, H., Sugimoto, Y., Magi, S., Itasaki, R., Okada-Hatakeyama, M., Kurata, H., 2017. Robustness analysis of the detailed kinetic model of an ErbB signaling network by using dynamic sensitivity. PloS One 12, e0178250. https://doi.org/10.1371/journal.pone.0178250

Matsuura, K., Canfield, K., Feng, W., Kurokawa, M., 2016. Metabolic Regulation of Apoptosis in Cancer. Int. Rev. Cell Mol. Biol. 327, 43–87. https://doi.org/10.1016/bs.ircmb.2016.06.006

Mayr, U., Serra, D., Liberali, P., 2019. Exploring single cells in space and time during tissue development, homeostasis and regeneration. Development 146, dev176727. https://doi.org/10.1242/dev.176727

Mendoza, M.C., Er, E.E., Zhang, W., Ballif, B.A., Elliott, H.L., Danuser, G., Blenis, J., 2011. ERK-MAPK Drives Lamellipodia Protrusion by Activating the WAVE2 Regulatory Complex. Mol. Cell 41, 661–671. https://doi.org/10.1016/j.molcel.2011.02.031

Meyer, T., 1991. Cell signalling by second messenger waves. Cell 64, 675–678. https://doi.org/10.1016/0092-8674(91)90496-L

Meyer, T., Teruel, M.N., 2003. Fluorescence imaging of signaling networks. Trends Cell Biol. 13, 101–106. https://doi.org/10.1016/s0962-8924(02)00040-5

Miki, H., Fukuda, M., Nishida, E., Takenawa, T., 1999. Phosphorylation of WAVE Downstream of Mitogen-activated Protein Kinase Signaling*. J. Biol. Chem. 274, 27605–27609. https://doi.org/10.1074/jbc.274.39.27605

Ming-Kuei Hu, 1962. Visual pattern recognition by moment invariants. IEEE Trans. Inf. Theory 8, 179–187. https://doi.org/10.1109/TIT.1962.1057692

Miranti, C.K., Brugge, J.S., 2002. Sensing the environment: a historical perspective on integrin signal transduction. Nat. Cell Biol. 4, E83-90. https://doi.org/10.1038/ncb0402-e83

Mohammad, R.M., Muqbil, I., Lowe, L., Yedjou, C., Hsu, H.-Y., Lin, L.-T., Siegelin, M.D., Fimognari, C., Kumar, N.B., Dou, Q.P., Yang, H., Samadi, A.K., Russo, G.L., Spagnuolo, C., Ray, S.K., Chakrabarti, M., Morre, J.D., Coley, H.M., Honoki, K., Fujii, H., Georgakilas, A.G., Amedei, A., Niccolai, E., Amin, A., Ashraf, S.S., Helferich, W.G., Yang, X., Boosani, C.S., Guha, G., Bhakta, D., Ciriolo, M.R., Aquilano, K., Chen, S., Mohammed, S.I., Keith, W.N., Bilsland, A., Halicka, D., Nowsheen, S., Azmi, A.S., 2015. Broad targeting of resistance to apoptosis in cancer. Semin. Cancer Biol. 35 Suppl, S78–S103. https://doi.org/10.1016/j.semcancer.2015.03.001

Monge-Alvarez, J., Hoyos-Barcelo, C., Lesso, P., Casaseca-de-la-Higuera, P., 2019. Robust Detection of Audio-Cough Events Using Local Hu Moments. IEEE J. Biomed. Health Inform. 23, 184–196. https://doi.org/10.1109/JBHI.2018.2800741

Moran, M.F., Koch, C.A., Anderson, D., Ellis, C., England, L., Martin, G.S., Pawson, T., 1990. Src homology region 2 domains direct protein-protein interactions in signal transduction. Proc. Natl. Acad. Sci. 87, 8622–8626. https://doi.org/10.1073/pnas.87.21.8622

Moyer, J.D., Barbacci, E.G., Iwata, K.K., Arnold, L., Boman, B., Cunningham, A., DiOrio, C., Doty, J., Morin, M.J., Moyer, M.P., Neveu, M., Pollack, V.A., Pustilnik, L.R., Reynolds, M.M., Sloan, D., Theleman, A., Miller, P., 1997. Induction of apoptosis and cell cycle arrest by CP-358,774, an inhibitor of epidermal growth factor receptor tyrosine kinase. Cancer Res. 57, 4838–4848.

Murphy, L.O., Smith, S., Chen, R.-H., Fingar, D.C., Blenis, J., 2002. Molecular interpretation of ERK signal duration by immediate early gene products. Nat. Cell Biol. 4, 556–564. https://doi.org/10.1038/ncb822

Muthuswamy, S.K., Gilman, M., Brugge, J.S., 1999. Controlled dimerization of ErbB receptors provides evidence for differential signaling by homo- and heterodimers. Mol. Cell. Biol. 19, 6845–6857. https://doi.org/10.1128/MCB.19.10.6845

Mylonis, I., Chachami, G., Samiotaki, M., Panayotou, G., Paraskeva, E., Kalousi, A., Georgatsou, E., Bonanou, S., Simos, G., 2006. Identification of MAPK Phosphorylation Sites and Their Role in the Localization and Activity of Hypoxia-inducible Factor-1α*. J. Biol. Chem. 281, 33095–33106. https://doi.org/10.1074/jbc.M605058200

Nakakuki, T., Birtwistle, M.R., Saeki, Y., Yumoto, N., Ide, K., Nagashima, T., Brusch, L., Ogunnaike, B.A., Okada-Hatakeyama, M., Kholodenko, B.N., 2010. Ligand-specific c-Fos expression emerges from the spatiotemporal control of ErbB network dynamics. Cell 141, 884–896. https://doi.org/10.1016/j.cell.2010.03.054

Nakamura, T., Gulick, J., Colbert, M.C., Robbins, J., 2009. Protein tyrosine phosphatase activity in the neural crest is essential for normal heart and skull development. Proc. Natl. Acad. Sci. 106, 11270–11275. https://doi.org/10.1073/pnas.0902230106

Napoli, I., Mercaldo, V., Boyl, P.P., Eleuteri, B., Zalfa, F., De Rubeis, S., Di Marino, D., Mohr, E., Massimi, M., Falconi, M., Witke, W., Costa-Mattioli, M., Sonenberg, N., Achsel, T., Bagni, C., 2008. The Fragile X Syndrome Protein Represses Activity-Dependent Translation through CYFIP1, a New 4E-BP. Cell 134, 1042–1054. https://doi.org/10.1016/j.cell.2008.07.031

Nayal, A., Webb, D.J., Brown, C.M., Schaefer, E.M., Vicente-Manzanares, M., Horwitz, A.R., 2006. Paxillin phosphorylation at Ser273 localizes a GIT1–PIX–PAK complex and regulates adhesion and protrusion dynamics. J. Cell Biol. 173, 587–589. https://doi.org/10.1083/jcb.200509075

Negro, A., Brar, B.K., Lee, K.-F., 2004. Essential roles of Her2/erbB2 in cardiac development and function. Recent Prog. Horm. Res. 59, 1–12. https://doi.org/10.1210/rp.59.1.1

Newbern, J., Zhong, J., Wickramasinghe, R.S., Li, X., Wu, Y., Samuels, I., Cherosky, N., Karlo, J.C., O'Loughlin, B., Wikenheiser, J., Gargesha, M., Doughman, Y.Q., Charron, J., Ginty, D.D., Watanabe, M., Saitta, S.C., Snider, W.D., Landreth, G.E., 2008. Mouse and human phenotypes indicate a critical conserved role for ERK2 signaling in neural crest development. Proc. Natl. Acad. Sci. 105, 17115–17120. https://doi.org/10.1073/pnas.0805239105

Nguyen, K.A., Intriago, R.E., Upadhyay, H.C., Santos, S.J., Webster, N.J.G., Lawson, M.A., 2010. Modulation of gonadotropin-releasing hormone-induced extracellular signal-regulated kinase activation by dual-specificity protein phosphatase 1 in LbetaT2 gonadotropes. Endocrinology 151, 4882–4893. https://doi.org/10.1210/en.2009-1483

Obatake, N., Shiu, A., Tang, X., Torres, A., 2019. Oscillations and bistability in a model of ERK regulation. J. Math. Biol. 79, 1515–1549. https://doi.org/10.1007/s00285-019-01402-y

Okoshi, R., Shu, C.-L., Ihara, S., Fukui, Y., 2013. Scattering of MCF7 cells by heregulin ß-1 depends on the MEK and p38 MAP kinase pathway. PloS One 8, e53298. https://doi.org/10.1371/journal.pone.0053298

Ostrakhovitch, E.A., Cherian, M.G., 2005. Inhibition of extracellular signal regulated kinase (ERK) leads to apoptosis inducing factor (AIF) mediated apoptosis in epithelial breast cancer cells: the lack of effect of ERK in p53 mediated copper induced apoptosis. J. Cell. Biochem. 95, 1120–1134. https://doi.org/10.1002/jcb.20484

Parker, M.I., Nikonova, A.S., Sun, D., Golemis, E.A., 2020. Proliferative signaling by ERBB proteins and RAF/MEK/ERK effectors in polycystic kidney disease. Cell. Signal. 67, 109497. https://doi.org/10.1016/j.cellsig.2019.109497

Parmenter, T.J., Kleinschmidt, M., Kinross, K.M., Bond, S.T., Li, J., Kaadige, M.R., Rao, A., Sheppard, K.E., Hugo, W., Pupo, G.M., Pearson, R.B., McGee, S.L., Long, G.V., Scolyer, R.A., Rizos, H., Lo, R.S., Cullinane, C., Ayer, D.E., Ribas, A., Johnstone, R.W., Hicks, R.J., McArthur, G.A., 2014. Response of BRAF-mutant melanoma to BRAF inhibition is mediated by a network of transcriptional regulators of glycolysis. Cancer Discov. 4, 423–433. https://doi.org/10.1158/2159-8290.CD-13-0440

Parsons, J.T., Horwitz, A.R., Schwartz, M.A., 2010. Cell adhesion: integrating cytoskeletal dynamics and cellular tension. Nat. Rev. Mol. Cell Biol. 11, 633–643. https://doi.org/10.1038/nrm2957

Patel, A.L., Shvartsman, S.Y., 2018. Outstanding questions in developmental ERK signaling. Dev. Camb. Engl. 145. https://doi.org/10.1242/dev.143818

Pérez Millán, M., Turjanski, A.G., 2015. MAPK's networks and their capacity for multistationarity due to toric steady states. Math. Biosci. 262, 125–137. https://doi.org/10.1016/j.mbs.2014.12.010

Phuc, L.T.M., Taniguchi, A., 2017. Epidermal Growth Factor Enhances Cellular Uptake of Polystyrene Nanoparticles by Clathrin-Mediated Endocytosis. Int. J. Mol. Sci. 18. https://doi.org/10.3390/ijms18061301

Pinsino, A., Roccheri, M.C., Costa, C., Matranga, V., 2011. Manganese interferes with calcium, perturbs ERK signaling, and produces embryos with no skeleton. Toxicol. Sci. Off. J. Soc. Toxicol. 123, 217–230. https://doi.org/10.1093/toxsci/kfr152

Raina, D., Fabris, F., Morelli, L.G., Schröter, C., 2022. Intermittent ERK oscillations downstream of FGF in mouse embryonic stem cells. Dev. Camb. Engl. 149. https://doi.org/10.1242/dev.199710

Rauen, K.A., 2013. The RASopathies. Annu. Rev. Genomics Hum. Genet. 14, 355–369. https://doi.org/10.1146/annurev-genom-091212-153523

Richard, D.E., Berra, E., Gothié, E., Roux, D., Pouysségur, J., 1999. p42/p44 Mitogen-activated Protein Kinases Phosphorylate Hypoxia-inducible Factor 1α (HIF-1α) and Enhance the Transcriptional Activity of HIF-1*. J. Biol. Chem. 274, 32631–32637. https://doi.org/10.1074/jbc.274.46.32631

Rivera, V.M., Miranti, C.K., Misra, R.P., Ginty, D.D., Chen, R.H., Blenis, J., Greenberg, M.E., 1993. A growth factor-induced kinase phosphorylates the serum response factor at a site that regulates its DNA-binding activity. Mol. Cell. Biol. 13, 6260–6273. https://doi.org/10.1128/mcb.13.10.6260-6273.1993

Roskoski, R.J., 2012. ERK1/2 MAP kinases: structure, function, and regulation. Pharmacol. Res. 66, 105–143. https://doi.org/10.1016/j.phrs.2012.04.005

Ryu, H., Chung, M., Dobrzyński, M., Fey, D., Blum, Y., Lee, S.S., Peter, M., Kholodenko, B.N., Jeon, N.L., Pertz, O., 2015. Frequency modulation of ERK activation dynamics rewires cell fate. Mol. Syst. Biol. 11, 838. https://doi.org/10.15252/msb.20156458

Saba-El-Leil, M.K., Frémin, C., Meloche, S., 2016. Redundancy in the World of MAP Kinases: All for One. Front. Cell Dev. Biol. 4, 67. https://doi.org/10.3389/fcell.2016.00067

Sanderson, M.P., Dempsey, P.J., Dunbar, A.J., 2006. Control of ErbB signaling through metalloprotease mediated ectodomain shedding of EGF-like factors. Growth Factors 24, 121–136. https://doi.org/10.1080/08977190600634373

Santos, A., Tsafou, K., Stolte, C., Pletscher-Frankild, S., O'Donoghue, S.I., Jensen, L.J., 2015. Comprehensive comparison of large-scale tissue expression datasets. PeerJ 3, e1054. https://doi.org/10.7717/peerj.1054

Sauer, T., Yorke, J.A., Casdagli, M., 1991. Embedology. J. Stat. Phys. 65, 579–616. https://doi.org/10.1007/BF01053745

Saxton, R.A., Sabatini, D.M., 2017. mTOR Signaling in Growth, Metabolism, and Disease. Cell 168, 960–976. https://doi.org/10.1016/j.cell.2017.02.004

Serasinghe, M.N., Wieder, S.Y., Renault, T.T., Elkholi, R., Asciolla, J.J., Yao, J.L., Jabado, O., Hoehn, K., Kageyama, Y., Sesaki, H., Chipuk, J.E., 2015. Mitochondrial Division Is Requisite to RAS-Induced Transformation and Targeted by Oncogenic MAPK Pathway Inhibitors. Mol. Cell 57, 521–536. https://doi.org/10.1016/j.molcel.2015.01.003

Shamir, A., Buonanno, A., 2010. Molecular and cellular characterization of Neuregulin-1 type IV isoforms. J. Neurochem. 113, 1163–1176. https://doi.org/10.1111/j.1471-4159.2010.06677.x

Shankaran, H., Ippolito, D.L., Chrisler, W.B., Resat, H., Bollinger, N., Opresko, L.K., Wiley, H.S., 2009. Rapid and sustained nuclear–cytoplasmic ERK oscillations induced by epidermal growth factor. Mol. Syst. Biol. 5, 332. https://doi.org/10.1038/msb.2009.90

Shankaran, H., Wiley, H.S., 2010. Oscillatory dynamics of the extracellular signal-regulated kinase pathway. Curr. Opin. Genet. Dev. 20, 650–655. https://doi.org/10.1016/j.gde.2010.08.002

Shao, Y., Aplin, A.E., 2012. ERK2 phosphorylation of serine 77 regulates Bmf pro-apoptotic activity. Cell Death Dis. 3, e253–e253. https://doi.org/10.1038/cddis.2011.137

Shen, C.-H., Yuan, P., Perez-Lorenzo, R., Zhang, Y., Lee, S.X., Ou, Y., Asara, J.M., Cantley, L.C., Zheng, B., 2013. Phosphorylation of BRAF by AMPK Impairs BRAF-KSR1 Association and Cell Proliferation. Mol. Cell 52, 161–172. https://doi.org/10.1016/j.molcel.2013.08.044

Sigismund, S., Argenzio, E., Tosoni, D., Cavallaro, E., Polo, S., Di Fiore, P.P., 2008. Clathrin-Mediated Internalization Is Essential for Sustained EGFR Signaling but Dispensable for Degradation. Dev. Cell 15, 209–219. https://doi.org/10.1016/j.devcel.2008.06.012

Siromolot, A.A., Krynina, O.I., Kolybo, D.V., Komisarenko, S.V., 2020. Antiproliferative and apoptotic effects of anti-human HB-EGF neutralizing polyclonal antibodies in vitro. Exp. Oncol. 42, 25–30. https://doi.org/10.32471/exp-oncology.2312-8852.vol-42-no-1.14145

Slack-Davis, J.K., Eblen, S.T., Zecevic, M., Boerner, S.A., Tarcsafalvi, A., Diaz, H.B., Marshall, M.S., Weber, M.J., Parsons, J.T., Catling, A.D., 2003. PAK1 phosphorylation of MEK1 regulates fibronectin-stimulated MAPK activation. J. Cell Biol. 162, 281–291. https://doi.org/10.1083/jcb.200212141

Smitz, J., Cortvrindt, R., Hu, Y., 1998. Epidermal growth factor combined with recombinant human chorionic gonadotrophin improves meiotic progression in mouse follicle-enclosed oocyte culture. Hum. Reprod. Oxf. Engl. 13, 664–669. https://doi.org/10.1093/humrep/13.3.664

Spelat, R., Ferro, F., Curcio, F., 2012. Serine 111 Phosphorylation Regulates OCT4A Protein Subcellular Distribution and Degradation. J. Biol. Chem. 287, 38279–38288. https://doi.org/10.1074/jbc.M112.386755

Stacey, D.W., Kung, H.-F., 1984. Transformation of NIH 3T3 cells by microinjection of Ha-ras p21 protein. Nature 310, 508–511. https://doi.org/10.1038/310508a0

Stallaert, W., Brüggemann, Y., Sabet, O., Baak, L., Gattiglio, M., Bastiaens, P.I.H., 2018. Contact inhibitory Eph signaling suppresses EGF-promoted cell migration by decoupling EGFR activity from vesicular recycling. Sci. Signal. 14.

Stanoev, A., Mhamane, A., Schuermann, K.C., Grecco, H.E., Stallaert, W., Baumdick, M., Brüggemann, Y., Joshi, M.S., Roda-Navarro, P., Fengler, S., Stockert, R., Roßmannek, L., Luig, J., Koseska, A., Bastiaens, P.I.H., 2018. Interdependence between EGFR and Phosphatases Spatially Established by Vesicular Dynamics Generates a Growth Factor Sensing and Responding Network. Cell Syst. 7, 295-309.e11. https://doi.org/10.1016/j.cels.2018.06.006

Steinkamp, M.P., Low-Nam, S.T., Yang, S., Lidke, K.A., Lidke, D.S., Wilson, B.S., 2014. erbB3 is an active tyrosine kinase capable of homo- and heterointeractions. Mol. Cell. Biol. 34, 965–977. https://doi.org/10.1128/MCB.01605-13

Sundberg-Smith, L.J., Doherty, J.T., Mack, C.P., Taylor, J.M., 2005. Adhesion Stimulates Direct PAK1/ERK2 Association and Leads to ERK-dependent PAK1 Thr212 Phosphorylation*. J. Biol. Chem. 280, 2055–2064. https://doi.org/10.1074/jbc.M406013200

Takens, F., 1981. Detecting strange attractors in turbulence, in: Rand, D., Young, L.-S. (Eds.), Dynamical Systems and Turbulence, Warwick 1980. Springer Berlin Heidelberg, Berlin, Heidelberg, pp. 366–381.

Tanimura, S., Takeda, K., 2017. ERK signalling as a regulator of cell motility. J. Biochem. (Tokyo) 162, 145–154. https://doi.org/10.1093/jb/mvx048

Tsukada, Y., Aoki, K., Nakamura, T., Sakumura, Y., Matsuda, M., Ishii, S., 2008. Quantification of Local Morphodynamics and Local GTPase Activity by Edge Evolution Tracking. PLoS Comput. Biol. 4, e1000223. https://doi.org/10.1371/journal.pcbi.1000223

Twigg, S.R.F., Vorgia, E., McGowan, S.J., Peraki, I., Fenwick, A.L., Sharma, V.P., Allegra, M., Zaragkoulias, A., Akha, E.S., Knight, S.J.L., Lord, H., Lester, T., Izatt, L., Lampe, A.K., Mohammed, S.N., Stewart, F.J., Verloes, A., Wilson, L.C., Healy, C., Sharpe, P.T., Hammond, P., Hughes, J., Taylor, S., Johnson, D., Wall, S.A., Mavrothalassitis, G., Wilkie, A.O.M., 2013. Reduced dosage of ERF causes complex craniosynostosis in humans and mice and links ERK1/2 signaling to regulation of osteogenesis. Nat. Genet. 45, 308–313. https://doi.org/10.1038/ng.2539

Ueda Takeshi, Watanabe-Fukunaga Rie, Fukuyama Hidehiro, Nagata Shigekazu, Fukunaga Rikiro, 2004. Mnk2 and Mnk1 Are Essential for Constitutive and Inducible Phosphorylation of Eukaryotic Initiation Factor 4E but Not for Cell Growth or Development. Mol. Cell. Biol. 24, 6539–6549. https://doi.org/10.1128/MCB.24.15.6539-6549.2004

Ünal, E.B., Uhlitz, F., Blüthgen, N., 2017. A compendium of ERK targets. FEBS Lett. 591, 2607–2615. https://doi.org/10.1002/1873-3468.12740

Váradi, T., Schneider, M., Sevcsik, E., Kiesenhofer, D., Baumgart, F., Batta, G., Kovács, T., Platzer, R., Huppa, J.B., Szöllősi, J., Schütz, G.J., Brameshuber, M., Nagy, P., 2019. Homo- and Heteroassociations Drive Activation of ErbB3. Biophys. J. 117, 1935–1947. https://doi.org/10.1016/j.bpj.2019.10.001

Vicente-Manzanares, M., Ma, X., Adelstein, R.S., Horwitz, A.R., 2009. Non-muscle myosin II takes centre stage in cell adhesion and migration. Nat. Rev. Mol. Cell Biol. 10, 778–790. https://doi.org/10.1038/nrm2786

Villaseñor, R., Kalaidzidis, Y., Zerial, M., 2016. Signal processing by the endosomal system. Curr. Opin. Cell Biol. 39, 53–60. https://doi.org/10.1016/j.ceb.2016.02.002

von Kriegsheim, A., Baiocchi, D., Birtwistle, M., Sumpton, D., Bienvenut, W., Morrice, N., Yamada, K., Lamond, A., Kalna, G., Orton, R., Gilbert, D., Kolch, W., 2009. Cell fate decisions are specified by the dynamic ERK interactome. Nat. Cell Biol. 11, 1458–1464. https://doi.org/10.1038/ncb1994

Wagner, M.J., Stacey, M.M., Liu, B.A., Pawson, T., 2013. Molecular Mechanisms of SH2- and PTB-Domain-Containing Proteins in Receptor Tyrosine Kinase Signaling. Cold Spring Harb. Perspect. Biol. 5, a008987–a008987. https://doi.org/10.1101/cshperspect.a008987

Wallot, S., Mønster, D., 2018. Calculation of Average Mutual Information (AMI) and False-Nearest Neighbors (FNN) for the Estimation of Embedding Parameters of Multidimensional Time Series in Matlab. Front. Psychol. 9, 1679. https://doi.org/10.3389/fpsyg.2018.01679

Wang, S., Allen, N., Vickers, T.A., Revenko, A.S., Sun, H., Liang, X.-H., Crooke, S.T., 2018. Cellular uptake mediated by epidermal growth factor receptor facilitates

the intracellular activity of phosphorothioate-modified antisense oligonucleotides. Nucleic Acids Res. 46, 3579–3594. https://doi.org/10.1093/nar/gky145

Warbug, O., 1956. On the origin of cancer cells. Science 123, 309–314. https://doi.org/10.1126/science.123.3191.309

Waters, K.M., Cummings, B.S., Shankaran, H., Scholpa, N.E., Weber, T.J., 2014. ERK Oscillation-Dependent Gene Expression Patterns and Deregulation by Stress Response. Chem. Res. Toxicol. 27, 1496–1503. https://doi.org/10.1021/tx500085u

Webb, D.J., Donais, K., Whitmore, L.A., Thomas, S.M., Turner, C.E., Parsons, J.T., Horwitz, A.F., 2004. FAK–Src signalling through paxillin, ERK and MLCK regulates adhesion disassembly. Nat. Cell Biol. 6, 154–161. https://doi.org/10.1038/ncb1094

Webber, C.L., n.d. Chapter 2. Recurrence Quantification Analysis of Nonlinear Dynamical Systems 69.

Worster, D.T., Schmelzle, T., Solimini, N.L., Lightcap, E.S., Millard, B., Mills, G.B., Brugge, J.S., Albeck, J.G., 2012. Akt and ERK control the proliferative response of mammary epithelial cells to the growth factors IGF-1 and EGF through the cell cycle inhibitor p57Kip2. Sci. Signal. 5, ra19. https://doi.org/10.1126/scisignal.2001986

Xu, Q., Zhang, Q., Ishida, Y., Hajjar, S., Tang, X., Shi, H., Dang, C.V., Le, A.D., 2017. EGF induces epithelial-mesenchymal transition and cancer stem-like cell properties in human oral cancer cells via promoting Warburg effect. Oncotarget 8, 9557–9571. https://doi.org/10.18632/oncotarget.13771

Yan, Y., Gong, Y., Guo, Y., Lv, Q., Guo, C., Zhuang, Y., Zhang, Y., Li, R., Zhang, X., 2012. Mechanical strain regulates osteoblast proliferation through integrin-mediated ERK activation. PloS One 7, e35709. https://doi.org/10.1371/journal.pone.0035709

Yang, J., Weinberg, R.A., 2008. Epithelial-mesenchymal transition: at the crossroads of development and tumor metastasis. Dev. Cell 14, 818–829. https://doi.org/10.1016/j.devcel.2008.05.009

Yang, J.-M., Bhattacharya, S., West-Foyle, H., Hung, C.-F., Wu, T.-C., Iglesias, P.A., Huang, C.-H., 2018. Integrating chemical and mechanical signals through dynamic coupling between cellular protrusions and pulsed ERK activation. Nat. Commun. 9, 4673. https://doi.org/10.1038/s41467-018-07150-9

Yang, J.-Y., Zong, C.S., Xia, W., Yamaguchi, H., Ding, Q., Xie, X., Lang, J.-Y., Lai, C.-C., Chang, C.-J., Huang, W.-C., Huang, H., Kuo, H.-P., Lee, D.-F., Li, L.-Y., Lien, H.-C., Cheng, X., Chang, K.-J., Hsiao, C.-D., Tsai, F.-J., Tsai, C.-H., Sahin, A.A., Muller, W.J., Mills, G.B., Yu, D., Hortobagyi, G.N., Hung, M.-C.,

2008. ERK promotes tumorigenesis by inhibiting FOXO3a via MDM2-mediated degradation. Nat. Cell Biol. 10, 138–148. https://doi.org/10.1038/ncb1676

Yarden, Y., Sliwkowski, M.X., 2001. Untangling the ErbB signalling network. Nat. Rev. Mol. Cell Biol. 2, 127–137. https://doi.org/10.1038/35052073

Ye, Q., Cai, W., Zheng, Y., Evers, B.M., She, Q.-B., 2014. ERK and AKT signaling cooperate to translationally regulate survivin expression for metastatic progression of colorectal cancer. Oncogene 33, 1828–1839. https://doi.org/10.1038/onc.2013.122

Yin, J.C., Platt, M.J., Tian, X., Wu, X., Backx, P.H., Simpson, J.A., Araki, T., Neel, B.G., 2017. Cellular interplay via cytokine hierarchy causes pathological cardiac hypertrophy in RAF1-mutant Noonan syndrome. Nat. Commun. 8, 15518. https://doi.org/10.1038/ncomms15518

Ying, Q.-L., Wray, J., Nichols, J., Batlle-Morera, L., Doble, B., Woodgett, J., Cohen, P., Smith, A., 2008. The ground state of embryonic stem cell self-renewal. Nature 453, 519–523. https://doi.org/10.1038/nature06968

Yoon, S., Seger, R., 2006. The extracellular signal-regulated kinase: Multiple substrates regulate diverse cellular functions. Growth Factors 24, 21–44. https://doi.org/10.1080/02699050500284218

Zbilut, J.P., Giuliani, A., Webber, C.L., 1998. Detecting deterministic signals in exceptionally noisy environments using cross-recurrence quantification. Phys. Lett. A 246, 122–128. https://doi.org/10.1016/S0375-9601(98)00457-5

Zhang, B., Zhang, Y., Liu, J., Wang, B., 2021. FGFF Descriptor and Modified Hu Moment-Based Hand Gesture Recognition. Sensors 21. https://doi.org/10.3390/s21196525

Zhang, X., Gureasko, J., Shen, K., Cole, P.A., Kuriyan, J., 2006. An Allosteric Mechanism for Activation of the Kinase Domain of Epidermal Growth Factor Receptor. Cell 125, 1137–1149. https://doi.org/10.1016/j.cell.2006.05.013

Zhao, J., Yuan, X., Frödin, M., Grummt, I., 2003. ERK-Dependent Phosphorylation of the Transcription Initiation Factor TIF-IA Is Required for RNA Polymerase I Transcription and Cell Growth. Mol. Cell 11, 405–413. https://doi.org/10.1016/S1097-2765(03)00036-4

Zhihu Huang, Jinsong Leng, 2010. Analysis of Hu's moment invariants on image scaling and rotation, in: 2010 2nd International Conference on Computer Engineering and Technology. Presented at the 2010 2nd International Conference on Computer Engineering and Technology, pp. V7-476. https://doi.org/10.1109/ICCET.2010.5485542

7 Acknowledgements

I would firstly like to thank Prof. Dr. Philippe Bastiaens for giving me the opportunity to be a part of this interesting and complex project.

I would like to thank all my TAC members, Dr. Peter Bieling, Dr. Christian Schröter, and PD. Dr. Aneta Koseska for their valuable input during our meetings, and their support throughout these 4 years. Special thanks to Dr. Astrid Kramer for her comments on the manuscript.

Thank you, Astrid and Tanja, for their help with all the administrative work, especially during these hectic pandemic times. Also, thanks to Lucia for welcoming me to the institute and for her help in organizing the IMPRS events.

To the 4 Frauen (Luig, Manu, Michel, Schutz), your support during the first two years of my Ph.D. was invaluable. Frau Schutz, I probably wouldn't have known what to do if it weren't for you.

To all the members of Department 2, those who've moved on and those who've stayed. Thank you for listening to me, helping me, being there for me, and your teachings. Dr. Seidel, thank you very much for your help during my pseudo-biochemist phase and your help with the assembling of my thesis

A mi familia venezolana, esparcida por el mundo. Muchas gracias por sus palabras de aliento y por su entendimiento. El camino que nos tocó, no ha sido ni fácil ni justo, pero sé que hemos mantenido nuestros valores y nuestra humanidad. Espero que podamos reunirnos pronto y, en algún momento, reconstruir Venezuela. A mis padres, es por ustedes que vivo, por su crianza, soy quien soy y por su apoyo he logrado lo que he logrado. No podré devolverles los años vida que les han robado, pero espero que con mi trabajo pueda darles una mejor calidad de vida a su porvenir.

A mi querida esposa, muchas gracias por todo. Tu constante apoyo incondicional y tu compañía hicieron posible culminar esta etapa.

Chciałbym bardzo podziękować mojej polskiej rodzinie. Wasze wsparcie przez te wszystkie lata było niesamowite. Od samego początku czułem się przez Was zrozumiany, wspierany i kochany. Dzięki Wam mam nowe miejsce w moim sercu, które mogę nazwać "domem". Podziękowania dla Taty, Mamy, Wojtka, Babci, Cioci i Wujka.

お仕舞です
麻奴衣流 神歩素

8 Matlab scripts

ERK activity kinetic parameters calculation

```
for kk=1:numel(List_var)
     CURVE=eval(List_var{kk});
     [n,m]=size(CURVE);
     for j=1:n
     cont=cont+1;
    y=CURVE(j,:);

ccont=y-min(y);
ccont=ccont./max(ccont);

Smooth_curve=sgolayfilt(ccont,1,5);
c(1)=0;
vv=gradient(Smooth_curve);


for i=1:180
c(i)=(vv(i)>0)+(vv(i+1)>0)+(vv(i+2)>0)+(vv(i+3)>0)+(vv(i+4)>0)+(vv(i+5)>0)+
(vv(i+6)>0)+(vv(i+7)>0)+(vv(i+8)>0)+(vv(i+9)>0)+(vv(i+10)>0)+(vv(i+11)>0);
end

RT(j)=find(c>=11,1)*3.108;
MSp(j)=max(vv)*60/3.108;
Tmax=find(vv==max(vv));
try
Tstab(j)=find(vv(Tmax:end)<0,1)+Tmax;
catch
    Tstab(j)=m;
end
eval(strcat('RT_',List_var{kk},'(j)=','RT(j);'))
eval(strcat('MSp_',List_var{kk},'(j)=','MSp(j);'))
eval(strcat('Tstab_',List_var{kk},'(j)=','Tstab(j);'))
vv=[];
Tmax=[];

     end
     cont=0;
     MSp=[];
     RT=[];
     CURVE=[];
     Tstab=[];

end
```

AMI Function

```
function [v,lag]=ami(x,y,lag)
%Usage: [v,lag]=ami(x,y,lag)
%
% Calculates the mutual average information of x and y with a possible lag.
```

```
%
%
% v is the average mutual information. (relative units see below)
% x & y is the time series. (column vectors)
% lag is a vector of time lags.
%
% (A peak in V for lag>0 means y is leading x.)
%
% v is given as how many bits x and y has in common relative to how
% many bits is needed for the internally binned representation of x or y.
% This is done to make the result close to independent bin size.
%
if nargin==0
    error('You should provide a time series.');
end
if nargin<2
    y=x;
end
x=x(:);
y=y(:);
n=length(x);
if n~=length(y)
    error('x and y should be same length.');
end
if nargin<3
    lag=0;
    if nargin<2
        lag=0:min(n/2-1,20); %compatible with mai.m
    end
else
    lag=round(lag);
end
% The mutual average information
x=x-min(x);
x=x*(1-eps)/max(x);
y=y-min(y);
y=y*(1-eps)/max(y);
v=zeros(size(lag));
lastbins=nan;
for ii=1:length(lag)
    abslag=abs(lag(ii));

    % Define the number of bins
    bins=floor(1+log2(n-abslag)+0.5);%as mai.m
    if bins~=lastbins
        binx=floor(x*bins)+1;
        biny=floor(y*bins)+1;
    end
    lastbins=bins;
    Pxy=zeros(bins);

    for jj=1:n-abslag
        kk=jj+abslag;
        if lag(ii)<0
            temp=jj;jj=kk;kk=temp;%swap
        end
        Pxy(binx(kk),biny(jj))=Pxy(binx(kk),biny(jj))+1;
    end
    Pxy=Pxy/(n-abslag);
    Pxy=Pxy+eps; %avoid division and log of zero
    Px=sum(Pxy,2);
    Py=sum(Pxy,1);
```

```
    q=Pxy./(Px*Py);

    q=Pxy.*log2(q);

    v(ii)=sum(q(:))/log2(bins); %log2bins is what you get if x=y.
%   Equivalent formulation (slightly slower)
%     Hx=-sum(Px.*log2(Px));
%     Hy=-sum(Py.*log2(Py));
%     Hxy=-sum(Pxy(:).*log2(Pxy(:)));
%     v(ii)=Hx+Hy-Hxy;
end
```

FNN function

```
function [embedm fnn1 fnn2]=fnn(y,maxm)

% Usage: This function  calculates corrected false nearest neighbour.

% Inputs:
%   y  is a  vertical vector of time series.
%   maxm: maximum value of embedding dimension.

% Output:
%   embedm: proper value for embedding dimension.
%   fnn1: First criteria of false nearest neighbors.
%   fnn2: second criteria of false nearest neighbors.



%_____________________________________________________________________________
y=y(:);
RT=15;
AT=2;
sigmay=std(y);
[nyr,nyc]=size(y);
%Embedding matrix
m=maxm;

    EM=lagmatrix(y,0:m-1);

%EM after nan elimination.
EEM=EM(1+(m-1):end,:);
[rEEM cEEM]=size(EEM);

embedm=[];

for k=1:cEEM
fnn1=[];
fnn2=[];
   D=dist(EEM(:,1:k)');

   for i=1:rEEM-m-k

       d11 = min(D(i,1:i-1));
       d12=min(D(i,i+1:end));
       Rm=min([d11;d12]);
       l=find(D(i,1:end)== Rm);
```

```
        if Rm>0
        if l+m+k-1<nyr
        fnn1=[fnn1;abs(y(i+m+k-1,1)-y(l+m+k-1,1))/Rm];
        fnn2=[fnn2;abs(y(i+m+k-1,1)-y(l+m+k-1,1))/sigmay];
        end
        end
    end
    Ind1=find(fnn1>RT);
    Ind2=find(fnn2>AT);
    if length(Ind1)/length(fnn1)<.1 && length(Ind2)/length(fnn1)<.1;
    embedm=k; break

    end
end
```

Unthresholded recurrence plot calculation

```
function M= RP_cal(X)

%%
%Input X should be the time delay embedded series to be analyzed.
%
%
%

[m,~]=size(X);
A_rp1=zeros(m);

 for i=1:m
    for j=1:m
          A_rp1(i,j)=sqrt(sum((X(i,:)-X(j,:)).^2)) ;
    end
 end

 M=A_rp1;
```

Unthresholded Cross-recurrece plot calculation

```
function M= CrossRP_cal(X1,X2)

%%
%
%
%

[m,~]=size(X1);
A_rp1=zeros(m);

 for i=1:m
    for j=1:m
          A_rp1(i,j)=sqrt(sum((X1(i,:)-X2(j,:)).^2)) ;
    end
 end

 M=A_rp1;
```

Recurrence plot quantification

```
function [RR,DET,ENTR,L,pp,S,Lmax] = Recu_RQA(RP,I)

% Recurrence quantification analysis of recurrence plots
% RP:  the Recurrence Plot
% I:   the indication marks (I=0 RP is the symmetry matrix
%                            I=1 RP is the asymmetry matrix)

% RR:   Recurrence rate RR, The percentage of recurrence points in an RP
%       Corresponds to the correlation sum;
% DET:  Determinism DET, The percentage of recurrence points which form
%       diagonal lines
% ENTR: Entropy ENTR, The Shannon entropy of the probability distribution
of the diagonal
%       line lengths p(l)
% L:    Averaged diagonal line length L, The average length of the diagonal
lines

%% pp probability of the length distribuition

%% S Length distribuition


Lmin=2;

if nargin < 2
    I=0;
end

N1=size(RP,1);

Yout=zeros(1,N1);

for k=2:N1
    On=1;
    while On<=N1+1-k
        if RP(On,k+On-1)==1
            A=1;off=0;
            while off==0 && On~=N1+1-k
                if RP(On+1,k+On)==1
                    A=A+1;On=On+1;
                else
                    off=1;
                end
            end
            Yout(A)=Yout(A)+1;
        end
        On=On+1;
    end
end
if I==0
    S=2*Yout;
end

if I==1
```

```
    RP=RP';
    for k=2:N1
        On=1;
        while On<=N1+1-k
            if RP(On,k+On-1)==1
                A=1;off=0;
                while off==0 && On~=N1+1-k
                    if RP(On+1,k+On)==1
                        A=A+1;On=On+1;
                    else
                        off=1;
                    end
                end
                Yout(A)=Yout(A)+1;
            end
            On=On+1;
        end
    end
    S=Yout;
end

%% calculate the recurrence rate (RR)
SR=0;
for i=1:N1
    SR=SR+i*S(i);
end
RR=SR/(N1*(N1-1));

%% calculate the determinism (%DET)
if SR==0
    DET=0;
else
    DET=(SR-sum(S(1:Lmin-1)))/SR;
end

%% calculate the ENTR = entropy (ENTR)
S(1)=[]; Delete the non isolated recurrences
pp=S/sum(S);
entropy=0;
F=find(S(Lmin:end));
l=length(F);
if l==0
    ENTR=0;
Else
    F=F+Lmin-1;
    ENTR=-sum(pp(F).*log(pp(F)));
end

%% calculate Averaged diagonal line length (L)
L=(SR-sum([1:Lmin-1].*S(1:Lmin-1)))/sum(S(Lmin:end));
Lmax=max(find(S));
```